Quantum Backreaction Effects in Macroscopic Systems

Black Holes and Inflation

Lukas Eisemann

München 2023

Quantum Backreaction Effects in Macroscopic Systems

Black Holes and Inflation

Lukas Eisemann

Dissertation
der Fakultät für Physik
der Ludwig-Maximilians-Universität
München

vorgelegt von
Lukas Eisemann
aus Braunschweig

München, den 21. September 2023

Erstgutachter: Prof. Dr. Gia Dvali
Zweitgutachter: Prof. Dr. Andreas Weiler
Tag der mündlichen Prüfung: 28. November 2023

Zusammenfassung

Diese Arbeit befasst sich mit zwei Effekten in makroskopischen Systemen, die nur sichtbar werden, wenn man die Quantennatur des Systems berücksichtigt. Damit diese Effekte stark werden, ist eine hohe Mikrozustandsentartung erforderlich, was die Untersuchung ihrer Manifestation in de Sitter und schwarzen Löchern (SL) motiviert.

Der erste Teil befasst sich mit der quantenmechanischen Beschreibung von Phänomenen der Teilchenerzeugung in einem Hintergrund. Die übliche semiklassische Behandlung solcher Szenarien erlaubt oft eine nichtperturbative Analysemethode. Wir zeigen, dass die Auflösung des Hintergrunds als N-Teilchen-Zustand eine vollständig quantenmechanische perturbative Analyse ermöglicht, welche die semiklassischen nichtperturbativen Ergebnisse produziert und es erlaubt, darüber hinaus zu gehen. Sowohl in einem Modell mit zwei Skalaren als auch in der Skalar-QED können wir so die Teilchenerzeugung in zeitabhängigen Feldern in Form von $n \to 2$ Annihilationsprozessen darstellen. Rückwirkungseffekte werden insbesondere im Fall $n \sim N$ innerhalb eines einzigen Prozesses dramatisch, d.h. das nahezu klassische System geht nicht-graduell in einen Quantenzustand von wenigen hochenergetischen Teilchen über. Wir stellen fest, dass eine solche "Quantenmechanisierung" (quantumization) im Allgemeinen stark unterdrückt ist. Im Gegensatz dazu können die umgekehrten, "klassisierenden" (classicalizing) Übergänge, $2 \to N$, potentiell ohne Unterdrückung erfolgen, da die Entartung des N-Teilchen-Zustands in einer konsistenten Theorie ausreichend hoch sein kann. Im Fall von $N \to 2$ bewirkt eine solche Entartung nur in dem Maße eine Verstärkung, wie die entarteten Zustände innerhalb einer anfänglichen Superposition abgedeckt sind. Ein SL, das durch einen gebundenen Zustand von N Gravitonen beschrieben wird, besitzt somit einen Zustand, der gegenüber einem Einprozesszerfall instabil ist. Wir kommentieren die Möglichkeit, dass ein nahezu klassisches SL das erforderliche Maß an Superposition auf relevanten Zeitskalen erzeugt.

Der zweite Teil befasst sich mit dem so genannten Speicherlast- (memory burden) Effekt, der universell für Systeme mit hoher Speicherkapazität besteht und einen graduellen Zerfall des Systems unterbindet. Wir untersuchen anhand eines Prototypmodells, ob dieser Effekt vermieden werden kann, indem gespeicherte Quanteninformation von einem Satz von Freiheitsgraden auf einen anderen umgeschrieben wird. Wir stellen fest, dass ein solcher durch Umschreiben ermöglichter Zerfall nur sehr langsam im Vergleich zum Anfangsstadium des Zerfalls voranschreiten kann, d.h. der Zerfall bleibt effektiv unterdrückt. Sowohl bei de Sitter als auch bei SL manifestiert sich der Effekt in einer Abweichung von der semiklassischen Entwicklung der thermischen Teilchenemission und wird spätestens nach

einer Anzahl von Emissionen in der Größenordnung der Entropie stark. Die gespeicherte Quanteninformation, die für den Effekt verantwortlich ist, stellt ein Quanten-Haar dar und kann um den Wirkungseintritt herum beginnen, freigesetzt zu werden. Wenn die Inflation nicht lange vor diesem Zeitpunkt endete, können die Abdrücke dieser primordialen Information beobachtbar sein. Für SL eröffnet die effektive Stabilisierung nach dem Halbzerfall in Abwesenheit anderer starker Effekte destabilisierender Art ein neues Fenster für kleine primordiale SL als dunkle Materie.

Abstract

This thesis is concerned with two effects in macroscopic systems that are only revealed when taking into account the system's quantum nature. For these effects to become strong, a high microstate degeneracy is essential, which motivates investigating their manifestation in de Sitter and black holes (BHs).

The first part is concerned with the quantum description of phenomena of particle creation in a background. The common semiclassical treatment of such scenarios often allows for a nonperturbative method of analysis. We show that resolving the background as an N-particle state allows for a fully quantum perturbative analysis that produces the semiclassical nonperturbative results and allows to go beyond. In a model of two scalars as well as in scalar QED, we thus produce particle creation in time-dependent fields in terms of $n \to 2$ annihilation processes. Effects of backreaction in particular become dramatic within a single process in the case $n \sim N$, i.e., the near-classical system non-gradually transitions into a quantum state of a few highly energetic particles. We find that such "quantumization" is in general highly suppressed. By contrast, the reverse, "classicalizing" transitions, $2 \to N$, may be unsuppressed because the degeneracy of the N-particle state can be sufficiently high in a consistent theory. For the case of $N \to 2$, such degeneracy is causing an enhancement only to the extent that the degenerate states are covered within an initial superposition. A BH described in terms of a bound state of N gravitons thus possesses a state unstable to single-process decay. We comment on the possibility of a near-classical BH generating the required level of superposition on relevant time scales.

The second part is concerned with the so-called memory burden effect, which is universal to systems of high memory capacity and stops any gradual decay of the system. We study a prototype model to investigate whether the effect may be avoided by rewriting stored quantum information from one set of degrees of freedom to another one. We find that such rewriting-facilitated decay can proceed only very slowly compared to the initial stage of decay, s.t. the decay effectively remains suppressed. In both de Sitter and BHs, the effect manifests in a deviation from the semiclassical evolution of thermal particle emission and becomes strong the latest after a number of emissions on the order of the entropy. The stored quantum information responsible for the effect constitutes a quantum hair and may start to get released around the onset. If inflation ended not long before that time, the imprints of that primordial information can be observable. For BHs, in the absence of other strong effects of destabilizing kind, the effective stabilization after half-decay opens a new window for small primordial BHs as dark matter.

Publications

The present thesis is based on research that I conducted at the LMU München as well as the Max-Planck-Institute for Physics and the results of which have been published in ref. [1, 2, 3]. In particular, part I of this thesis is based on work that has been done in collaboration with Gia Dvali and has been published in

1. G. Dvali and L. Eisemann, "Perturbative understanding of nonperturbative processes and quantumization versus classicalization," Phys. Rev. D **106** (2022), 125019, [2211.02618]

Part II is based on research done in collaboration with Gia Dvali, Marco Michel, and Sebastian Zell, which has been published in

2. G. Dvali, L. Eisemann, M. Michel and S. Zell, "Universe's Primordial Quantum Memories," JCAP **03** (2019), 010 [1812.08749].

3. G. Dvali, L. Eisemann, M. Michel and S. Zell, "Black hole metamorphosis and stabilization by memory burden," Phys. Rev. D **102** (2020), 103523, [2006.00011].

As is conventional in high energy physics, the authors of these papers share the principal authorship and are listed alphabetically. The main objective of this thesis is to put the results into context as well as present them in a unified way. Thus, the presentation in this thesis follows that of the above papers closely, although new material has been added. In particular, equations and figures have been reproduced ad verbatim. We also point out that the results obtained and published in the above collaborations have since in part been reported in the dissertations of some of the collaborators. Explicitly, results of [2] were reported by Sebastian Zell in [4] and the results of both [2] and [3] were reported by Marco Michel in [5].

Contents

Chapter 1

Introduction

Context

The theory of quantum gravity is well-defined within quantum field theory for sub-Planckian energies (see, e.g., ref. [6]). However, an open problem is not just its extension to higher energies, the so-called UV-completion, but also to clarify what quantum gravity predicts at low energies. Famous solutions of General Relativity, the classical theory of gravity, such as black holes (BHs) and de Sitter spacetime are assumed to correspond to nonperturbative states in the quantum theory that persist in the classical limit. However, those states and their exact evolution are unknown. An active field of research therefore is concerning quantum corrections to the known (semi-)classical evolution of those states. With the work presented in this thesis we hope to contribute to such understanding.

BHs and de Sitter spacetime, which cannot be described within Newtonian gravity, not only have many fascinating properties but are also at the center of several important open questions in fundamental physics and cosmology.

Let us review some of the established properties of BHs and de Sitter as well as touch on some ideas regarding BHs in the context of quantum gravity and particle physics in general.

Within General Relativity, BHs are the objects of the highest possible mass density (see, e.g., ref. [7]). They may form in the gravitational collapse of matter and subsequently grow by accreting further matter, giving them a prominent role in astrophysical modelling (see, e.g., ref. [8]). For an outside observer, there exists an event horizon, meaning that no physical signal from beyond the horizon can reach the observer [7]. The Bekenstein bound on the possible entropy of a system of finite extent [9] is saturated by BHs [10], implying there has to be an enormous number of internal degrees of freedom that can carry information while having an effectively vanishing energy cost of excitation. Furthermore, that entropy scales with the area of the BH as opposed to the ordinary case of scaling with a system's volume [10]. BHs have been shown to radiate all existing particle species with an approximately thermal spectrum for as long as the corresponding energy loss is

negligible as compared to the BH mass [11], a phenomenon known as Hawking-radiation.

In cosmology, BHs have attracted attention in the context of dark matter, a type of matter motivated by the current cosmological standard model ΛCDM and constrained by observations to make up around 20% of the universe's current mass (see, e.g., [12]). Cold dark matter would be nonrelativistic and interact electromagnetically only rather weakly. BHs that would have formed sufficiently early in the universe's history, so-called primordial BHs, could in principle account for part or all of the cold dark matter (see, e.g., [13]). Such an explanation arguably would have the appeal of not requiring the existence of unknown particles.

Via the existence of BHs, gravity likely limits the possible masses elementary particles may have: a particle of mass much heavier than M_P would have a Compton wavelength much smaller than its gravitational radius and thus may be expected to constitute a BH. States at the crossover with a mass around M_P are expected to neither behave like a quantum particle nor like a near-classical BH [14].

In addition to the formation from gravitational collapse, BHs are also expected to be created in trans-Planckian particle collisions (see, e.g., [15]), matching the semi-classical intuition that if the impact parameter is smaller than the gravitational radius corresponding to the center of mass energy, a BH should be formed.

Combining the above expectations, the idea of self-completeness of gravity [16] entails that there is no UV-completion of gravity in terms of additional particles but instead BHs are the only new trans-Planckian states.

Within the idea of classicalization [17], the possibility of such a nonperturbative mechanism of UV-completion is argued to generalize to quantum field theories that share certain key properties of gravity. This would make BHs a representative of "classicalons", the resonances appearing at trans-cutoff energies in such a theory. As an explicit example, a derivative self-interaction of the Higgs boson at a scale between the highest experimentally probed one and the Planck scale could lead to classicalizing behaviour in the absence of new elementary particles restoring perturbative unitarity [17, 18].

A proposal for a BH quantum state is provided by the N-Portrait [19], according to which BHs are bound states of gravitons. Combined with the idea of self-completion, this would imply that at energies both below and above M_P, the degrees of freedom are merely gravitons. We are going to come back to the N-Portrait and its implications for the quantum evolution of BHs below.

As remarkable as some of the BH properties are, some of them have been shown to be shared by a family of objects called "saturons" [20]: these objects are achieving maximal and area-form entropy as well as exhibiting a slow release of information. Explicit examples of saturon states within renormalizable quantum field theories have demonstrated that such properties are not specific to gravity [21].

Many of the BH properties mentioned above are shared by de Sitter spacetime. In addition, de Sitter has important applications in cosmology in the approximate description of an inflationary stage [22] as well as of a present dark-energy-dominated stage [12]. In high analogy to BHs, there also exists an event horizon for the observer [12]. Likewise, particles are created in a thermal spectrum, a phenomenon known as Gibbons-Hawking-

radiation [23]. A de Sitter patch viewed as a system of the size of the horizon, shares the remarkable information properties of a BH: an area-form entropy saturating the Bekenstein bound [23].

Quantum corrections to the evolution of BHs and de Sitter spacetime may be of various kinds. Both Hawking- and Gibbons-Hawking-radiation are derived using the classical solutions of a BH and de Sitter spacetime as an external background for quantum fields. Such a semi-classical description represents a conscious approximation that necessarily breaks down after a certain time if gravity is quantum in nature and takes part in the dynamics.

It has been argued [24] that the semi-classical description predicts the breakdown of its validity in terms of a deviation from thermality of the radiation spectrum after a time on the order of half-decay, even if the energy loss due to the radiation is taken into account in terms of self-similar evaporation with a shrinking horizon and mass. In order to make more quantitative predictions for the quantum mechanical evolution one has to, in principle, go beyond such a description and commit to a quantum mechanical model.

Before outlining the types of quantum corrections our work is related to, let us briefly mention other quantum corrections that have been proposed.

Within the above-mentioned N-Portrait [19], measurable effects of a global charge of a BH have been identified, constituting a so-called BH-hair, which is absent only in the semi-classical limit [25]. In the same quantum mechanical model, growing inner entanglement [26] as well as growing entanglement with the radiated Hawking quanta [27] have been found to be another cause for deviation from the semi-classical description.

An aspect of quantum mechanical evolution that part of our work concerns is non-gradual decay. BHs are, in general, not protected by any symmetries against "explosion" into a few particles. Within quantum field theories simpler than gravity, we investigate condensate decay processes of many particles to two. Leaning on the N-Portrait for BHs, we draw conclusions for BHs.

Another quantum mechanical effect that any system of high entropy has been argued to be exposed to [28] is the so-called memory burden effect, which is a gradually building resistance against any prolonged gradual decay of such a system. In the work presented here, we investigate how this effect plays out in simplified model systems and draw conclusions for BHs and de Sitter spacetime upon appropriate parameter choices.

Outline and Results

After giving a big picture of our work at the end of the previous section, in the following, we are going to provide a more detailed description as well as the results of our studies. Alongside, we are going to outline the presentation in this thesis.

Our research has been carried out along two distinct lines and correspondingly this thesis consists of two parts.

Chapter 2, which constitutes part I, contains our work on many-particle scattering processes.

Within a model of two scalar fields as well as in scalar quantum electrodynamics, in 3+1 dimensions, we analyze three cases of condensate decay. Before going to a fully quantum treatment, for each case, we find or cite the semiclassical prediction for particle creation in the respective classical background where the energy of the produced particles is high compared to the characteristic frequency of the background. Resolving the backgrounds in terms of a many-particle state allows for a fully quantum description of the decay in terms of a generic number n out of N condensate particles annihilating in a single connected process in favour of a pair of particles. In the regime of high n, the semi-classical non-perturbative prediction and quantum perturbative prediction match and imply a strong suppression of the processes.

Specifically, in section 2.2, we demonstrate this for the case of a two-scalar-model with a $\phi^2\chi^2$-interaction. Section 2.3 repeats the analysis for the example of a condensate of charged scalar electrons decaying into a pair of photons with energy large compared to the electron mass. In section 2.4, we consider a condensate of massive photons, corresponding to an oscillating electric field, in which a pair of scalar electrons near mass threshold is produced. In section 2.5, we establish the regimes in which the rate can be calculated reliably in perturbation theory.

The fully quantum approach has the advantage to allow for consistently taking into account the backreaction. This is required in particular in the dramatic case of $n \sim N$, i.e., decay within a single process, which we focus on in section 2.6. Endowing the systems studied with additional internal symmetries provides clear-cut examples for the potential interplay of enhancement due to microstate degeneracy on the one hand and suppression of the $2 \to N$ S-matrix elements on the other. We find that as long as the system is approximately classical, single-process decay is dominated by gradually proceeding decay and evolution of entanglement. However, such effective stability against non-gradual decay may be lost in the case that the system loses classicality (while remaining macroscopic) by evolving into an entangled superposition that accesses a sufficiently large microstate degeneracy. For the more complicated systems of BHs, this points to a mechanism of destabilization against explosive quantum evolution.

Part II of the thesis contains our studies on the memory burden effect.

The focus of our work is to investigate to what extent the memory burden effect, which we have briefly described in section 1, can be avoided in general and, in particular, in BHs and de Sitter. As has been argued in [28], the quantum information stored in a system of high entropy or, more generally, of enhanced memory capacity, microscopically is carried in modes of near-vanishing excitation gaps and, correspondingly, the energy cost of the stored information is raised by any departure of the system from the state around which those near-gapless degrees of freedom exist. The memory burden effect denotes the ensuing backreaction that slows down any such evolution. In particular, this happens in the case of a gradual decay of the system. In the absence of an efficient release of the stored

information to the environment, it has been argued in ref. [28] that the only conceivable way of avoiding the memory burden effect is a process called rewriting. Namely, if the system possesses further sets of modes that become gapless at a later stage of the decay and onto which the system manages to offload the information in the process. The goal of the present work is to find whether systems can realize such rewriting-powered decay at all and to quantify the parameter dependence of the speed of such decay.

To this end, we study a prototype model (presented in section 3.1), which has been proposed in ref. [28] as the simplest possible model exhibiting the memory burden effect as well as the possibility of rewriting. Besides the benefit of calculational accessibility, such an approach offers an understanding of the dynamics of the memory burden in isolation. We thus attempt to find universal properties of systems of high entropy. The universality of behaviour is of course limited by the onset of other effects specific to a given system. But since for BHs the evolution past the initial stage of Hawking-like evaporation is unknown, any insight into of the post-semiclassical stage is valuable. In addition to analytic considerations presented in sections 3.1, 3.3, and 3.3.2, we perform an extensive numerical time-evolution of the full system (section 3.2). The evolution reveals the conditions under which rewriting takes place as well as the dependence on the size of the system.

In chapter 4, we investigate the implications of the above findings for the memory burden effect in BHs and de Sitter. In section 4.1, we identify the appropriate parameter scaling with the size of a BH and find a strong slowdown of decay after the onset of the memory burden effect, which takes place the latest by half-decay. Since such stabilization would imply that small primordial BHs would still exist today, in section 4.2, we comment on the effects on the parameter space for primordial BHs constituting dark matter. In section 4.1, we also comment on other possibilities for evolution past half-decay that cannot be ruled out within the prototype model analyzed. In section 4.3 we discuss the manifestation of the memory burden effect in de Sitter spacetime. We find a slowdown of Gibbons-Hawking radiation accompanied by enhanced release of the stored quantum information.

Part I

Many-Particle Processes

Chapter 2

Perturbative Understanding of Non-Perturbative Processes and Single-Process Decay

2.1 Introduction

Physical effects in quantum field theory are often categorized as *non-perturbative* when the associated physical quantity, e.g., a transition rate, is not given in terms of a perturbative power series in a relevant coupling constant.

For instance, the Hawking evaporation rate of a black hole is proportional to the inverse of the Newtonian coupling. Like many other cases of particle production from an external classical field, this effect is therefore commonly deemed non-perturbative.

However, in many examples, resolving the background field in terms of a many-particle state reveals that the effects may in fact be obtained perturbatively. The apparent non-perturbativity can then be seen to be a consequence of the scaling of the mean occupation N of the many-particle state.

For instance, a black hole in the theory of ref.s [19, 30] is resolved in terms of an N-graviton state, where N is set by G_N^{-1}. Hawking evaporation in that model is obtained from a perturbative depletion process resulting from the re-scattering of the constituent gravitons. The initial state Bose-enhancement of the process results in factors of N in the expression for the rate, accounting for the seemingly non-perturbative scaling.

Any understanding of non-perturbative mean-field effects in a perturbative fully quantum treatment also comes with the benefit to make certain corrections accessible. These are corrections coming from quantum effects of the individual particles and are $1/N$-suppressed. In their accumulation, they may even lead to a complete breakdown of the background-field treatment. This notion was initially introduced in the context of the black hole N-portrait [19], and was later termed *quantum breaking* in ref. [26].

For the case of a black hole, it has been argued [25, 31, 27, 3] that quantum breaking occurs the latest after the black hole has lost on the order of half its mass.

The quantum resolution of backgrounds in terms of N-particle states has also been termed "corpuscular" treatment and has been applied to a range of systems other than black holes. The corpuscular resolution of the de Sitter metric has been explored in ref.s [27, 32, 33, 2, 34, 35, 36]. Specifically, such representation as an N-graviton state on top of a Minkowski-vacuum has been argued [34] to be obligatory within the S-matrix formulation of gravity, as a classical de Sitter background does not constitute a valid S-matrix vacuum. The corpuscular description recovers Gibbons-Hawking particle creation [23] as a perturbative re-scattering process of the constituent gravitons into all existing particle species. It has been argued in ref.s [27, 32, 33, 34, 35] that there are quantum backreaction effects, in particular, related to developing entanglement, of order $1/N$ and that these build up to cause a gradual breakdown of the semi-classical description.

In ref. [37], a corpuscular analysis of the decaying field of cosmic axions along the same lines has been carried out. Ref.s [38, 39] investigate by different methods the occurrence of quantum breaking in the evolution of coherent states. Further aspects of the corpuscular treatment of the de Sitter metric may be found in ref.s [40, 41, 42].

In all the cases mentioned, the result of the fully quantum treatment captures the non-perturbative semiclassical effect in the infinite-N limit.

The present study continues the above line of research through an analysis of many-particle processes. In different quantum field theoretic systems of basic importance, we study particle production in a background field, both in a semi-classical treatment and in a fully quantum one.

In the quantum picture, we calculate the rate for annihilation processes involving an arbitrary number n out of the N constituent quanta. This allows us, in particular, to investigate the regime in which the energy of the created particles strongly exceeds the oscillation frequency of the classical background. In that regime, we show that the leading order perturbative prediction in the quantum treatment reproduces the non-perturbative semiclassical prediction in the limit

$$g^2 \to 0, \quad \frac{N}{Vm^3} \to \infty, \quad g^2\frac{N}{Vm^3} = \text{fixed}\,, \tag{2.1}$$

where m is the mass of the background-field constituent particles and V is the volume. For finite values of the coupling g^2 and the particle number density N/V, loop corrections constrain the regime of validity of the prediction. We outline that regime of n and N in terms of g^2. The advantage of the quantum treatment is the possibility of consistently taking into account effects of backreaction, such as generation of entanglement and depletion of the initially occupied field.

We study three different cases. The first one is within a model of two scalar fields that interact via a cross-coupling $g^2\phi^2\chi^2$. We consider processes of χ-creation from a ϕ-condensate. More precisely, in the semiclassical treatment, the fields are quantized around the external classical ϕ-field that oscillates in time, giving rise to particle-creating instabilities. Such models have been studied, among other things, in the context of reheating after inflation [43].

In the quantum treatment, the ϕ-condensate is instead given in terms of a state of ϕ-particles at rest with an occupation peaked around N. The process of a pair of χ-quanta being created at a certain energy is then resolved in terms of an annihilation process of the corresponding number of n ϕ-particles.

In the remaining two cases, we demonstrate the presence of the correspondence in systems with gauge symmetry. In one case we consider a pair of photons created from a condensate of scalar electrons and positrons. In the other example, we study scalar electron-positron creation in a time-dependent electric field or, respectively, in a many-photon annihilation process.

A particularly interesting regime is $n \sim N$, which is relevant to the understanding of classical-to-quantum transitions and even quantum-to-classical. It is an open question when and how fast a near-classical system can reach a regime in which the classical approximation ceases to be good. This time-scale t_Q has been called *quantum break-time* in ref. [26]. The appropriate scale of reference is the scale inherent in the initial classical state.

In ref. [26] it was shown that quantum breaking proceeds most quickly in systems that also possess a classical instability, i.e., a Lyapunov exponent. Namely, in such a system t_Q can scale logarithmically with the number N of the system's constituents.

For systems without such classical instability, it has been argued that t_Q is macroscopic in N [27, 32, 33]. Such scaling is the result of a gradually proceeding transition involving many processes of low n. This has been argued to be the dominant road to quantum breaking for black holes [19, 25, 31, 27, 3], as well as for de Sitter [27, 32, 33, 2, 34, 35].

On the other hand, quantum breaking within a single process requires $n \sim N$ and is expected to be negligible. As a name for this intriguing regime, we introduce the term *quantumization*. The analysis performed here provides explicit examples in quantum field theories of fundamental importance.

The reverse, a transition from a state of a few energetic particles to a classical state of many soft quanta, has been termed *classicalization* [17, 44, 18, 45, 46, 20]. Up to the phase space integration, both quantumization and classicalization are based on the same S-matrix element between number eigenstates of occupation 2 and N.

The square of such matrix elements has been argued on general grounds to be bounded from above by e^{-N} [20]. All known explicit examples conform to this bound. In particular, this is the case for the $2 \to N$ graviton scattering amplitude obtained in [45]. Our results in the present study likewise adhere to the bound and in some regimes feature an even stronger suppression.

Apart from the S-matrix element, the effective transition rate is also determined by the available microstate degeneracy of the final state. Since the potential degeneracy of an N-particle is vastly higher than that of a 2-particle state, classicalization may in fact proceed efficiently in certain theories, while quantumization is expected to be universally suppressed [46, 20]. In particular, such interplay has been argued to be in place for black holes in their description in the N-portrait [19]: Their high entropy balances the smallness of the $2 \to N$ matrix element and creation in a transplanckian collision may be unsuppressed. On the other hand, their decay within a single process is suppressed and instead, the evolution proceeds via gradual decay. Since efficient classicalization requires the final states to have

an entropy close to saturating the bound, such states have been termed "saturons" [20].

The analysis presented here provides clean cases that demonstrate under what conditions transitions $2 \to N$ and $N \to 2$ can proceed with high probability.

2.2 Case 1: $\phi^2\chi^2$

Let us consider the following model of two scalars:

$$L = \frac{1}{2}\partial_\mu\phi\partial^\mu\phi - \frac{1}{2}m^2\phi^2 + \frac{1}{2}\partial_\mu\chi\partial^\mu\chi - \frac{1}{2}m_\chi^2\chi^2 - g^2\phi^2\chi^2\,. \tag{2.2}$$

This permits the classical solution of one field oscillating in time and the other vanishing:

$$\phi_B(t) = \phi_0\cos(mt)\;, \quad \chi_B = 0\,, \tag{2.3}$$

In a semiclassical treatment, we may quantize the fluctuations around the background (2.3):

$$\hat{\phi} = \phi_B + \hat{\delta\phi}\,, \quad \hat{\chi} = \hat{\delta\chi}\,. \tag{2.4}$$

Let us consider the initial state with no excitations around the background:

$$|t_0\rangle = |0\rangle_{\delta\phi}|0\rangle_\chi\,. \tag{2.5}$$

The background affects the propagation of the fluctuations and makes this state unstable. Thus, there are transitions from this "vacuum" state, for instance

$$0 \to 2\chi\,. \tag{2.6}$$

Let us now look at the same phenomenon in a fully quantum treatment. The ϕ-condensate then instead is described in terms of the initial state

$$|t_0\rangle = |N\rangle_\phi\,|0\rangle_\chi\,. \tag{2.7}$$

Here, $|N\rangle_\phi$ is supposed to denote a state of ϕ-particles all in the same 3-momentum mode, namely, $\vec{p} = 0$. N denotes the mean occupation number of a superposition centered around it. In the following considerations, the difference among different superpositions vanishes in the limit (2.1). We are going to comment on the particularly simple cases of a coherent state and a number state. For definiteness, unless otherwise stated, in the following we assume a number state.

With this, χ-pair creation is thus given by the processes

$$N\phi \to (N-n)\phi + 2\chi\,, \tag{2.8}$$

where the final ϕ-particles are meant to be in the mode $\vec{p} = 0$ as well. Processes with scattered ϕs in the final state also exist, of course. However, compared to (2.8), they are suppressed by extra powers of the coupling g^2 and vanish in the limit (2.1). An exception to

this are diagrams with only forward-scattered ϕs, but they contribute to the same process (2.8) (see also sec. 2.5).

Since the ϕ-field has no fundamental self-interaction, in the regime where the induced self-coupling is negligible, the energetics of the condensate to a good approximation are given by

$$\frac{N}{V} = \frac{m\phi_0^2}{2}\,, \tag{2.9}$$

which provides a relation between the quantum and classical parameters. With this, the limit (2.1) can be expressed in semi-classical terms as

$$g^2 \to 0\,, \quad \frac{\phi_0^2}{m^2} \to \infty\,, \quad g^2\frac{\phi_0^2}{m^2} = \text{fixed}\,. \tag{2.10}$$

In the following, we are going to analyze creation of χ-pairs both in the quantum-perturbative and in the semiclassical-non-perturbative treatment. Although the quantum calculation is generic, we are going to focus on the case of χ-momenta $k \equiv |\vec{k}|$ corresponding to

$$n \gg \frac{g\phi_0}{m}\,. \tag{2.11}$$

2.2.1 Coherent States and Background Fields

Before we get to the actual calculations, it is worth revisiting the general correspondence [47] between calculations in a semiclassical approximation and those done in a fully quantum framework involving coherent states. Consider a coherent state $|c\rangle$ with the property $\langle c|\hat{\phi}(t)|c\rangle = \phi_B(t)$ and $\langle c|\hat{\chi}(t)|c\rangle = \chi_B(t)$, where $\hat{\phi}(t)$ and $\hat{\chi}(t)$ are evolving according to the free Hamiltonian and ϕ_B and χ_B constitute classical solutions of the free Hamiltonian. The S-matrix operator of the full theory between such a state $|c\rangle$ then coincides with the S-matrix operator of the theory quantized in a semiclassical manner around a background:

$$\langle c, B|\hat{S}|c, A\rangle_{\phi,\chi} = \langle B|\hat{S}[\phi_B, \chi_B]|A\rangle_{\delta\phi,\delta\chi}\,. \tag{2.12}$$

Here, the states $|A\rangle$ and $|B\rangle$ denote arbitrary number eigenstates of modes that are not part of the background. As we are going to see later, whether an expansion in powers of the field strength converges depends also on how many particles are involved in the process. In the perturbative regime, Eq. (2.12) in particular tells us that we have to find agreeing results for the processes (2.6) and (2.8). The differences can be due to solely deviations of the initial and final ϕ-state from $|c\rangle$. These deviations are independent of the model at hand and vanish as $\sim N^{-1}$ in the limit (2.1). The calculations in the $\phi^2\chi^2$-model as well as those in scalar QED therefore constitute explicit instances of the identity (2.12).

2.2.2 Quantum Calculation

At the leading order in g^2N, the amplitude corresponding to the process (2.8) is given in terms of a single diagram (see fig. 2.1). The accompanying factors may be found via

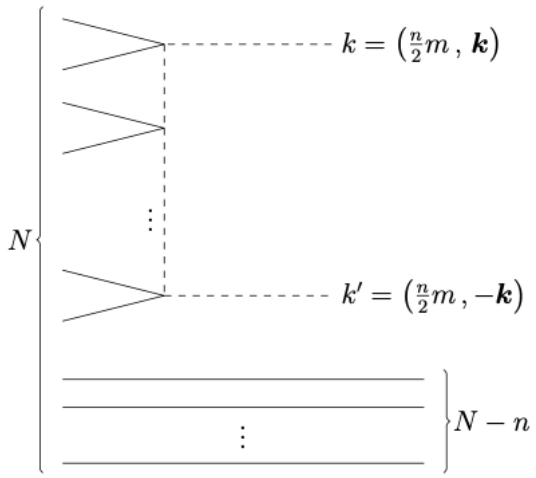

Figure 2.1: Diagrammatic representation of the leading order terms in perturbation theory contributing to the amplitude of the process (2.8). This diagram as well as the following ones have been created using *TikZ-Feynman* [48].

the following bookkeeping. The number of Wick contractions and Taylor-coefficient of the relevant term of the S-matrix operator cancel each other up to a factor of $2^{n/2}$. Projecting each Wick contraction onto the initial state of n ϕ-particles in the same momentum mode results in a factor $n!/\sqrt{n!}$. The squared amplitude is therefore given by $2^n n!|d|^2$, where d is the value of the diagram.

Let q_l denote the virtual momentum in the propagator following the lth insertion of a pair of ϕ-legs. Then one has $q_l^\mu = 2lm\delta_0^\mu - k^\mu$ and thus the propagators contribute to d a factor of

$$\prod_{l=1}^{n/2-1} \left(q_l^2 - m_\chi^2\right)^{-1} = (-1)^{n/2-1} m^{2-n}\, n^2\, 2^{-n}\, (n/2)!^{-2}\,. \tag{2.13}$$

The phase space integration is independent of the scattering angle since the initial state does not carry angular momentum. Perturbatively, the energy conservation implies

$$nm = 2\left(m_\chi^2 + k^2\right)^{1/2}\,. \tag{2.14}$$

This implies a kinematic threshold for the multiplicity n given by

$$n > n_0 \equiv \frac{2m_\chi}{m}\,. \tag{2.15}$$

One thus obtains for the tree-level rate for $n\phi \to 2\chi$ (more details on the calculation can

be found in appendix A)

$$\Gamma_{n\phi\to 2\chi} = \frac{1}{4\pi} V m^4 \sqrt{1-\frac{n_0^2}{n^2}}\, n^4 \left(\frac{g^2}{4Vm^3}\right)^n \frac{n!}{(n/2)!^4}\,. \tag{2.16}$$

As can be seen from (2.16), perturbation theory does not break down for high values of n. The initial N quanta generate a combinatoric enhancement of (see A)

$$C_{Nn} = \binom{N}{n} = \frac{N^n}{n!}\left(1+\mathcal{O}\left(\frac{n^2}{N}\right)\right)\,. \tag{2.17}$$

With this, the leading order rate for the process (2.8) is

$$\Gamma \equiv C_{Nn}\Gamma_{n\phi\to 2\chi} \sim \left(\frac{e^2}{2n^2}\frac{g^2\phi_0^2}{m^2}\right)^n\,. \tag{2.18}$$

Here, we have used relation (2.9), the Stirling approximation for the factorial, and omitted factors that scale less strongly with n than exponentially.

For early times, the evolution of n_k, the expected occupation number density of χs per momentum $\vec{k}$, is given by $n_k(t) \sim \Gamma\, t$. However, final-state Bose enhancement cannot be neglected at later times. This leads to the enhanced effective rate of (for details, see appendix A)

$$\Gamma_{\text{eff}} \sim \left(1+2n_k+\mathcal{O}\left(\frac{n_k^2 n^2}{N}\right)\right)\Gamma\,, \tag{2.19}$$

and thus

$$n_k(t) \sim \exp\left(2\Gamma t\right)\,, \quad n_k \gtrsim 1\,. \tag{2.20}$$

Thus, the quantum rate (2.18) and the semiclassical prediction are related by

$$\Gamma \sim \frac{\dot{n}_k}{n_k}\,. \tag{2.21}$$

Effects like depletion or evolution of entanglement can of course correct the evolution (2.20), but those corrections can be neglected as long as the number of depleted quanta is much smaller than N.

2.2.3 Semiclassical Calculation

The equations of motion for both $\delta\phi$ and χ simplify in the limit (2.10). The equation for $\delta\phi$ is

$$\left(\partial^2+m^2\right)\delta\phi = -2\left(d_t^2+m^2\right)\phi_B - 2g^2\chi^2\left(\phi_B+\delta\phi\right) = \mathcal{O}\left(g\right)\,, \tag{2.22}$$

where the terms involving only the background ϕ_B vanish due to (2.3). The equation for χ is

$$\left(\partial^2 + m_\chi^2\right)\chi = -2g^2\chi\left(\phi_B + \delta\phi\right)^2 = -2g^2\phi_B^2\chi + \mathcal{O}\left(g\right) . \tag{2.23}$$

One sees that, in the limit (2.10), $\delta\phi$ decouples as a free field, while χ has a time-dependent contribution to its mass due to the background.

In order to obtain the non-perturbative prediction of particle creation from the above equations, we can follow for example ref.s [49, 50]. The evolution of the expected number of χs in the case of a linear equation of the form (2.23) can be obtained in terms of the mode function v_k. The latter is defined via the mode expansion of the field operator as

$$\hat{\chi}(x) = \int d^3k \left(v_k(t)\hat{a}_0(\vec{k})e^{i\vec{k}\cdot\vec{x}} + h.c.\right) , \tag{2.24}$$

where $\hat{a}_0(\vec{k})$ and its Hermitean conjugate are the time-independent annihilation and creation operators. Only the mode function is time-dependent and follows the equation

$$\left(d_t^2 + \omega_k^2(t)\right) v_k = 0 , \tag{2.25}$$

with

$$\omega_k^2(t) \equiv m_\chi^2 + k^2 + 2g^2\phi_0^2\cos^2(mt) . \tag{2.26}$$

The expected particle creation in terms of v_k is given by

$$n_k(t) \equiv \langle 0|\hat{n}_k(t)|0\rangle = \frac{1}{2\omega_k}\left(|\dot{v}_k|^2 + \omega_k^2|v_k|^2\right) - \frac{1}{2} . \tag{2.27}$$

Here, $\hat{n}_k$ is the time-evolved operator of the number density of χ-particles per mode $\vec{k}$. The initial conditions of v_k are constrained by the requirement of being consistent with the commutation relations of the operators as well as that of initially defining the lowest energy state. The equation (2.25) with (2.26) takes the form of a Mathieu equation.

In the high multiplicity regime (2.11), the Mathieu equation allows an approximate solution, whose derivation can be found in ref. [51]. Let us parametrize equations (2.25) and (2.26) as

$$d_t^2 x + \omega_0^2\left(1 + h\cos\left(\gamma t\right)\right) x = 0 , \tag{2.28}$$

with the correspondence

$$\begin{aligned} \omega_0^2 &\leftrightarrow \overline{\omega_k}^2 \equiv m_\chi^2 + k^2 + g^2\phi_0^2 , \\ h &\leftrightarrow \frac{g^2\phi_0^2}{\overline{\omega_k}^2} , \\ \gamma &\leftrightarrow 2m . \end{aligned} \tag{2.29}$$

The equation (2.28) is known to exhibit so-called parametric resonance, i.e., some of its solutions exhibit exponential growth between the cycles of period $\tau \equiv 2\pi/\gamma$:

$$x(t+\tau) = e^{s\tau}x(t) , \tag{2.30}$$

where $s > 0$ is the parameter of instability. Such scaling implies for the particle number

$$\frac{n_k(t+\tau)}{n_k(t)} \sim \exp(2s\tau)\,, \tag{2.31}$$

and, with coarse-graining over several periods,

$$\frac{\dot{n}_k}{n_k} \sim s\,. \tag{2.32}$$

For $h \ll 1$, ref. [51] prove that there is parametric resonance in the bands

$$\gamma = \frac{2\omega_0}{l} + \epsilon\,, \quad l \in \mathbb{N} \tag{2.33}$$

and that the maximal value of the exponent within these bands scales as

$$s \sim h^l\,, \tag{2.34}$$

as does the width ϵ. From comparing (2.14) and (2.33), one sees the correspondence $l \leftrightarrow n/2$. With this, one sees from (2.21) and (2.32) that the quantum rate (2.18) is to be compared with s for $2l$:

$$s \sim h^{2l} \leftrightarrow \left(\frac{g^2\phi_0^2}{m^2}\frac{1}{n^2}\right)^n\,, \tag{2.35}$$

where we have used (2.29) and $h \ll 1$. As can be seen, there is complete agreement with the parametric scaling of (2.18).

2.3 Case 2: Scalar QED

As a second example, we are going to consider scalar QED without elementary self-coupling of the scalar,

$$L = D_\mu\phi(D^\mu\phi)^\dagger - m^2\phi^\dagger\phi - \frac{1}{4}F_{\mu\nu}F^{\mu\nu}\,, \tag{2.36}$$

where $D_\mu \equiv \partial_\mu - igA_\mu$. We are going to analyze an analogous situation as we did in the previous example, where now the roles of ϕ and χ are played by the complex scalar ϕ and the vector A, respectively. Specifically, we investigate in the semiclassical treatment the out-of-the-vacuum creation of a photon pair in the background

$$\phi_B = \phi_B^\dagger = \phi_0\cos(mt)\,, \quad A_B^\mu = 0\,. \tag{2.37}$$

In the fully quantum treatment, on the other hand, we investigate the many-particle annihilation processes

$$\frac{N}{2}s^- + \frac{N}{2}s^+ \to \frac{N-n}{2}s^- + \frac{N-n}{2}s^+ + 2\gamma\,. \tag{2.38}$$

The relation between quantum and classical parameters is now given by

$$\frac{N}{V} = m\phi_0^2\,. \tag{2.39}$$

With this, the double scaling limit (2.1) in semiclassical terms takes the same form as (2.10).

2.3.1 Quantum Calculation

Since in addition to the analogous 4-point vertex $g^2 A_\mu A^\mu \phi^\dagger \phi$ there is also the 3-point vertex $igA^\mu \phi^\dagger \partial_\mu \phi + h.c.$, rather than a single one there is now a large variety of inequivalent Wick contractions that contribute to the process (2.38) at leading order, $(Ng^2)^n$.

However, upon projecting the Wick contractions onto the initial and final state, the special condensate kinematics in combination with gauge redundancy makes all but one of the corresponding diagrams vanish, which can be seen as follows. Any diagram in which an incoming scalar pair is connected by a single 3-point vertex vanishes because the equal momenta in the initial condensate make the derivative result in a factor of zero. This throws out all diagrams with shapes other than the one shown in fig. 2.1, where now the dotted lines represent a photon and the 4-point vertices drawn either represent the elementary 4-point vertex or an effective one consisting of two 3-point vertices with one internal ϕ-line,

$$-ig^2 \frac{q^\mu_{2l+2} q^\nu_{2l}}{q^2_{2l+1} - m^2} \,, \tag{2.40}$$

where l is the number of vertices preceding the vertex. In any diagram that involves at least one effective vertex like (2.40), two momenta q_l are contracted only with orthogonal photon polarization vectors:

$$q^\mu_l \, \epsilon_\mu \left(q_{l'}, r\right) = 0 \,, \quad \forall \; l, l' \,. \tag{2.41}$$

The orthogonality holds only for transverse polarizations r, but non-transverse polarizations do not occur, since in the numerators of the photon-propagators they are projected out by the outgoing transverse photons. This leaves one again with only a single non-zero diagram, namely that consisting only of elementary 4-point vertices. The value of the diagram differs from the case of the 2-scalar model only by the factor

$$\epsilon^*_\mu(k, r) \epsilon^{*\mu}(k', r') = \delta_{r,r'} \,. \tag{2.42}$$

Thus the tree-level rate for $\frac{n}{2} s^- + \frac{n}{2} s^+ \to 2\gamma$ for each of the two polarizations coincides with (2.16).

For an initial number of $N > n$ condensate quanta, there is again a combinatoric enhancement

$$C_{Nn} = \binom{N/2}{n/2}^2 \sim 2^{-n} \frac{N^n}{(n/2)!^2} \left(1 + \mathcal{O}\left(\frac{n^2}{N}\right)\right) \,, \tag{2.43}$$

where the Stirling approximation for the factorial has been used.

Combining this with (2.39), we obtain for the leading order rate of the process (2.38)

$$\Gamma \equiv C_{Nn} \Gamma_{\frac{n}{2}, \frac{n}{2} \to 2\gamma} \sim \left(\frac{e^2}{2n^2} \frac{g^2 \phi_0^2}{m^2}\right)^n \,. \tag{2.44}$$

Here, again the Stirling approximation has been used and factors that scale less strongly with n than exponentially have been omitted. More details on the above calculation can be found in appendix A.

2.3.2 Semiclassical Calculation

The limit (2.10) simplifies the equations of motion also in the present case. Further simplifications arise taking into account that the background ϕ_B has a vanishing current and obeys a harmonic equation. With the notation

$$x \equiv \mathrm{Re}\,\delta\phi\,, \quad y \equiv \mathrm{Im}\,\delta\phi\,, \tag{2.45}$$

the equations for $\delta\phi$ are therefore

$$\left(\partial^2 + m^2\right) x = \mathcal{O}\left(g\right) \tag{2.46}$$

and

$$\left(\partial^2 + m^2\right) y = gA^\mu \partial_\mu \phi_B + g\partial_\mu \left(A^\mu \phi_B\right) + \mathcal{O}\left(g\right)\,. \tag{2.47}$$

The equation for A_μ is

$$\partial_\mu F^{\mu\nu} = 2g^2\phi_B^2 A^\nu - 2g\left(\phi_B \partial^\nu y - y\partial^\nu \phi_B\right) + \mathcal{O}\left(g\right)\,. \tag{2.48}$$

As can be seen, x decouples as a free field in the limit (2.10).

Upon projecting out the non-transverse part of A_μ, we obtain the equation for the transverse polarizations:

$$\left(\partial^2 - 2g^2\phi_B^2\right) A_T^j = \mathcal{O}\left(g\right)\,. \tag{2.49}$$

We see that, as in the 2-scalar example, the propagating photon degrees of freedom decouple from the fluctuations $\delta\phi$. The interaction of y and the Coulomb degree of freedom encoded in A_0 and A_L^j gives rise to creation of s^+s^-. We are going to restrict the analysis to processes of photon creation and are left with analogous equations to solve, namely, (2.49) takes the form of a Mathieu equation, that the mode functions of the two transverse photon polarizations obey,

$$\left(d_t^2 + \omega_k^2(t)\right) v_{k,r} = 0\,, \tag{2.50}$$

where now

$$\omega_k^2(t) \equiv k^2 + 2g^2\phi_0^2\cos^2(mt)\,. \tag{2.51}$$

We may again parametrize this equation as in (2.28) with an analogous version of (2.29). With this, we obtain as the semiclassical prediction for the rate

$$\frac{\dot{n}_{k,r}}{n_{k,r}} \sim \left(\frac{g^2\phi_0^2}{m^2}\frac{1}{n^2}\right)^n\,. \tag{2.52}$$

As in the previous example, we see complete agreement of parametric scaling between the results (2.44) and (2.52).

2.4 Case 3: Scalar QED with Massive Photon

For the third case, we consider again scalar QED, but now with a massive photon:

$$L = D_\mu\phi(D^\mu\phi)^\dagger - m_e^2\phi^\dagger\phi - \frac{1}{4}F_{\mu\nu}F^{\mu\nu} + \frac{1}{2}m^2A_\mu A^\mu\,. \tag{2.53}$$

Consider now an interchange of roles of the selectron and the photon in the previous example. That means we are looking at pair creation in an electric field. In the semiclassical treatment, the fields are quantized around the background

$$A_B^\mu = \delta_z^\mu\frac{E_0}{m}\cos(mt)\ , \quad \phi_B = 0\,, \tag{2.54}$$

which gives rise to out-of-the-vacuum creation of s^+s^-. On the other hand, in a fully quantum treatment, this takes the form of a many-photon-annihilation process,

$$N\gamma \to (N-n)\,\gamma + s^+s^-\,. \tag{2.55}$$

The quantum and classical parameters in this scenario are approximately related via

$$\frac{N}{V} = \frac{1}{2m}E_0^2\,. \tag{2.56}$$

Thus, the semi-classical limit is given by (2.10) upon replacing ϕ_0 by E_0/m. The solution (2.54) amounts to the background electromagnetic field

$$F_{0j} = \delta_j^z E_0\sin(\omega t)\ , \quad F_{kj} = 0\,, \tag{2.57}$$

where the frequency is given by $\omega = m$. The field is purely electric and nonzero only in the z-direction.

For the case of spinor QED, similar processes have been analyzed in the author's master's thesis [52]. The more involved spin structure of that model allowed only for a calculation with circular photon polarizations, which compared to the case of linear polarization leads to additional suppression of the amplitudes close to the mass threshold.

The field (2.57) can be used as an approximation, for instance, of the field created in the antinodes of superposing laser light, on length scales short compared to the wavelength, $2\pi/\omega$. In the case of an optical or X-ray laser and the real electron mass, the minimum number of photons required for pair creation is very large, $n_0 \equiv 2m_e/m \gg 1$. By contrast, in the previous examples, the threshold number was arbitrary for generic m_χ and $n_0 = 2$ due to $m_\gamma = 0$, respectively. As we are going to see shortly, for the present case of $m_e \gg m$, the dominant process is the one closest to the threshold,

$$n = n_0 + \delta\,, \quad 0 < \delta \leq 1\,. \tag{2.58}$$

For $n \sim n_0$, the perturbative regime (2.11) reads

$$\frac{gE_0}{mm_e} \ll 1\,. \tag{2.59}$$

2.4.1 Semiclassical Result

The semiclassical rate of pair-production in an electric background field of the form(2.57) averaged over a period of oscillation is already known and has been found in ref.s [53, 54] (see also ref. [55]) The result is valid in the regime of $n_0 \gg 1$ and $E_0 \ll m_e^2/g$ and interpolates between the following two asymptotic expressions. For $\frac{gE_0}{m_e\omega} \gg 1$, the rate is asymptotic to

$$\Gamma \sim \frac{V m_e^4}{2\sqrt{2}\pi^4} \left(\frac{gE_0}{m_e 2}\right)^{5/2} \exp\left(-\pi \frac{m_e^2}{gE_0}\right) . \tag{2.60}$$

As to be expected, this reproduces the suppression obtained by Schwinger for the case of a constant electric field [56]. In the opposite regime, $\frac{gE_0}{m_e\omega} \ll 1$, the rate asymptotes to

$$\Gamma \sim \frac{V m_e^4}{(2\pi)^{5/2}} e^{-2\delta} \left(\frac{\omega}{m_e}\right)^{5/2} \left(\frac{e}{4}\frac{gE_0}{m_e\omega}\right)^{2(n_0+\delta)} \mathrm{Erfi}\left(\sqrt{2\delta}\right) . \tag{2.61}$$

This second regime is also called the multi-photon regime and coincides with the regime (2.59). Indeed we are going to obtain (2.61) from an n-photon process (2.55) in the perturbative quantum calculation in the following section.

2.4.2 Quantum Calculation

In contrast to the previous example, in the present case, all the different Wick contractions also result in non-zero diagrams. Close to the kinematic threshold, however, the amplitude is dominated by only one particular diagram. This is again the diagram constructed purely out of the 4-point vertex $g^2\phi^\dagger\phi A_\mu A^\mu$, corresponding to the diagram shown in fig. 2.1, where now plain lines represent photons and dashed ones the selectron. Let us consider only the contribution to the rate based on the square of that diagram and denote it by $\delta\Gamma_4$. There are of course contributions from interference terms as well, but they are still subleading near the threshold. The result for this leading term may be expressed through the value of the rate (2.16) in the 2-scalar example as

$$\delta\Gamma_4 = 2^{-n-1}\Gamma_{n\phi\to 2\chi} . \tag{2.62}$$

The relative factor of 2^{-n} is due to the lesser number of Wick contractions corresponding to the fact that ϕ is a complex field. Similarly, the additional relative factor of $1/2$ is because the final particles are not identical. In all other diagrams, one or more photons are inserted through a 3-point vertex. Let us consider the extreme case of the diagram constructed only from 3-point vertices (see fig. 2.2). Let us again consider the contribution to the rate from only its square and denote it by $\delta\Gamma_3$. The calculation goes rather similar (for details, see appendix A) and has the result

$$\frac{\delta\Gamma_3}{\delta\Gamma_4} = \frac{e^{2n}}{8n}\left(1-\frac{n_0^2}{n^2}\right)^n \sim \frac{e^{2n}}{8n}\left(\frac{2\delta}{n_0}\right)^n . \tag{2.63}$$

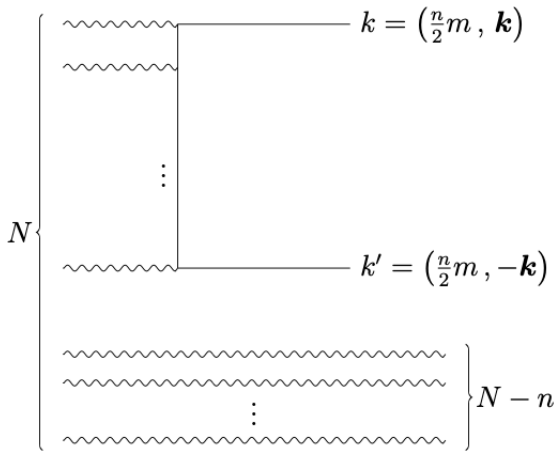

Figure 2.2: One of the terms contributing to the amplitude of the process (2.55).

Here, the second relation is true for the dominant process (2.58). As can be seen, for sufficiently small δ/n_0, the contribution is negligible. This indicates that near the threshold a 3-point vertex yields a suppression factor and that thus for the process (2.58) the all-4-point diagram (fig. 2.1) approximates the amplitude well. Therefore, we have

$$\Gamma_{n\gamma\to s^+s^-} = \delta\Gamma_4\left(1+\mathcal{O}\left(\delta\right)\right) . \tag{2.64}$$

The initial state Bose-enhancement contributes the same combinatoric enhancement factor as in (2.17). With that and the relation (2.56) between N and E_0, we have

$$\Gamma \sim \frac{1}{8\pi^3}Vm^4\sqrt{1-\frac{n_0^2}{n^2}}n^2\left(\frac{e}{4}\frac{gE_0}{m_e m}\frac{n_0}{n}\right)^{2n} , \tag{2.65}$$

where the Stirling approximation for the factorial has been used. To make the agreement with (2.61) explicit, one may use the relations $1-(n_0/n)^2 \sim 2\delta/n_0$ as well as $(n_0/n)^{2n} \approx e^{-2\delta}$, which hold for the process (2.58). Keeping in (2.61) only the leading order of

$$\mathrm{Erfi}\left(\sqrt{2\delta}\right) = 2\sqrt{\frac{2}{\pi}}\sqrt{\delta}\left(1+\frac{2}{3}\delta+\mathcal{O}\left(\delta^2\right)\right) , \tag{2.66}$$

one sees that the agreement is complete. For $\delta \ll 1$, the relative error is therefore $\sim \delta$ while for $\delta = 1$ it is ≈ 0.6. More details on the above calculation can be found in appendix A.

2.5 Parameter Regimes

In the previous sections, for the example of three different models, we have examined the rate of a many-particle process of the form $n \to 2$. In a specific regime, we obtained a

result that scales as $\sim (g^2N)^n$. In this section, we are going to investigate more closely the limits of validity of this leading-order approximation. We are going to refer to the $\phi^2\chi^2$-model for definiteness, but the following equally holds for the other two examples.

2.5.1 Semiclassical Limit

In the limit (2.1), simplifications of two kinds arise. One is the vanishing of the backreaction from the created χ-particles on the initial ϕ-state. Another is the vanishing of any loop corrections, which are of higher order in g^2.

Consequently, any non-perturbative approach that uses a semiclassical approximation and disregards radiative corrections becomes exact. The semiclassical calculations employed and referenced in the three examples we have examined fall into this category.

The obtained result can be interpreted as the resummation of a set of diagrams that remain non-zero in the limit (2.1). These diagrams are of the same order in N and in g^2, i.e., $\sim (g^2N)^{n+k}$. In the leading order, $k = 0$, they coincide with the diagrams we have evaluated in the quantum perturbative analysis. At higher orders, $k \geq 1$, those are diagrams with k rescattered ϕ-particles, but all into the initial mode. They may thus be termed forward scattering diagrams.

For the regime (2.11) (regime (2.59), respectively), which in terms of N is given by

$$n^2 \gg \frac{g^2N}{Vm^3}\,, \tag{2.67}$$

the results of the preceding sections show that all diagrams beyond the leading order, $k \geq 1$, can safely be neglected. When moving towards the opposite regime, however, their resummation manifests in two effects. One is an effective contribution to the particle masses that affects the kinematic threshold. The other is a change in the behaviour of the particle-creation rate away from a power-law growth with coupling and field strength transitioning to a weaker scaling before the rate becomes large.

For the cases reducing to the Mathieu-equation (in sec.s 2.2 and 2.3), this corresponds to the crossover from narrow to broad resonance. For the case of pair-creation in an alternating electric field (sec. 2.4), the crossover can be seen in the asymptotics (2.60) and (2.61). In the parameter plane of n and $g\phi_0/m$, the perturbative and non-perturbative regimes can be schematically represented as in fig. 2.3. The other regimes shown will be discussed below.

2.5.2 Finite g^2

Away from the limit (2.1), the finite values of N and g^2 give rise to various quantum corrections.

Some corrections fall into the category of backreaction, such as depletion or evolution of entanglement. These are suppressed by $1/N$ and thus are negligible as long as they have not built up over a sufficiently large number of processes.

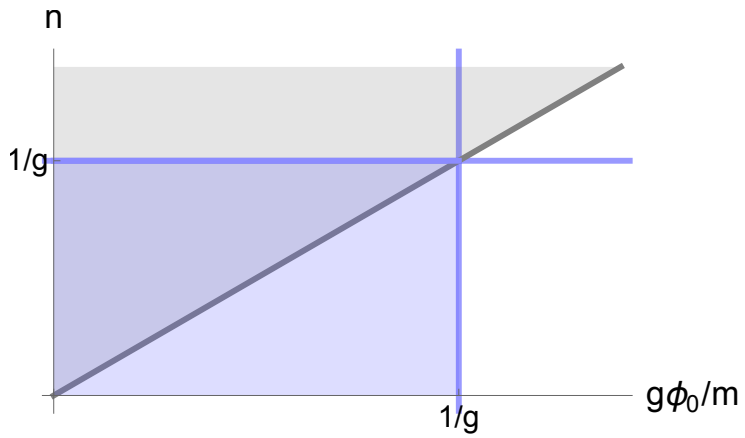

Figure 2.3: Schematic representation of regime boundaries: Above the grey diagonal line, non-perturbative corrections are negligible (see (2.67)). Additional regimes for finite g^2 (and the example of negligible m_χ): To the left of the blue vertical line, loop corrections to the potential are negligible (see (2.69)); Below the blue horizontal line, contributions of loop-induced diagrams are negligible (see (2.74)). The overlap of coloured areas is the resulting regime in which the calculation is perturbative in both g^2N and g^2, i.e., both non-perturbative and quantum corrections to the leading order approximation are negligible. This plot and all following ones have been created using *Mathematica* [29].

Similarly, an extra power of the coupling g^2 accompanies corrections to the amplitude from a single loop or contributions to the total rate from processes with a single (non-forward) scattered ϕ-quantum.

In the following analysis, we aim to identify and estimate additional loop effects that could be significant even when $g^2 \ll 1$. To simplify the discussion, we will focus on the case where the mass m_χ is negligible.

Effective potential

We begin by considering the 1-loop-corrected potential [57], which for $\chi = 0$ is given by

$$V_{1Loop}(\phi, 0) = \frac{m^2}{2}\phi^2 + \frac{g^4\phi^4}{16\pi^2}\left(\log\left(\frac{2g^2\phi^2}{\mu^2}\right) - \frac{3}{2}\right) . \tag{2.68}$$

Here, the parameters are defined in the $\overline{\text{MS}}$-scheme. For sufficiently high ϕ-values, the loop-correction becomes significant and as a result both (2.3) and (2.9), which give the time evolution $\phi(t)$ and the energetics relating N and ϕ_0, respectively, do not hold anymore, thus invalidating the considerations of the preceding sections. From (2.68), we see that such quantum corrections can be neglected only as long as (with a choice of $\mu \sim m$)

$$\frac{\phi_0}{m} \ll \frac{1}{g^2} , \tag{2.69}$$

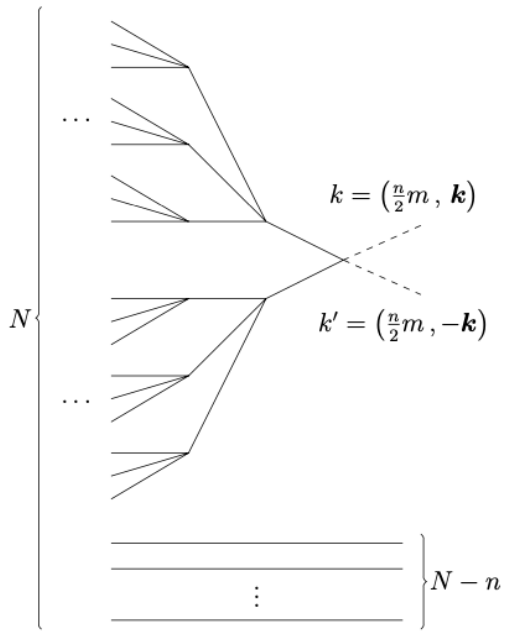

Figure 2.4: "Symmetrically branching tree" (SBT) diagram: Diagram contributing to the amplitude of the process $n\phi \to 2\chi$ based on only a single cross-coupling vertex and otherwise only the quartic self-coupling of ϕ (with the most symmetric shape possible).

which may be read as a bound on the initial state parameter N (or ϕ_0) in terms of the theory parameter g^2 (see fig. 2.3).

Diagrams with different n-scaling

A different type of quantum correction may arise from diagrams with many loops. While such diagrams are suppressed by much higher powers of g^2 compared to the leading order, they may compensate that suppression by a different scaling with n. The novel shapes of Wick contractions allowed for by loops in turn may lead to a different momentum flow through the corresponding diagram, affecting the n-scaling. Specifically, a nonzero quartic self-coupling of the ϕ-field allows for the "symmetrically branching tree" (SBT) diagram (see fig. 2.4), which is well known for its strong scaling with n [58, 59].

The elementary cross-coupling induces the required self-coupling via a χ-loop (see fig. 2.5), which contributes to the SBT-diagram the momentum-dependent vertex

$$v_4\left(q^2\right) = -\frac{ig^4}{16\pi^2}\left(\log\left(\frac{4q^2}{\mu^2}\right) - 2 + i\pi\right) + \mathcal{O}\left(g^6\right)\,, \tag{2.70}$$

where the value of q^2 depends on the position of the vertex in the diagram. From fig.s 2.4 and 2.5, one sees that $m^2 \leq q^2 \leq \frac{1}{9}n^2m^2$. Thus the momentum dependence of the vertex is not hiding any significant n-scaling and $4!|v_4| \sim g^4$ is a good approximation throughout the diagram.

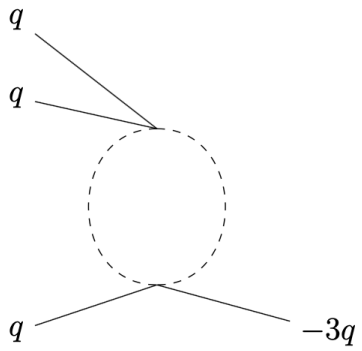

Figure 2.5: Momentum dependent 4-ϕ-vertex induced by a χ-loop with momenta as occurring in the SBT diagram (fig. 2.4)

Let us consider the contribution to the rate from only the square of the SBT diagram. It can be calculated in a way analogous to one found in ref.s [58, 59] (for details, see appendix A). The following schematic representation of the result suffices for our purpose:

$$\delta\Gamma_{SBT} \sim \left(\frac{c}{Vm^3}\right)^n n!\,, \quad c \sim g^4\,. \tag{2.71}$$

Perturbation theory can be seen to break down for

$$n \gtrsim n_{max} \equiv \frac{Vm^3}{c}\,. \tag{2.72}$$

The contribution (2.71) becomes significant as compared to the leading order rate (2.16) when

$$n \gtrsim n_{eq} \equiv \sqrt{g^2/c}\,. \tag{2.73}$$

This can be seen to happen well before the breakdown. For an exact statement, further diagrams as well as interference among them of course have to be taken into account. However, Eq. (2.73) may serve to indicate the n-regime where contributions due to loop-induced couplings become important.

From this, we obtain for the parametric bound of validity of the leading order approximation (2.16):

$$n \ll \frac{1}{g}\,. \tag{2.74}$$

This does not involve the initial state parameter ϕ_0. The combination of this bound with the previously obtained ones is shown in fig. 2.3. One sees that the combined bounds leave a finite area in the parameter plane of n and $g\phi_0/m$ where corrections of higher order in either g^2 or g^2N can be neglected.

2.6 Efficiency of Many-Particle Processes

In this section, we are going to discuss the potential for processes of high multiplicity to be unsuppressed. For this, we are going to extend the models considered by internal symmetries, which bring into play enhancement due to degeneracy. We also comment on potential implications for black holes.

2.6.1 Overview

In the decay processes considered, for the case of $n \sim N$, the two final particles carry an order-one fraction of the initial energy. If the initial state is a coherent state such a process constitutes a transition from a classical to a quantum state. In general, when and how fast the classical approximation for a system can lose validity is still an open question.

An important concept in this regard is *macro-quantumness* (introduced within the black hole N-portrait [19]). The term macro-quantumness [31, 60] describes the observation that quantum effects of order $1/N$ can lead to features that are not describable in classical terms, such as the emergence of black hole hair [25].

In ref. [26], the question was raised about how quickly classicality breaks down, which was termed "quantum breaking", and the corresponding timescale was referred to as the "quantum break-time", t_Q. This question was further explored in ref.s [27, 33].

In ref. [26]. it has been demonstrated that in an N-particle system with a Lyapunov instability, the quantum break-time can be extremely short, with only a logarithmic dependence on N,

$$t_Q = \lambda^{-1} \ln(N) \,, \tag{2.75}$$

with λ the Lyapunov exponent. This phenomenon was explicitly demonstrated for the case of a $1+1$-dimensional condensate of bosons on a ring with attractive interactions in [26] (a more recent discussion of this model can be found in [61]). By contrast, if a system does not possess any classical instability, the quantum break-time behaves differently. In such cases, the following general bound on the quantum break-time has been argued to hold in [33]:

$$t_Q \gtrsim \frac{N}{N^2 \Gamma_{2\to 2}} \,. \tag{2.76}$$

Here, $\Gamma_{2\to 2}$ represents the re-scattering rate of a pair of constituents. The initial state Bose-enhancement $C_{Nn} = N(N-1)/2$ is what gives rise to the factor N^2 in the denominator. Equation (2.76) implies that the quantum breaking of a condensate requires order N scattering events to occur. For the self-coupled scalar example of ref. [33], expression (2.76) was independently reproduced using different techniques in ref. [38].

Put differently, the primary mechanism for quantum breaking involves the gradual loss of coherence due to the scattering of a small number of constituents into external quanta. This is distinct from non-gradual single-process transitions involving many constituents. As we have seen and will discuss further below, in stable classical systems, single-process transitions to a quantum state are suppressed.

We refer to these types of transitions as *quantumization* in this study. Although this term can have a broader definition, we specifically use it to describe the process of transitioning from an initially classical state to a quantum state with a small number of constituents. Thus, they also fall into the category of transitions from macroscopic to microscopic systems.

The reverse phenomenon, where a few-particle quantum state transitions to a classical state in a single process, has been termed classicalization [17, 44, 45, 18, 46, 20]. Our analysis provides insight into the physics of both quantumization and classicalization processes as well as their very different manifestations.

Notably, while unsuppressed classicalization can occur in some systems, quantumization is always suppressed. This may initially seem counterintuitive, as both processes are based on the same fundamental phenomenon: the transition between a small and large number of particles. Specifically, for "small" and "large" numbers let us consider a two-particle state $|\,2\rangle$ and a state $|\,n\rangle$ with $n \gg 1$ quanta. We are going to assume that both states can be approximated as valid asymptotic S-matrix states.

The square of the S-matrix element $|\,\langle 2\,|\,\hat{S}\,|\,n\rangle\,|^2$ constitutes the basis of both transition probabilities. It is indeed always suppressed. Using general arguments based on the effective Hamiltonian and the locality of the Hilbert space, one can prove that at weak coupling and large n, this element has an upper bounded (see ref. [20], which improves on ref. [46]),

$$|\,\langle 2\,|\,\hat{S}\,|\,n\rangle\,|^2 \lesssim e^{-n}\,. \tag{2.77}$$

However, the total transition probability is obtained by summing the squared matrix element over the degeneracy of the final states [19],

$$\Gamma_{i\to f} \propto \sum_f |\,\langle 2\,|\,\hat{S}\,|\,n\rangle\,|^2\,. \tag{2.78}$$

The degeneracy factors can be drastically different depending on whether the final state is $\langle 2\,|$ or $\langle n\,|$. Specifically, the degeneracy of n-particle states can be exponentially large [20] whereas the degeneracy of two-particle states cannot be without compromising the validity of the theory. This difference is the fundamental reason why quantumization and classicalization are manifested in nature in such distinct ways.

While quantumization is always suppressed, a given degeneracy of the n-particle state does cause an enhancement of the process $n \to 2$, if the initial state is in a superposition. For $n \sim N$, this would correspond to the single-process decay of a macroscopic that has departed from classicality.

In the following two subsections, we will examine the potential for realization of $n \to 2$ and $2 \to n$ processes in more detail based on our results. We will refer to the $\phi^2\chi^2$-model for definiteness, although it applies to the other models as well.

2.6.2 Suppressed Processes

The inequality (2.76) gives a reason why quantumization effects are usually not observed in everyday life. For instance, in telecommunications, the interaction between electromagnetic

waves and charged particles does not pose a challenge in the form of transitions to mostly quantum states. Similarly, it is not expected that objects which are not directly observed will undergo quantumization. For example, as mentioned already in the introduction, a black hole is not expected to decay into a pair of high-energy photons, despite the absence of a conservation law that would forbid such a transition.

The systems studied above allow us to identify the mechanism underlying the suppression of quantumization. In these systems, the process of quantumization would involve the transition $n \to 2$ with $n \sim N$. In such a case, the created particle pair carries an order-one fraction of the mean energy stored in the initial coherent state. However, since the basic S-matrix element is suppressed, for the transition to have a chance of occurring, the rate requires an enhancement due to combinatorial factors associated with either the initial or final states or both.

As for the initial-state Bose enhancement, it is important to note that increasing the initial occupation number of quanta beyond a certain level, $N \sim g^{-4}$, will render the weak coupling treatment invalid. This is due to two reasons: firstly, in such a regime, the collective interaction with all other particles substantially modifies the dispersion relation of each individual particle. Secondly, Lyapunov instabilities occur in the condensate for such high N, leading to a deviation of the classical background from the coherently oscillating field (2.3). Looking at the one-loop effective potential (2.68), which corrects the free oscillations for amplitudes ϕ_0 exceeding m/g^2, one arrives at the same conclusion. Therefore, our treatment is only valid as long as the condition (2.69) is satisfied, which in terms of N is given by

$$N \ll \frac{Vm^3}{g^4} \,. \tag{2.79}$$

In light of the above, let us compare the minimal decay time of a condensate decaying into a particle pair with the timescale of an oscillation, $\sim m^{-1}$, or with the timescale of complete gradual decay,

$$\tau_{gradual} \lesssim N\,\Gamma_{2\to 2}^{-1} \sim m^{-1} N \frac{Vm^3}{g^4} \,. \tag{2.80}$$

The above upper bound is rather mild since it neglects the effects of initial state Bose-enhancement (which is accounted for in (2.76)) as well as the cumulative Bose-enhancement due to the created χ-particles, which corresponds to the occurrence of parametric resonance in the Mathieu equation (2.25). However, we will demonstrate that during timescales on the order of (2.80), non-gradual decay is still negligible.

We can introduce a parameter r to parametrize the range of n corresponding to $n \sim N$, since the coherent superposition has non-zero support for other occupations, including ones higher than N. We can then sum the rates for processes with $N/r \leq n \leq r\,N$ (with appropriate rounding, and with values of $r \gtrsim 10$ being reasonable). This range of n remains in the perturbative regime (2.67) as long as

$$r^2 \ll NVm^3/g^2 \,. \tag{2.81}$$

Let us denote the occupation numbers in the coherent superposition by $n + n'$, where n' is the number of unscattered initial quanta. To obtain an upper bound on the effective combinatoric enhancement, we evaluate

$$\sum_{n'=0}^{\infty} |\langle n'|\hat{a}^n|c\rangle|^2 = \sum_{n'=0}^{\infty} \binom{n+n'}{n} |\langle 0|\hat{a}^n|n\rangle\langle n+n'|c\rangle|^2 = \frac{N^n}{n!} |\langle 0|\hat{a}^n|n\rangle|^2 \,. \tag{2.82}$$

Here, the occupations of the number states such as $|n\rangle$ and of the coherent state $|c\rangle$ are all referring to the same mode and $\hat{a}|c\rangle = \sqrt{N}|c\rangle$. Thus, for the rate of non-gradual decay we have

$$\Gamma_{n\sim N} \sim \sum_{n=N/r}^{r\,N} \frac{N^n}{n!} \Gamma_{n\to 2} \,. \tag{2.83}$$

When the result (2.16) holds for $\Gamma_{n\to 2}$, the timescale $\Gamma^{-1}_{n\sim N}$ is significantly greater than (2.80), provided that (2.81) is satisfied. On the other hand, if the scaling (2.71) is valid, then the range of n for the summation is within the perturbative unitarity bound (2.72) if $N \leq n_{max}/r$, which is equivalent to (2.79). Even in this case, we observe that $\Gamma^{-1}_{n\sim N}$ is much larger than (2.80).

As for enhancement due to final-state degeneracy, the rate of the quantumization transition cannot be sufficiently enhanced, either, since an exponential increase in the 2-particle degeneracy would cause the theory to be strongly coupled.

For an illustration, consider the possibility of increasing the degeneracy of final states by introducing an additional internal quantum number, such as a "flavor" quantum number $j = 1, 2, ..., N_f$, for the χ-particles. For instance, if χ_j forms an N_f-dimensional representation of the $SO(N_f)$ symmetry group, the rate (2.16) of the transition $n\phi \to 2\chi$ is enhanced by a factor of N_f. However, for the ϕ- and χ-particles to remain valid, i.e., weakly interacting, degrees of freedom, the collective coupling has to respect the bound

$$N_f g^4 \lesssim 1 \,. \tag{2.84}$$

Beyond this regime, the loop expansion breaks down, and the degrees of freedom change. The bound (2.84) prevents the final-state degeneracy from being able to compensate the matrix element (2.77).

The above considerations also show why any non-gradual generation of entanglement from an initially classical state should be suppressed. For example, the $SO(N_f)$-invariant 2-particle state

$$|\,2\rangle = \frac{1}{\sqrt{N_f}} \sum_{j=1}^{N_f} |\,\chi_j\rangle \times |\,\chi_j\rangle \,, \tag{2.85}$$

is entangled with respect to the flavour quantum number. The rate of its creation from the initial state of n ϕs, however, is likewise strongly suppressed. In a classically stable system, rather than in a single process, the generation of entanglement happens gradually over a time scale of (2.76) [27, 3, 35].

2.6.3 Potentially Unsuppressed Processes

As already mentioned, in the case of classicalizing transitions, based on the inverse process $2 \to n$, many of the above aspects play out differently [44, 45, 46, 20]. For a given pair of initial and final states, the absolute values of S-matrix elements for transitions in either direction, $|S_{2\to n}|$ and $|S_{n\to 2}|$, are of course exactly equal. Compared to the allowed degeneracy of a 2-particle state, however, that of the n-particle final state may be high enough to balance the suppression of the matrix element. Such degeneracy is the key ingredient in the microscopic explanation of the classicalization phenomenon [46, 20].

In the example of the process $2\chi \to n\phi$, the number of final states is exponentially enhanced if ϕ_j carries an $SO(N_f)$ index [20]. By symmetry, the matrix elements for transition to each member of the same irreducible representation are equal and the rate is enhanced by the dimensionality of the representation. In our example, an invariant state of n ϕs has degeneracy $C_{N_f+n,n} = (N_f+n)!/n!N_f!$, which scales as e^n for $N_f \sim n$. By this, we do not mean to imply that a simple $\phi^2\chi^2$-theory necessarily exhibits classicalization at an order-one rate, but instead wish to demonstrate the different potential of enhancement inherent to a classicalizing transition $2 \to n$ versus a quantumizing one, $n \to 2$.

Due to such enhancement actualized via the sum over final states, unsuppressed production of n-particle states with high entropy, known as saturons, is expected in 2-particle collisions at sufficiently high energy [20]. According to ref. [19], one known example of a saturon in nature is given by black holes.

Several other instances of classicalization have been identified outside of gravity. In ref. [62], it has been proposed that the Color Glass Condensate of gluons in QCD [63] may constitute a saturated entropy state. Correspondingly, the creation of such a state in proton collision would constitute a classicalization process. In ref. [20], it has been suggested that confinement in QCD with a large number of colors is explained by the formation of a saturated state of gluons due to high color degeneracy.

In ref. [64], the creation of saturon bound states in $2 \to N$ process in the Gross-Neveu model [65] has been analyzed. The results imply a nonperturbative enhancement of the transition rate compensating the exponential suppression of the matrix element.

For a long time, it has been assumed [15, 66, 67, 68, 69] that the formation of a black hole can occur with order-one probability in the collision of two particles. This viewpoint is based in semiclassical reasoning, suggesting that a black hole will form when energy becomes localized within its own gravitational radius. The idea of self-completion of gravity [16] is based on this expected behaviour.

In the absence of a microscopic theory of a black hole, the quantum mechanism behind its unsuppressed formation naturally cannot be verified or understood. Such microscopic theory is given by the black hole N-portrait [19]. In that model, a black hole is a condensate of N soft gravitons, with the microstate entropy scaling as $\sim N$.

According to this theory, the formation of a black hole in a 2-particle collision can be understood as a process of classicalization, $2 \to N$, where a highly degenerate state of N gravitons is created [19]. Although the transition probability to each individual microstate is suppressed by e^{-N} due to the high multiplicity involved [45, 70], the total probability

of black hole formation is order one. The suppression is balanced by the non-perturbative enhancement due to the degeneracy of the N-graviton state, which accounts for the black hole entropy [19, 45].

As is clear from the discussion in the preceding section, the many-particle nature of a near-classical black hole also provides an explanation for its stability against a non-gradual decay. While the decay process $N \to 2$ shares the exponentially suppressed S-matrix element with the formation process, $2 \to N$ [19, 45], the final 2-particle state cannot provide degeneracy large enough to overcome that suppression.

The concept of the decay of a black hole into a few particles may raise concern regarding perturbative validity since the decay products gravitate. If the decay products are created at distances not far exceeding the initial gravitational radius, their gravitational field is not negligible. However, at the level of calculation, this is accounted for by a dressing of the outgoing particles with a classical gravitational field in the form of a coherent state of secondary "softer" gravitons.

As we have mentioned, while quantumizing $n \to 2$ transitions are always suppressed, a transition $n \to 2$ may still become unsuppressed after the system has lost its classicality: a given degeneracy of the initial n-particle state does result in an enhancement if the initial state is in a superposition of the degenerate microstates. This enhancement is maximized by a uniform superposition in the sense that the absolutes of the coefficients of the independent states are equal. In that case, for a number of d degenerate states, the enhancement at the level of the square amplitude amounts to a factor of d. This is the same degree of enhancement as brought about by the sum over final states in the case of a final-state degeneracy of d. Let us consider as a specific example a flavour superposition of the initial state in the process $n\phi \to 2\chi$, where again ϕ_j carries an $SO(N_f)$ index. Thus, in our example, if the initial superposition is the normalized $SO(N_f)$-invariant sum over the entire representation space, the resulting enhancement at the level of the squared amplitude is by a factor of the dimensionality of the representation. For our example of an initial state of n ϕs, the enhancement is therefore again by the factor of $C_{N_f+n,n} = (N_f + n)!/n!N_f!$. Since, as mentioned, an initial state of such kind cannot be considered classical, such a transition also does not fall in our category of quantumization. Nonetheless, such transitions may play an important role in the evolution of macroscopic systems that have departed from classicality. Over the duration of its quantum break-time, an initially near-classical system can potentially evolve to the required level of superposition of its degenerate microstates.

In particular, for a black hole in the N-portrait, the protection against single-process decay thus will vanish if it evolves into a superposition covering close to all of its microstates. This can potentially happen in the process of the generation of maximal inner entanglement. Such entanglement has been argued [35] to be achievable on a time scale of $\sim N$ emissions. As an alternative mechanism, maximal entanglement is achieved on the logarithmically short time scale (2.75) in the presence of a classical instability [26]. It has been argued in ref. [3] (subject of part II of this thesis) that such instability could appear likewise after $\sim N$ emissions, i.e., order half-decay.

2.7 Summary

In this study, we have resolved non-perturbative phenomena of particle creation in coherently oscillating background fields in terms of perturbative many-particle quantum processes. This work represents a continuation of the research applied to systems like black holes [19] and de Sitter spacetime [19, 27] (for more references, see section 2.1).

In those studies as well as in the present one, a classical background is resolved by a quantum state with an occupation number centered around N. Here, we have investigated high-multiplicity processes, in which a generic number n out of N quanta annihilates in favour of an energetic pair. Specifically, we have studied in those terms three different cases of condensate decay in the simplest interacting scalar and gauge theories in 3+1 dimensions. We have shown the agreement of the non-perturbative semiclassical prediction and the perturbative quantum prediction in the double limit $g^2 \to 0$, $N \to \infty$, with $g^2 N$ fixed.

For finite values of the coupling g^2, we have established the regimes of perturbative validity for n and N in terms of g^2. The fully quantum treatment allows to consistently take into account the backreaction. This is relevant in particular in the interesting case of $n \sim N$, i.e., the system decays in a single process. This also represents a transition from a near-classical state to a quantum one, and correspondingly we have termed it *quantumization*. We have found that the suppression of the $N \to 2$ S-matrix element is so strong that the evolution is dominated instead by gradually proceeding decay. Correspondingly, the quantum break time t_Q, after which classicality is lost, is determined by processes of low n.

Our analysis may be directly extended to the case of particle creation in an oscillating background spin-2 field. A state of N massive gravitons corresponding to such background has been used as a resolution of de Sitter spacetime in ref. [33].

Thanks to their calculational accessibility, the systems studied here provide a clean laboratory for gaining insight into the conditions under which processes of high multiplicity may become efficient. To provide explicit cases, we have extended the models studied by internal symmetries, which bring into play an enhancement due to microstate degeneracy. We have demonstrated that within the bounds of weak coupling, the N-particle state, unlike the 2-particle state, may accommodate a degeneracy sufficient to balance the smallness of the matrix element.

In the case of the inverse process of $2 \to N$, which shares the same matrix element, the sum over final states causes an enhancement by a factor of the number of the degenerate microstates. Such a process is the basis of the phenomenon of *classicalization* [17]. It has been argued [19, 45] that an example of the discrepancy between classicalization and quantumization is provided by black holes conceived as N-graviton bound states: while their creation in 2-particle collisions may be unsuppressed thanks to the high entropy, near-classical black holes are effectively stable against explosion into a few quanta.

As for the enhancement of the transition $N \to 2$, we have pointed out that a given degeneracy of the initial N-particle state is actualized as an enhancement to the extent the state is a superposition covering the degenerate microstates. In particular, for a uniform

superposition over all degenerate states, the enhancement reaches the same level as in the classicalizing case. While a system in such a state cannot be regarded as classical, and the transition thus would not fall into the category of quantumization, a single-process decay of a macroscopic system would be no less spectacular. We have pointed out that a black hole can potentially evolve to the required level of superposition in the process of generating maximal inner entanglement. The latter has been argued [35, 3, 26] to be achievable on a time scale on the order of half-decay.

Thus, what we have demonstrated in the simple systems of oscillating fields in basic quantum field theories in particular points to the possibility of explosive evolution of the more complicated system of a black hole.

Part II

Memory Burden Effect

Introduction

In this part of the thesis we present our studies related to the memory burden effect [28], which is a phenomenon universally present in systems that achieve high memory capacity, and its implications for black holes (BHs) and de Sitter. As we are going to explain in more detail below, the effect consists of suppression of the system's decay due to a backreaction effect related to quantum information stored in the memory. The focus of our study is on the ability of systems to avoid the memory burden effect by rewriting the information among internal degrees of freedom. We find that the speed of decay facilitated by such rewriting decreases with increasing system size. The universal nature of the effect suggests applicability in particular to BHs and de Sitter as systems of maximal entropy.

Our work is part of a line of research [30, 71, 72, 73, 74, 75, 76, 77, 28, 2, 21, 78, 20] that aims to obtain new understanding about BHs by investigating much simpler systems that have in common a high memory capacity. Encouragingly, in those studies, many such systems have been shown to exhibit BH-like properties. This is despite abstracting from the geometric aspects of a BH. Since those simplified model systems in contrast to BHs are calculationally accessible, they may in turn allow to learn about BH behaviour beyond the validity of the semiclassical treatment. This line of research is distinct from a line of research focusing on an explicit microscopic model of a BH in terms of a bound state of gravitons with a wavelength on the order of the Schwarzschild radius, the so-called N-Portrait [19].

Without loss of generality, any physical system can be described in terms of quantum oscillators or modes. When considering a subset of those modes, their occupation pattern $|\, n_1, \ldots, n_K\rangle$ amounts to quantum information stored in the system. We can quantify the system's memory capacity at a given energy by the number of patterns that can be realized within a microscopic interval around that energy [75, 77]. A high memory capacity achieved through the above modes thus requires their gap to effectively vanish.

In [30, 71, 74, 75, 76, 77, 28, 2] it has been found that systems able to achieve high memory capacity do so through a universal mechanism. This mechanism has been called assisted gaplessness. As has been shown in the references cited above, in a suitable basis, there exists a mode, which we may call control mode, whose occupation n_0 controls the gap of a set of other modes, which we may call memory modes. For a certain critical occupation $n_0 = N_c$ of the control mode, due to the attractive interaction, the gap of the memory modes nearly vanishes.

The memory burden effect arises due to the back-reaction of the memory modes: any change of the control mode's occupation away from N_c leads to a growth of the memory modes' gap. To the extent they are occupied, this leads to an increased energy cost of the memory pattern. As a result, there is a building resistance against any evolution away from the critical occupation N_c. In particular, if n_0 is affected by the decay of the system, the memory burden leads to a suppression of the decay.

From the above, it is clear that a single near-gapless mode, which is highly occupied, will create a similar memory burden as a high number of such modes with the occupation distributed among them. The former case has been demonstrated [79] to be at work in

the case of a solitonic vacuum bubble whose decay is suppressed by a high occupation of a single Nambu-Goldstone mode localized inside.

As for the case of large K, the number of near-degenerate microstates grows exponentially with K. If apart from the total energy all other macro-observables also take the same value for those memory states, this will correspond to an entropy $S = \ln(n_{st}) \sim K$, where n_{st} is the number of distinct basic microstates $|\, n_1, \ldots, n_K\rangle$. From the above, it follows that the presence of the memory burden effect does not require the system to have high or even maximal entropy. On the other hand, any system saturating the Bekenstein bound on entropy will certainly exhibit the memory burden effect.

Understanding BH dynamics in terms of phenomena that are universal to systems of high memory capacity can be valuable since BH evolution past the initial stage of Hawking evaporation is unknown. This is because the semiclassical approximation by default cannot take into account quantum back-reaction effects and therefore breaks down the latest after the BH has lost on the order of half its initial mass. This means that contrary to a frequent assumption, there is no self-similar evaporation: due to quantum effects, a newly created BH is not equivalent to an old one that has arrived at the same mass after losing a sizeable fraction of its initial mass. Therefore, it is important to quantify those back-reaction effects and gain understanding of the possible BH evolution beyond half-decay.

In order to make progress in these questions, in our study, we will try to find universal features of a system under the influence of the memory burden effect. In [28], the evolution of a system subjected to the memory burden effect has already been analyzed. There, it has been found that the system's decay is stopped as soon as the memory burden effect sets in. The time of the set-in may be specific to a given system, but cannot be later than order half decay. A question raised in [28] is whether the memory burden can be alleviated or avoided. There, it has been argued that barring an efficient transfer of the stored information to the environment, the only conceivable way is via a mechanism called rewriting. Namely, if there exist other sets of memory modes that become gapless at a lower occupation of the control mode, N_c'. In such a case the system could synchronize the decay with the offload of the memory pattern to the next memory sector and thus avoiding a macroscopic increase of the energy cost for the stored quantum information.

The purpose of the present study is to investigate the mechanism of rewriting. To that end, we are going to analyze a model considered already in ref.s [74, 75, 76, 28, 2], which may be considered the simplest possible model exhibiting memory burden as well as the capability of rewriting. We aim to determine under what conditions rewriting takes place as well as the maximal speed of rewriting-powered decay depending on the parameters. In particular, we analyze the dependence on the system size.

After the analysis of the generic prototype model, we aim to apply the findings to the particular systems of BHs and deSitter. When choosing a scaling of the parameters appropriate to BHs, we find that after the set-in of MB, the maximal rewriting-powered decay speed is much smaller than the initial speed of Hawking evaporation.

As said before, the onset of memory burden takes place the latest after order half-decay. Since as systems of maximal entropy BHs and de Sitter must be subjected to the memory burden effect, the departure of their evolution from the semiclassical one thus has to be

dramatic the latest by half-decay. This constitutes a rigorous finding of the present study. The speculative part of our work concerns the evolution past half-decay. This is because, after half decay, the universality argument regarding the memory burden effect no longer holds since by that time other sources of quantum back-reaction, that are specific to BHs or de Sitter, may have accumulated to result in a strong effect.

The memory burden effect on its own implies a drastically slowed down decay rate amounting to an effective stabilization of BHs. As a different conceivable scenario, a BH may also develop a classical instability and disintegrate on a very short time scale.

Here, we are going to speculate on the stabilization of BHs with interesting consequences for PBHs. Since in that case, PBHs of small mass would still exist rather than having completely evaporated, many constraints on the fraction of DM constituted by PBHs would be invalidated. To illustrate this point, we consider some of those constraints and point out an exemplary scenario in which light PBHs appear to be able to constitute all of DM.

For de Sitter spacetime, we argue that the Gibbons-Hawking radiation is slowed down after t_Q, the onset of the MB. Simultaneously, the release of the quantum information becomes less suppressed. If inflation has lasted long enough to come close to t_Q, the resulting deviation from the semiclassical evolution may have left detectable imprints in the primordial density perturbations. Intriguingly, the quantum information thus accessible in the CMB would have been carried through the entire inflationary history.

Chapter 3

Avoiding Memory Burden by Rewriting: A Prototype Model Analysis

3.1 The Model

Following ref. [28], in this section, we are going to construct our prototype model. In order to gain intuition about the system, we put together sectors of the model in steps, analytically investigating its behaviour before getting to the full system, which requires numerics to solve it.

3.1.1 Assisted Gaplessness

We are going to start with a sector of the model that is able to dynamically achieve a number K of gapless modes, and correspondingly a large number of degenerate states. This part of the model follows ref.s [76, 75, 77]. Consider K bosonic modes with corresponding creation and annihilation operators satisfying the usual relations (here and throughout $\hbar = 1$)

$$[\hat{a}_j, \hat{a}_k^\dagger] = \delta_{jk}\,, \qquad [\hat{a}_j, \hat{a}_k] = [\hat{a}_j^\dagger, \hat{a}_k^\dagger] = 0\,, \tag{3.1}$$

where $k = 1, \dots K$. We denote by $\hat{n}_k = \hat{a}_k^\dagger \hat{a}_k$ and $|\, n_k\rangle$ the number operators and its eigenstates, respectively. ϵ_k denotes the energy gap in the free part of the Hamiltonian, $\hat{H} = \sum_k \epsilon_k \hat{n}_k$.

The state of those K modes can be expressed in terms of the basis states

$$|\, n_1, \dots, n_K\rangle \equiv |\, n_1\rangle \otimes |\, n_2\rangle \otimes \cdots \otimes |\, n_K\rangle\ , \tag{3.2}$$

where $n_1, \dots n_K$ can take arbitrary values. While the number of independent states scales exponentially with K, they may differ significantly in energy, depending on the associated gaps ϵ_k. Neglecting interactions of the modes, two different states $|\, n_1, \dots n_S\rangle$ and $|\, n'_1, \dots n'_S\rangle$ have energies that differ by $\sum_{k=1}^{K} \epsilon_k (n_k - n'_k)$. For there to be a large number

of effectively degenerate states, the gaps ϵ_k have to be correspondingly small. Specifically, the number of states that fits into a reference interval ΔE scales exponentially with K if the gaps satisfy $\epsilon_k \lesssim \Delta E/K$.

Let us include another mode $\hat{n}_0$, with creation and annihilation operators $\hat{a}_0^\dagger$, $\hat{a}_0$ likewise obeying Eq. (3.1). This mode differs by how it is coupling to the remaining modes via the following attractive interaction:

$$\hat{H} = \epsilon_0 \hat{n}_0 + \left(1 - \frac{\hat{n}_0}{N_c}\right) \sum_{k=1}^{K} \epsilon_k \hat{n}_k \,, \tag{3.3}$$

with a parameter $N_c \gg 1$.

The occupation of $\hat{n}_0$ effectively lowers the gaps of the modes $\hat{n}_k$. Their effective gaps in terms of n_0 read

$$\mathcal{E}_k = \left(1 - \frac{n_0}{N_c}\right) \epsilon_k \,. \tag{3.4}$$

Due to this property, we are going to refer to the mode $\hat{n}_0$ as the *control* mode and to the modes $\hat{n}_k$ as *memory* modes. For the critical occupation $n_0 = N_c$, the effective gaps of the modes $\hat{n}_k$ vanish. Correspondingly, all states of the form

$$|\, n_0 = N_c, n_1, \ldots, n_K \rangle \tag{3.5}$$

are degenerate in energy for arbitrary values of $n_1, \ldots, n_K$. The energy required to achieve such gaplessness and corresponding memory capacity is $\epsilon_0 N_c$.

In the situation where the maximal occupation for each $\hat{n}_k$ is given by d, the number of degenerate states is given by $(d+1)^K$. In the case that those states constitute microstates describing the same macrostate, the corresponding entropy is

$$S = K \ln(d+1) \,. \tag{3.6}$$

3.1.2 Memory Burden

We have noted that the occupation of the control mode affects the gap of memory modes. As we are going to discuss now, the converse is true as well, leading to the memory burden effect [28]. The altered effective gap of $\hat{n}_0$ comes to bear dynamically if the Hamiltonian allows for the transfer of excitations between $\hat{n}_0$ and other modes. Consider including a further mode $\hat{m}_0 = \hat{b}_0^\dagger \hat{b}_0$ with commutation relations analogous to Eq. (3.1) in the following way:

$$\hat{H} = \epsilon_0 \hat{n}_0 + \epsilon_0 \hat{m}_0 + \left(1 - \frac{\hat{n}_0}{N_c}\right) \sum_{k=1}^{K} \epsilon_k \hat{n}_k + C_0 \left(\hat{a}_0^\dagger \hat{b}_0 + \hat{b}_0^\dagger \hat{a}_0\right) \,, \tag{3.7}$$

The occupation number conserving coupling has strength parametrized by C_0. In a state without occupations of the memory modes, the choice of equal gaps of $\hat{n}_0$ and $\hat{m}_0$ allows for unsuppressed oscillation between them.

More generally, consider as the initial state

$$|\, i_1\rangle = \left| \underbrace{N_c, 0}_{n_0, m_0}, n_1, \ldots, n_K \right\rangle . \tag{3.8}$$

The Hamiltonian (3.7) does not allow the memory modes to take part in the dynamics and the evolution reduces to that of a two-mode system. The solution for the initial state (3.8) in terms of the expectation value of $\hat{n}_0$ is given by [28]:

$$n_0(t) = N_c \left(1 - \frac{4C_0^2}{4C_0^2 + \mu^2} \sin^2(\sqrt{C_0^2 + \mu^2/4}\, t) \right) , \tag{3.9}$$

where we defined

$$\mu \equiv -\sum_{k=1}^{K} \epsilon_k n_k / N_c \, . \tag{3.10}$$

As can be seen from (3.9), μ^2/C_0^2 affects both the amplitude of the oscillations and the frequency. In terms of the effective energy gaps (3.4), μ is given by

$$\mu = \sum_{k=1}^{K} n_k \frac{\partial \mathcal{E}_k}{\partial n_0} \, . \tag{3.11}$$

Let us consider exemplary parameter values of the system and the initial state that illustrate the effect of μ. In Fig. 3.1a, the solution (3.9) is plotted for an initial state with all $n_k = 0$, s.t. $\mu = 0$. The amplitude of the oscillation of $n_0(t)$ (and $m_0(t) = N_c - n_0(t)$) is unsuppressed, i.e., all energy stored in the mode $\hat{n}_0$ is offloaded to $\hat{m}_0$ before oscillating back. The same behaviour would be the case if the memory modes would not be part of the system at all. But a nonzero occupation of the memory modes changes the situation. If n_k and ϵ_k give rise to $\mu^2/C_0^2 \gtrsim 1$, the oscillation of $n_0(t)$ takes place with a sizeable suppression of the amplitude. An example of this is plotted in Fig. 3.1b. Effectively, information stored in the memory modes suppresses the evolution of the control mode away from its initial value. This is the essence of the memory burden effect.

With the system's memory being able to constrain its evolution so strongly, a natural question is whether there may be mechanisms to alleviate or avoid it. For given μ^2/C_0^2, a delay of the onset of the memory burden effect is achieved by the following modification of the Hamiltonian [28]:

$$\hat{H} = \epsilon_0 \hat{n}_0 + \epsilon_0 \hat{m}_0 + \left(1 - \frac{\hat{n}_0}{N_c} \right)^p \sum_{k=1}^{K} \epsilon_k \hat{n}_k + C_0 \left(\hat{a}_0^\dagger \hat{b}_0 + \hat{b}_0^\dagger \hat{a}_0 \right) . \tag{3.12}$$

Now, the effective energy gaps are given by

$$\tilde{\mathcal{E}}_k = \left(1 - \frac{n_0}{N_c} \right)^p \epsilon_k \, . \tag{3.13}$$

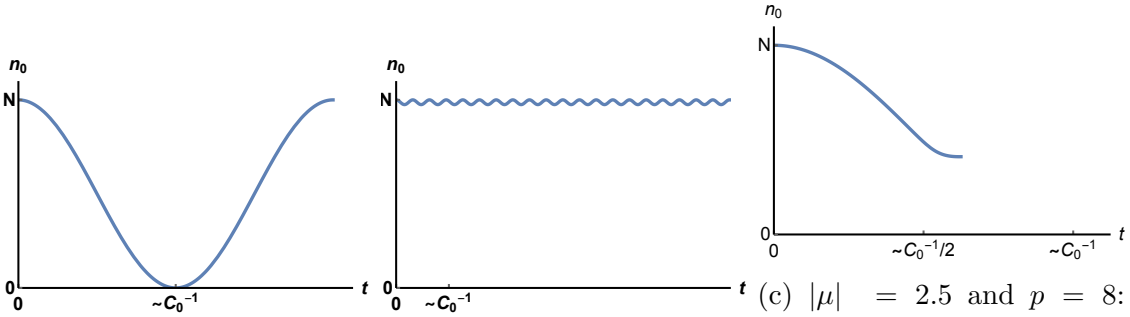

(a) $\mu = 0$: absence of memory burden. The expectation value n_0 oscillates freely with full amplitude.

(b) $|\mu| = 2.5$ (and $p = 1$): early backreaction due to memory burden ties n_0 to its initial value.

(c) $|\mu| = 2.5$ and $p = 8$: memory burden can be delayed up to a timescale on the order of half decay. Backreaction sets in at the latest at that point and stabilizes the system.

Figure 3.1: Plots of the time evolution of n_0 for $N_c = 25$ and $C_0 = \epsilon_0/\sqrt{N_c} = 1/5$. Figs. 3.1a and 3.1b follow from (3.9). Fig. 3.1c is an approximate solution of the system (3.12).

The parameter quantifying the memory burden defined in analogy to (3.11) is now

$$\tilde{\mu} = p \left(\frac{N_c - n_0}{N_c} \right)^{p-1} \mu \,. \tag{3.14}$$

Compared to the case of $p = 1$, this now depends on n_0 and can be seen to be initially suppressed by powers of $(N_c - n_0)/N_c$. Even in the absence of an exact solution for $p = 1$, we may expect that the onset of the memory burden effect is delayed only until $\tilde{\mu}$ has grown s.t. $\tilde{\mu}^2/C_0^2 \gtrsim 1$, i.e., in terms of n_0, until

$$N_c - n_0 \gtrsim N_c \left(\frac{C_0}{p|\mu|} \right)^{1/(p-1)} \,. \tag{3.15}$$

While (3.9) shows that, in the case of interest, $\mu^2/C_0^2 \gg 1$, the decay is frozen at $N_c - n_0 \sim N_c C_0^2/\mu^2$ for $p = 1$, (3.15) shows that the larger the value of p, the more delayed is the onset of the backreaction to larger values of $N_c - n_0$. So the value of p parametrizes the system's ability to buffer the decay: no system is of course expected to be able to maintain initially present gapless modes despite radiating away arbitrary amounts of its mass - but different systems may lose that ability at different stages of their decay. According to (3.15), for arbitrarily large values of p, the onset of backreaction can in principle be delayed arbitrarily. For plausible values of p and C_0^2/μ^2, one has an onset after $N_c - n_0 \sim N_c$, i.e., after order half decay. An example of such behaviour is plotted in Fig. 3.1c.

3.1.3 Rewriting

Apart from a system's potential ability to delay the onset of the memory burden effect, it is in principle conceivable that there are mechanisms to alleviate or avoid it, once it does

set in.

In ref. [28], it has been argued that barring an efficient channel to transfer the information stored in the memory modes onto external degrees of freedom, the only possible way involves offloading the information to a different set of memory modes that interact differently with the control mode. Such *rewriting* of the information may ensure that the energy cost of the information never gets too large as to freeze the decay of n_0. Specifically, following ref. [28], consider adding to the Hamiltonian a second set of memory modes, $\hat{n}'_{k'} = \hat{a}'^{\dagger}_{k'}\hat{a}'_{k'}$, $k' = 1, \ldots, K'$, that become gapless for a lower occupation of the control mode, $n_0 = N_c - \Delta N_c$. In addition, the memory modes are coupled to allow for rewriting to take place:

$$\begin{aligned}\hat{H} = {} & \epsilon_0 \hat{n}_0 + \epsilon_0 \hat{m}_0 + \left(1 - \frac{\hat{n}_0}{N_c}\right) \sum_{k=1}^{K} \epsilon_k \hat{n}_k + C_0 \left(\hat{a}_0^{\dagger}\hat{b}_0 + \hat{b}_0^{\dagger}\hat{a}_0\right) \\ & + \left(1 - \frac{\hat{n}_0}{N_c - \Delta N}\right) \sum_{k'=1}^{K'} \epsilon_{k'} \hat{n}'_{k'} + \sum_{k=1}^{K} \sum_{k'=1}^{K'} C_{k,k'} \left(\hat{a}_k^{\dagger}\hat{a}'_{k'} + \text{h.c.}\right) \\ & + \sum_{k=1}^{K} \sum_{\substack{l=1 \\ l \neq k}}^{K} \tilde{C}_{k,l} \left(\hat{a}_k^{\dagger}\hat{a}_l + \text{h.c.}\right) + \sum_{k'=1}^{K'} \sum_{\substack{l'=1 \\ l' \neq k'}}^{K'} \tilde{C}_{k',l'} \left(\hat{a}'^{\dagger}_{k'}\hat{a}'_{l'} + \text{h.c.}\right) . \end{aligned} \tag{3.16}$$

The coupling strength between the two memory sectors is set by the parameters $C_{k,k'}$. Similarly, we have included couplings $\tilde{C}_{k,l}$ between modes within each memory sector. In order to focus on the potential rewriting phenomenon we have gone back to the choice $p = 1$.

In an initial state as considered before, the second set of memory modes is not gapless:

$$|\, i\rangle = \Big| \underbrace{N_c, 0}_{n_0, m_0}, n_1, \ldots n_K, \underbrace{0, \ldots, 0}_{n'_1, \ldots, n'_{K'}} \Big\rangle \, . \tag{3.17}$$

However, the expectation value of the Hamiltonian is the same for the following state:

$$|\, f\rangle = \Big| \underbrace{N_c - \Delta N_c, \Delta N_c}_{n_0, m_0}, \underbrace{0, \ldots, 0}_{n_1, \ldots, n_K}, n'_1, \ldots, n'_{K'} \Big\rangle \, . \tag{3.18}$$

In this state of lower occupation of n_0, the second memory sector is gapless. The total occupation in the two memory sectors,

$$N_m \equiv \sum_{k=1}^{K} n_k + \sum_{k'=1}^{K'} n'_{k'} \, , \tag{3.19}$$

is conserved by the Hamiltonian (3.16).

Near the initial state (3.17), the second memory sector is certainly not effectively gapless if

$$\left|\mathcal{E}'_k\right| \gg \epsilon_0 \, . \tag{3.20}$$

As argued shortly below (see Eq. (3.22)), the milder bound

$$\left|\mathcal{E}_k^{'}\right| \gg \frac{\epsilon_0}{\sqrt{N_m}} \tag{3.21}$$

is sufficient.

The existence of the state (3.18) makes it conceivable that the system evolves to a state close to it by appropriately synchronizing the decay of n_0 and the rewriting from the $\hat{a}_k^\dagger$, $\hat{a}_k$-modes to the $\hat{a}_{k'}^{'\dagger}$, $\hat{a}_{k'}^{'}$-ones. However, it is not clear that the system will do so on a relevant time scale. In order to answer this question, we are going to numerically time-evolve the system.

3.1.4 Bounds on Couplings

The presence of the new couplings in (3.16) effectively alters the gaps of the memory modes in the following sense. Since the gaps and couplings within each memory sector are given in terms of a symmetric mode matrix, an orthogonal transformation exists that diagnoalizes it. This defines a new set of decoupled memory modes with gaps depending on the previous parameters. Requiring that those new gaps, $\mathcal{E}_{n,\text{eff}}$, not be too large to spoil the high entropy imposes bounds on the couplings. In the following, we are going to determine those bounds.

The maximal energy difference among different memory patterns is given by $N_m\mathcal{E}_{\text{eff}}$, if $\mathcal{E}_{\text{eff}}$ is a representative value. Taking into account that $\mathcal{E}_{n,\text{eff}}$ may be positive or negative, for large N_m, that maximal energy difference is more properly estimated by $\sqrt{N_m}\,|\mathcal{E}_{\text{eff}}|$. This latter estimate results in milder bounds on the couplings. In order for the different memory states to be effectively degenerate, it is sufficient that their energy differs by less than the elementary gap ϵ_0, resulting in the bound [1]

$$\mathcal{E}_{\text{eff}} \lesssim \frac{\epsilon_0}{\sqrt{N_m}}\,. \tag{3.22}$$

We start by determining the bounds on the couplings $\tilde{C}_{k,l}$ within one memory sector. We will assume that they all take values on the same order of magnitude. If there were only two modes in the first memory sector, the relevant part of the Hamiltonian is captured in terms of the following mode matrix:

$$\begin{pmatrix} 0 & \tilde{C}_{k,l} \\ \tilde{C}_{k,l} & 0 \end{pmatrix}. \tag{3.23}$$

Therefore, requiring the bound (3.22) implies $\tilde{C}_{k,l} \lesssim \epsilon_0/\sqrt{N_m}$. From here, the presence of K modes can be taken into account in the following way. Regarding the couplings within a single memory sector as independent samples from identical distributions with zero mean and unit variance, the resulting matrix (an extension of Eq. (3.23) to multiple modes)

[1] Note that without assuming contributions with random signs the constraint is $\mathcal{E}_{\text{eff}} \lesssim \frac{\epsilon_0}{N_m}$.

belongs to a Wigner Hermitian matrix ensemble. Wigner's semicircle law (as discussed in ref. [80]) states that the spectral distribution of this matrix converges and becomes independent of the dimension K when the matrix entries are rescaled by $1/\sqrt{K}$. In order not to disrupt the approximate gaplessness for the majority of modes we must therefore suppress the coupling constants by this extra factor:

$$\tilde{C}_{k,l} \lesssim \frac{\epsilon_0}{\sqrt{N_m}\sqrt{K}} \,. \tag{3.24}$$

This conclusion can also be reached by examining the expectation value of the off-diagonal elements in the Hamiltonian, following ref. [46]. This expectation value scales as $N_m \left|\tilde{C}_{k,l}\right|$ if the couplings take both positive and negative values, since then, for large N_m, N_m^2 non-zero terms only make a contribution on the order of N_m. To ensure that this energy is less than ϵ_0, we obtain the constraint

$$\tilde{C}_{k,l} \lesssim \frac{\epsilon_0}{N_m} \,. \tag{3.25}$$

For large K, a typical occupation has $N_m \sim K$, in which case the above bound agrees with Eq. (3.24).

Now consider the cross-couplings $C_{k,k'}$, i.e., the couplings between modes belonging to different memory sectors. We again assume all couplings to take values of the same order of magnitude. The mode matrix summarizing the relevant part of the Hamiltonian in that case reads (for $\Delta N_c \ll N_c$)

$$\begin{pmatrix} 0 & C_{k,k'} \\ C_{k,k'} & \epsilon_k \Delta N_c / N_c \end{pmatrix} . \tag{3.26}$$

From these effective gaps and couplings, we obtain upon diagonalizing $\mathcal{E}_{\text{eff}} \sim K C_{k,k'}^2 N/(\epsilon_k \Delta N_c)$. From (3.22), we then obtain the bound

$$C_{k,k'} \lesssim \frac{\sqrt{\epsilon_0 \epsilon_k \Delta N_c}}{\sqrt{K N_c}(N_m)^{1/4}} \,. \tag{3.27}$$

This constraint is less strong than (3.24) since $\epsilon_k \geq \epsilon_0$.

3.2 Time Evolution

The numerical time-evolution can of course proceed only with all parameter values in (3.16) specified. In order to deduce the parameter dependence of the system's behaviour, we repeat the evolution for many different values, as described in detail below. While we have in mind the special case of black holes, our selection of parameters is more general. Firstly, we set the free gaps of all memory modes in both sectors to be equal, $\epsilon_k = \epsilon_{k'} =: \epsilon_m$. Additionally, we assume that all couplings $C_{k,k'}$ and $\tilde{C}_{k,l}$ are of similar magnitude, and thus can be expressed as $C_{\text{m}} f_i(k,k')$, where $f_i(k,l)$ takes values of order one. To break the exchange symmetry $\hat{a}_k \leftrightarrow \hat{a}_l$, it is crucial that $f_i(k,l)$ are non-trivial. We choose them such that they effectively take random values in $|f_i(k,l)| \in [0.5;1]$, with both positive and

negative signs. [2] The operator $\epsilon_0 (\hat{n}_0 + \hat{m}_0)$ commutes with (3.16). Thus we can drop it from the Hamiltonian, since we only consider initial states that are eigenstates of this operator and it only leads to a trivial global phase. For convenience, we are going to use ϵ_0 as the basic energy unit. The above results in the following Hamiltonian:

$$\begin{aligned}\frac{\hat{H}}{\epsilon_0} = &\frac{\epsilon_m}{\epsilon_0}\left(1 - \frac{\hat{n}_0}{N_c}\right)\sum_{k=1}^{K}\hat{n}_k + \frac{C_0}{\epsilon_0}\left(\hat{a}_0^\dagger \hat{b}_0 + \hat{b}_0^\dagger \hat{a}_0\right) \\ &+ \frac{\epsilon_m}{\epsilon_0}\left(1 - \frac{\hat{n}_0}{N_c - \Delta N}\right)\sum_{k'=1}^{K'}\hat{n}'_{k'} + \frac{C_\mathrm{m}}{\epsilon_0}\Bigg\{\sum_{k=1}^{K}\sum_{k'=1}^{K'} f_1(k,k')\left(\hat{a}_k^\dagger \hat{a}'_{k'} + \mathrm{h.c.}\right) \\ &+ \sum_{k=1}^{K}\sum_{\substack{l=1\\ l\neq k}}^{K} f_2(k,l)\left(\hat{a}_k^\dagger \hat{a}_l + \mathrm{h.c.}\right) + \sum_{k'=1}^{K'}\sum_{\substack{l'=1\\ l'\neq k'}}^{K'} f_3(k',l')\left(\hat{a}_{k'}^{\prime\dagger}\hat{a}'_{l'} + \mathrm{h.c.}\right)\Bigg\}. \end{aligned} \tag{3.28}$$

From here on, we set $\epsilon_0 = 1$.

For the numerical analysis, we simplify the system by truncating all memory modes to qubits. This leads us to consider the initial state

$$|\,\mathrm{i}\rangle = \Big| N_c, 0, \underbrace{1, \ldots, 1}_{N_m}, 0, \ldots, 0 \Big\rangle\,, \tag{3.29}$$

where $\hat{n}_0$ is N_c-fold occupied, $\hat{m}_0$ is unoccupied, and the first N_m memory modes have one excitation each.

Unless stated otherwise, we use the following parameter values

$$\begin{aligned} &\epsilon_m = \sqrt{20}\,, \quad N_c = 20\,, \quad \Delta N_c = 12\,, \quad K = K' = 4\,, \\ &C_0 = 0.01\,, \quad N_m = 2\,, \end{aligned} \tag{3.30}$$

which determine the Hamiltonian and the initial state, except for the choice of the coupling C_m. We would like to emphasize that we have selected $N_m = K/2$ as it corresponds to the most probable state for large K.[3]

To numerically evolve the system, we utilize the approach and software documented in ref. [81], which is based on a Krylov subspace technique. In this method, the numerical error, i.e., the norm of the difference between the exact time-evolved state and its numerical approximation, is assigned a reliable upper bound. We set the error tolerance to be 10^{-6} for most systems, except for those with $K = 8$, for which we use a tolerance of 10^{-5}.

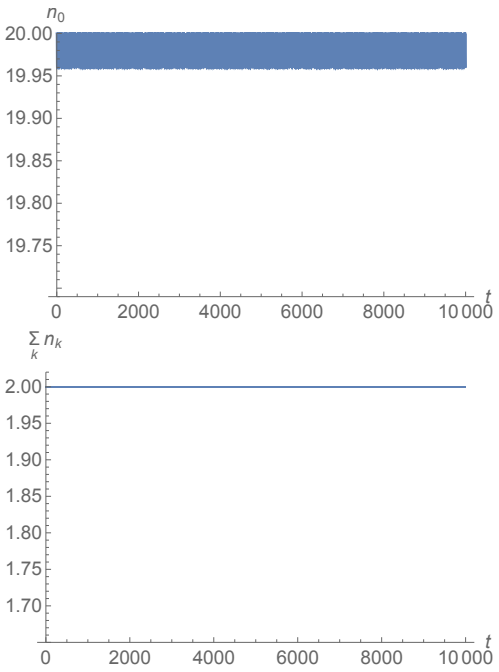

(a) $C_\mathrm{m} = 0$.

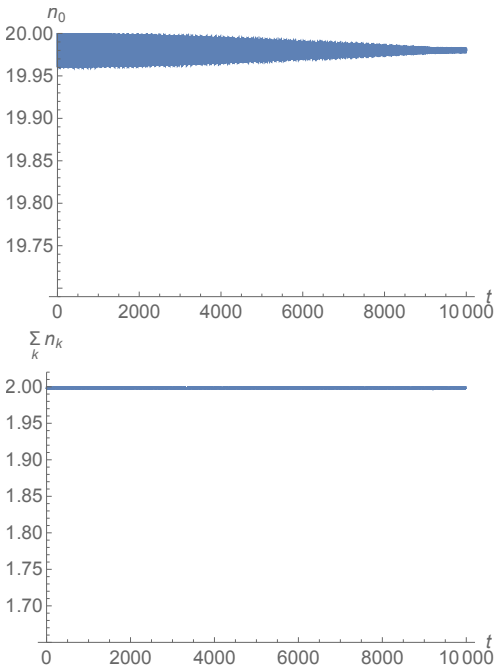

(b) $C_\mathrm{m} = 0.1$.

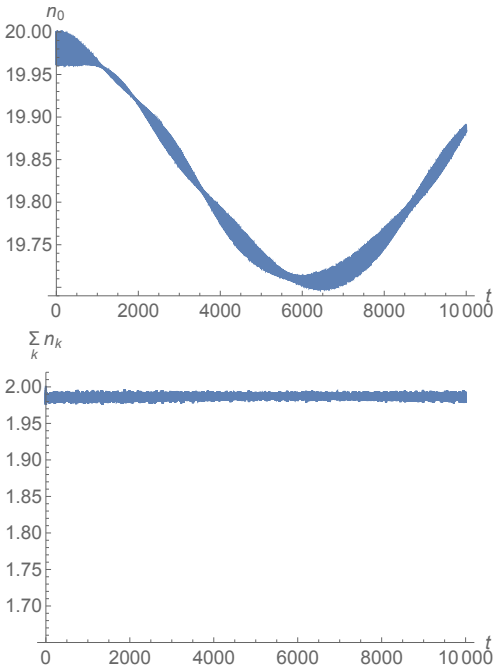

(c) $C_\mathrm{m} = 0.30055$.

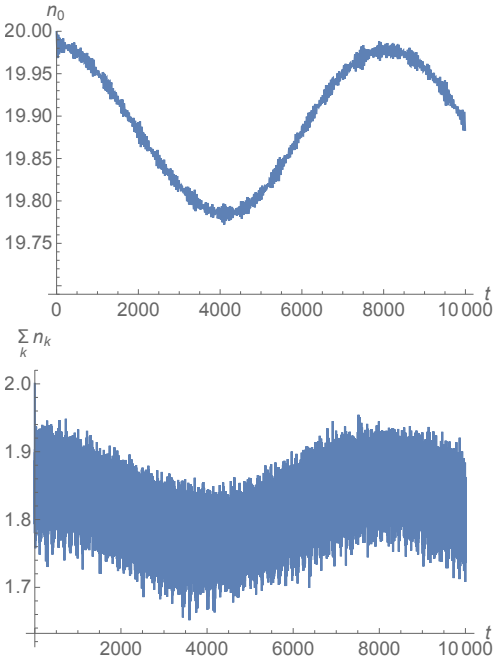

(d) $C_\mathrm{m} = 1.239$.

Figure 3.2: Time evolution of the initial state (3.29) for different values of C_m. Oscillations on a timescale of order 1 cannot be resolved graphically any more since we show very long timescales. n_0 is the expectation value of the occupation of the mode $\hat{a}_0$ and $\sum_k n_k$ that of the total occupation in the first critical sector. Time is plotted in units of $\epsilon_0^{-1}\hbar$.

3.2.1 Possibility of Rewriting

In Fig. 3.2, we present the time evolution of the initial state (3.29) for different values of $C_{\rm m}$. We show the expectation value n_0 of the occupation number of the $\hat{n}_0$-mode, as well as the expectation value of the total occupation of the first critical sector $\sum_{k=1}^{K}\hat{n}_k$. When $C_{\rm m}=0$ (see Fig. 3.2a), we can make the replacement $\sum_{k=1}^{K}\hat{n}_k \to N_m$ and $\sum_{k'=1}^{K'}\hat{n}'_{k'} \to 0$, and the system has the analytic solution (3.9). We observe that the critical sector remains stationary, and the amplitude of oscillations of $\hat{n}_0$ is heavily suppressed. This is the result of the memory burden effect[28] discussed in section 3.1.2.

For many nonzero values of $C_{\rm m}$, the system behaves similarly (see Fig. 3.2b). Although the time evolution of the system becomes more complicated, the amplitude of oscillations of n_0 remains small, and the critical sector effectively freezes.

However, there are certain $C_{\rm m}$ values for which the system behaves differently, and the amplitude of oscillations of n_0 distinctly increases, albeit on a significantly longer timescale (see Figs. 3.2c, 3.2d). As expected, this behavior accompanies a change in the occupation numbers in the critical sector. This change can occur either through an instantaneous jump (as in Fig. 3.2c) or through synchronous oscillations with n_0 (as in Fig. 3.2d). Although the second scenario is more intuitive, both are consistent with our expectation that a significant change in n_0 can only occur if rewriting in the critical sector also takes place.

Furthermore, the occupation transfer, and thus the information rewriting, is not complete. We anticipate that complete rewriting into the second sector of memory modes is only achievable after including additional sectors to which the $\hat{a}'_{k'}$-modes can transfer occupation number.

From now on, we are going to refer to the values of $C_{\rm m}$ for which partial rewriting takes place by *rewriting values*. For the parameter values used here (cf. (3.30)), rewriting values are rare. This is illustrated in Fig. 3.3a, where we plot the maximal amplitude of oscillations as a function of $C_{\rm m}$. We would like to mention that for other parameter choices, the system exhibits a higher abundance of rewriting values.

We close this section with an illustration of the system's behaviour for the choice of $p=2$ (see Eq. (3.12)). This change corresponds to replacing in the Hamiltonian $1-\hat{n}_0/N_c \to (1-\hat{n}_0/N_c)^2$ and $1-\hat{n}_0/(N_c-\Delta N_c) \to (1-\hat{n}_0/(N_c-\Delta N_c))^2$. As can be seen from Eq. (3.14), the memory burden in that case is reduced: using that, for $p=1$, N_c-n_0 can get as large as 0.3 (see Fig. 3.3a) we see that the memory burden is smaller by a factor of approximately 0.03. In order for the two systems $p=1$ and $p=2$ to have comparable amplitudes of oscillation of n_0 in the absence of rewriting (see Eq. (3.9)), we therefore need to rescale C_0 by the same factor, i.e., set $C_0=0.0003$. Other than that, the parameter choice Eq. (3.30) has been used. As described above for $p=1$, we numerically evolve the

[2]Specifically, we set $f_i(k,l) = \begin{cases} F_i(k,l)-1 & \text{for} \quad F_i<0.5 \\ F_i(k,l) & \text{for} \quad F_i\geq 0.5 \end{cases}$, where $F_i(k,l) = \left(\sqrt{2}(k+\Delta k_i)^3+\sqrt{7}(l+\Delta l_i)^5\right) \mod 1$. In addition, we set $\Delta k_1=\Delta k_2=1$, $\Delta k_3=K+1$, $\Delta l_1=\Delta l_3=K+1$ as well as $\Delta l_2=1$.

[3]This reasoning is only valid for macroscopic black holes with a mass much larger than the Planck mass, $M\gg M_p$, as K is mapped onto the entropy of a black hole.

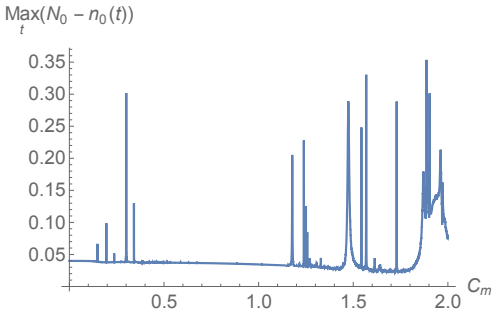

(a) $p = 1\,,\ C_0 = 0.01$

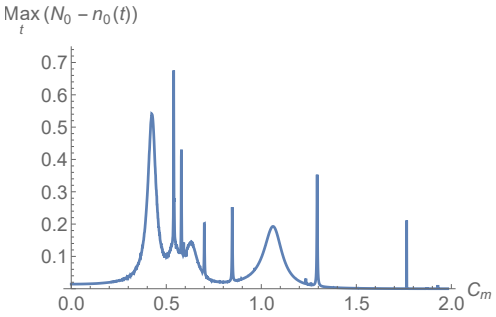

(b) $p = 2\,,\ C_0 = 0.0003$

Figure 3.3: Maximal amplitude of the expectation value of $\hat{n}_0$ for different values of C_m (with initial state (3.29)).

system for different values of C_m. The maximal amplitude observed for each C_m is shown in Fig. 3.3b. As can be seen, the qualitative behaviour of the system is the same as in the case of $p = 1$.

3.2.2 Scaling with System Size

We have seen that rewriting does indeed take place for certain values of the coupling C_m and the specific parameter values (3.30). Our next goal is to determine the dependence of the phenomenon on the system size. More specifically, we repeat the simulations for varied parameters in the Hamiltonian (3.28) and track the corresponding variation of the rewriting values of C_m. In addition, we track the corresponding variation of a certain characteristic of the rewriting process. Namely, we can define a rate Γ of rewriting as the ratio of the maximal amplitude of n_0 and the timescale on which this maximal value is attained. Γ gets the meaning of a decay rate if the oscillation among $\hat{a}_0$ and $\hat{b}_0$ is mapped on a decay. We will discuss this mapping in section 4.1.1. From here on, our analysis is restricted to the model with $p = 1$.

The details of the procedure are described in the appendix B. Here, we merely cite the observed scalings of C_m and Γ with the parameters varied:

- The initial occupation number N_c of $\hat{n}_0$ (which is also the critical occupation at which the first memory sector is gapless):

$$C_\mathrm{m} \sim N_c^{-1}\,, \qquad \Gamma \sim N_c^{-1} \tag{3.31}$$

- The free gap ϵ_m of the memory modes:

$$C_\mathrm{m} \sim \epsilon_m^1\,, \qquad \Gamma \sim \epsilon_m^0 \text{ (independent)} \tag{3.32}$$

- The coupling C_0 of $\hat{a}_0$ and $\hat{b}_0$:

$$C_\mathrm{m} \sim C_0^0 \text{ (independent)}\,, \qquad \Gamma \sim C_0^{1.4} \tag{3.33}$$

- The difference ΔN_c between the critical occupations of $\hat{a}_0$ making either of the two memory sectors gapless:

$$C_{\mathrm{m}} \sim (\Delta N_c/N_c)^{0.2}\,, \qquad \Gamma \sim (1 - \Delta N_c/N_c) \tag{3.34}$$

Concerning K and K', we can unfortunately only study three values due to numerical limitations, namely $K = K' = 4, 6, 8$. N_m is varied alongside as $N_m = K/2$. The results are shown in Fig. 3.4. With a parameterization of the dependence on K as

$$C_{\mathrm{m}} \sim K^{\beta_C}\,, \qquad \Gamma \sim K^{\beta_\Gamma}\,, \tag{3.35}$$

we may attempt to obtain a bound on the K-scaling despite the scarcity of available numerical results. When mapping the system on a BH later, it will become clear that the interesting bounds are a lower bound on the K-scaling of C_m and an upper bound on that of Γ.

For that, we proceed as follows. For $K = 6$, there are 11 rewriting values and corresponding rates, (C_m, Γ), whereas for $K = 8$, there are more. We average the 11 data points for $K = 6$ as well as 11 of the ones for $K = 8$. The latter are chosen to be the 11 lowest C_m values and the 11 highest Γ values. In order to get more conservative bounds, for C_m we exclude the data point of $K = 4$ and we include it for Γ. Performing a fit of (3.35) with the resulting data, we obtain

$$\beta_C \gtrsim -0.7 \tag{3.36}$$

and

$$\beta_\Gamma \lesssim -0.7\,. \tag{3.37}$$

Despite our attempt to generate a conservative estimate, we obviously have too little data for a reliable statement. Correspondingly, the actual values β_C and β_Γ may not obey the constraints (3.36) and (3.37).

Besides our tentative finding of decreasing Γ with growing K, we have also found that it decreases with growing N_c (see (3.31)). For a generic system, other parameters may vary arbitrarily with growing system size. For BHs, those variations are more constrained, as will be discussed in chapter 4. The above-mentioned findings already indicate that rewriting becomes less efficient for larger systems.

3.3 Analytic Considerations

3.3.1 Understanding of Results

In this section, we attempt to offer some analytic understanding of our results. For the sake of the argument, we make the simplifying assumptions that $K = K'$ and ϵ_k and $\epsilon_{k'} = \sqrt{N_c}\epsilon_0$ as well as vanishing couplings between memory modes of the same sector, $\tilde{C}_{k,l} = \tilde{C}_{k',l'} = 0$. $\epsilon_k = \epsilon_{k'} = \sqrt{N_c}\epsilon_0$. Without loss of generality, the cross-coupling matrix $C_{k,k'}$ can then

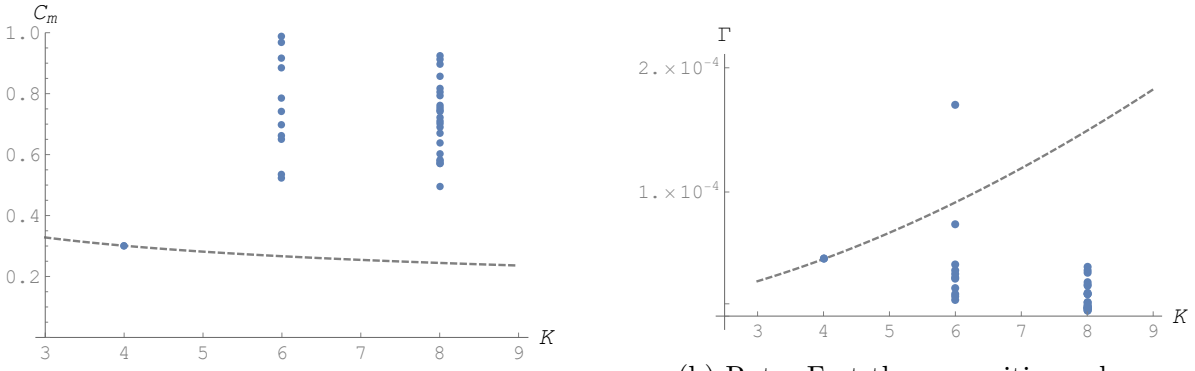

(a) Rewriting values of C_{m}

(b) Rates Γ at those rewriting values

Figure 3.4: Available data (blue dots) for the rewriting values of C_m and the rates Γ as function of $K = K'$, where we take $N_m = K/2$. The dashed curves are the constraints (4.10) and (4.11), that apply to a black hole. We see clear indications that for large black holes, rewriting is not fast enough to reproduce the semiclassical rate of evaporation.

be chosen diagonal since this can always be achieved by a unitary transformation. The Hamiltonian (3.16) is then

$$\begin{aligned}\hat{H} &= \epsilon_0 \hat{n}_0 + \epsilon_0 \hat{m}_0 + C_0 \left(\hat{a}_0^\dagger \hat{b}_0 + \hat{b}_0^\dagger \hat{a}_0\right) \\ &\quad + \mathcal{E} \sum_k \hat{n}_k + \mathcal{E}' \sum_k \hat{n}'_k \\ &\quad + \sum_k C_{k,k} \left(\hat{a}_k^\dagger \hat{a}'_k + \text{h.c.}\right) ,\end{aligned} \tag{3.38}$$

where

$$\mathcal{E} \equiv \left(1 - \frac{\hat{n}_0}{N_c}\right) \sqrt{N_c} \epsilon_0 \,, \tag{3.39}$$

and

$$\mathcal{E}' \equiv \left(1 - \frac{\hat{n}_0}{N_c - \Delta N_c}\right) \sqrt{N_c} \epsilon_0 \,. \tag{3.40}$$

For the initial state (3.17), $n_0 = N_c$, and thus

$$\mathcal{E} = 0 \,, \;\; \mathcal{E}' = -\frac{\sqrt{N_c}\Delta N_c}{N_c - \Delta N_c} \epsilon_0 \simeq -\frac{\Delta N_c}{\sqrt{N_c}} \epsilon_0 < 0 \,, \tag{3.41}$$

where the approximate equality holds for $\Delta N_c \ll N_c$. Due to the negative sign of the second gap, there are states with energy much lower compared to the initial state (3.17). An example is given by the state

$$|\,\text{low}\rangle = \Big| \underbrace{N_c, 0}_{n_0, m_0}, 0, \ldots 0, \underbrace{n_1, \ldots, n_K}_{n'_1, \ldots, n'_K} \Big\rangle \,. \tag{3.42}$$

Compared to (3.17), the occupations of the memory sectors are exchanged, while n_0 and m_0 are the same. The energy difference of the two states (3.42) and (3.17) is negative and macroscopically large. In terms of the memory burden, which in this case reads $\mu = -N_c^{-1/2}\epsilon_0 \sum_k n_k$, this energy difference can be expressed as

$$\langle \mathrm{low} \,|\, \hat{H} \,|\, \mathrm{low} \rangle - \langle \mathrm{i} \,|\, \hat{H} \,|\, \mathrm{i} \rangle = \mathcal{E}' \sum_k n_k \sim \Delta N_c \mu \,. \tag{3.43}$$

As far as the expectation value of the Hamiltonian is concerned, there appears no obstacle to intermediate deformations of the initial state (3.17) smoothly connecting to the final state (3.18): The exchanges of excitations among n_k and n'_k on the one hand and n_0 and m_0 on the other hand can proceed such that the associated negative and positive changes in energy balance. From this perspective, it appears possible that the system can indeed overcome the memory burden via rewriting. Such an expectation has also been put forward in ref. [28]. However, our results are very different.

Rather, we find that the rewriting-facilitated decay does not proceed efficiently. In the following, we attempt to identify the reason for this. As detailed above, the conservation of the expectation value of the Hamiltonian requires that the degrees of freedom a_0, b_0 on the one hand and a_k, a'_k on the other hand evolve in synchronized fashion. However, there may of course still exist other barriers to such an evolution. One such barrier appears to be constituted by the splitting of energy levels among the relevant degrees of freedom, as we will now discuss in detail.

The time evolution near the initial state (3.17) can be described as a set of coupled 2×2 problems, with the Hamiltonians

$$\hat{H} = \sum_k \begin{matrix} \hat{a}_k^\dagger \\ \hat{a}_k'^\dagger \end{matrix} \begin{pmatrix} \hat{a}_k & \hat{a}_k' \\ 0 & C_{k,k} \\ C_{k,k} & \mathcal{E}' \end{pmatrix} + \begin{matrix} \hat{a}_0^\dagger \\ \hat{b}_0^\dagger \end{matrix} \begin{pmatrix} \hat{a}_0 & \hat{b}_0 \\ \epsilon_0 + \mu & C_0 \\ C_0 & \epsilon_0 \end{pmatrix} . \tag{3.44}$$

The systems are coupled because $\mathcal{E}'$ is a function of n_0 and μ is a function of $\sum_k n_k$. In order to obtain a qualitative understanding of the behaviour of the system, we may solve the system iteratively. In the zeroth order, $\mathcal{E}'$ and μ are treated as constants. The resulting variations of n_0 and n_k obtained in this way are then fed into $\mathcal{E}'$ and μ for the next iteration and so on. In this way, within each iteration, the systems are decoupled. Then the large level-splittings as compared to the couplings in the above 2×2 matrices already indicate the suppression of the evolution. Namely, we have from (3.9)

$$\delta n_0 \sim -N_c \frac{C_0^2}{\mu^2} \quad \text{and} \quad \delta n_k \sim -\frac{C_{k,k}^2}{\mathcal{E}'^2} \,. \tag{3.45}$$

From (3.10) and (3.40), we see that the resulting variations of $\mathcal{E}'$ and μ are given by

$$\frac{\delta\mu}{\mu} \sim \frac{C_{k,k}^2}{\mathcal{E}'^2} \quad \text{and} \quad \frac{\delta\mathcal{E}'}{\mathcal{E}'} \sim \frac{C_0^2}{\mu^2} \,. \tag{3.46}$$

In the next iteration, the picture remains unaffected if these relative variations are very small. This is of course the case for $C_0^2 \ll \mu^2$ and $C_{k,k}^2 \ll \mathcal{E}'^2$. For any interesting parameter choice, $C_0^2 \ll \mu^2$ is fulfilled since otherwise there would be no strong memory burden effect in the first place. The condition $C_{k,k}^2 \ll \mathcal{E}'^2$ is implied by the bound on $C_{k,k}$, Eq. (3.27), in the interesting case of $N_c \sim K \sim N_m \gg 1$. Explicitly, combining (3.27) and (3.41), we obtain

$$\frac{C_{k,k}^2}{\mathcal{E}'^2} \lesssim \frac{\sqrt{N_c}}{K\sqrt{N_m}\Delta N_c} \sim \frac{1}{N_c \Delta N_c} \,. \tag{3.47}$$

Thus, for large systems and relevant parameter choices, the iteration series converges rapidly, indicating that the system is effectively confined to the initial state.

3.3.2 Role of Number Non-Conservation

In the prototype system introduced and investigated until now, the interactions are strictly number-conserving. In this section, we are going to argue that the possible effects of number-non-conservation cannot change our findings.

More explicitly, in the interactions considered so far, the creation of an excitation of an $\hat{a}'_{k'}$-mode always comes with the destruction of an $\hat{a}_k$-quantum. Likewise, the destruction of a particle in the control mode $\hat{a}_0$ comes with the creation of a particle in the $\hat{b}_0$-mode.

We have found that the memory burden effect is strong enough to halt the process before the extra sectors $(\hat{a}'_{k'}, \hat{b}_0)$ can get significantly populated. This means that the inverse transition processes can barely play a role in the time evolution of the system.

This indicates that transitions generated by the particle number non-conserving interactions of similar strengths could not overcome the memory burden effect, either. In the following, we are going to estimate this explicitly for some examples of number non-conserving interactions.

Decay of control mode

We start by considering number non-conserving interactions between the $\hat{a}_0$- and $\hat{b}_0$-mode. For this purpose, we approximate the memory burden μ as a constant parameter.

Let us replace the number conserving mixing among the $\hat{a}_0$- and $\hat{b}_0$-mode in (3.7) by the following number-non-conserving one,

$$\hat{H} = (\epsilon_0 + \mu)\hat{a}_0^\dagger \hat{a}_0 \, + \epsilon_0 \hat{b}_0^\dagger \hat{b}_0 + C_0(\hat{a}_0 \hat{b}_0 + \hat{a}_0^\dagger \hat{b}_0^\dagger) \,. \tag{3.48}$$

Here we take the parameter C_0 real and of the same strength as in the number-conserving version (3.7), $C_0 \sim \epsilon_0/N_c$. This strength is required for a half-decay time of the $\hat{a}_0$-mode of $t \sim N_c/\epsilon_0$ when $\mu = 0$, as follows from (3.9). At the level of our toy model, this scaling imitates the scaling of the black hole half-decay time in units of the typical energy of the Hawking quanta.

The following Bogoliubov transformation diagonalizes the Hamiltonian (3.48):

$$\hat{a}_0 = u\hat{\alpha} - v\hat{\beta}^\dagger \,, \qquad \hat{b}_0 = u\hat{\beta} - v\hat{\alpha}^\dagger \,. \tag{3.49}$$

Here, $\hat{\alpha}$ and $\hat{\beta}$ are the eigenmodes and

$$v^2 = \frac{1}{2}\left(\frac{1}{\sqrt{1-\frac{4C_0^2}{(2\epsilon_0+\mu)^2}}} - 1\right), \tag{3.50}$$

$$u^2 = \frac{1}{2}\left(\frac{1}{\sqrt{1-\frac{4C_0^2}{(2\epsilon_0+\mu)^2}}} + 1\right). \tag{3.51}$$

For $N_m \sim N_c$, the memory burden is given by $\mu \sim -\epsilon_0\sqrt{N_c}$. With $C_0 \sim \epsilon_0/N_c$, from (3.50) we have

$$v^2 \simeq \frac{C_0^2}{\mu^2} \sim \frac{1}{N_c^3}\,, \quad u^2 = 1 + \mathcal{O}(1/N_c^3)\,, \tag{3.52}$$

We see that the depletion coefficient v^2 is tiny. Comparing this to (3.9), we see that it is suppressed by the same factor C_0^2/μ^2 as the amplitude in the case of a number conserving mixing.

The Bogoliubov approximation offers another way of understanding why the number conserving and number non-conserving cases behave comparably in the situation where $\hat{a}_0$-mode is macroscopically occupied and the occupation of $\hat{b}_0$ never becomes high. In this approximation, the operators of the $\hat{a}_0$-mode are replaced by c-numbers, $\hat{a}_0 = \sqrt{N_c}\,,\ \hat{a}_0^\dagger = \sqrt{N_c}$.[4] The number non-conserving Hamiltonian (3.48) then is:

$$\hat{H} = \epsilon_0 \hat{b}_0^\dagger \hat{b}_0 + C_0\sqrt{N_c}(\hat{b}_0^\dagger + \hat{b}_0)\,. \tag{3.53}$$

This Hamiltonian for $\hat{b}_0$ is diagonalized by the canonical transformation

$$\hat{b}_0 = \hat{\beta} - C_0\sqrt{N_c}/\epsilon_0\,. \tag{3.54}$$

From this one sees that in the β-vacuum the occupation number of the $\hat{b}_0$-mode is

$$\langle \hat{b}_0^\dagger \hat{b}_0 \rangle = \frac{C_0^2 N_c}{\epsilon_0^2}\,. \tag{3.55}$$

The depletion can be seen to be suppressed by $C_0/\epsilon_0 \sim 1/N_c$. Therefore the memory burden effect cannot be avoided regardless of whether particle number is conserved.

Lastly, let us consider number non-conserving transitions of a $\hat{a}_0$-quantum into several $\hat{b}_0$-quanta. Since each extra $\hat{b}_0$ has to contribute an additional factor of $1/\sqrt{N_c}$ to the coefficient, i.e., the coefficient of the term $\hat{a}_0\hat{b}_0^l$ scales as $\epsilon_0/N_c^{l/2}$, the effect of such terms is likewise negligible.

[4] This is justified (self-consistently) as long as the departure of $\hat{a}_0$ from $\sqrt{N_c}$ is small.

Decay of memory modes

When allowing for a number non-conserving decay of the memory modes, the following issue has to be considered.

Near the initial state, the effective gap of the second set of the memory modes is negative for odd values of p. In the case of a number conserving Hamiltonian, the sign of the gap plays no role in the memory burden effect. This has allowed us to focus our analysis on the simplest version of (3.13) in $p = 1$.

On the other hand, as soon as number non-conserving transitions among the memory modes are admitted, a negative sign of the effective gap may lead to "tachyonic" type instabilities in the form of excitations created out of the vacuum. Whether such instabilities occur is completely distinct from whether the memory burden is alleviated. However, the answer to the second question can be made unnecessarily difficult to find in the presence of the instabilities. Therefore, below, we are going to implement a positive gap.

Let us begin by considering a Hamiltonian that mixes the memory modes in a number non-conserving way:

$$\begin{aligned}\hat{H} = {} & \mathcal{E}_k \hat{n}_k + \mathcal{E}_{k'} \hat{n}'_{k'} + \\ & + C_{k,k'} \left(\hat{a}_k \hat{a}'_{k'} + \text{h.c.} \right) .\end{aligned} \tag{3.56}$$

For the sake of the argument, we have simplified the structure present in the Hamiltonian (3.16) and paired up modes from the two memory sets. This decoupling lets each pair evolve separately with the evolution governed by a 2×2 matrix. The qualitative picture is not different in the more involved scenario.

The effective gaps $\mathcal{E}_k$ and $\mathcal{E}_{k'}$ as before depend on n_0. This n_0-dependence needs to be such that they reach zero at different values of n_0 with a macroscopic level-splitting, i.e.,

$$\begin{aligned}&\mathcal{E}_k = 0 \, , \mathcal{E}_{k'} \gg \epsilon_0, \qquad \text{for } n_0 = N_c, \\ &\mathcal{E}_{k'} = 0 \, , \mathcal{E}_k \gg \epsilon_0, \qquad \text{for } n_0 = N_c - \Delta N_c.\end{aligned} \tag{3.57}$$

For the first sector, we can, for instance, take

$$\mathcal{E}_k \equiv \left(1 - \frac{\hat{n}_0}{N_c} \right) \epsilon_k \, , \tag{3.58}$$

as before. For the second sector, possibilities include

$$\mathcal{E}_{k'} \equiv \left(1 - \frac{\hat{n}_0}{N_c - \Delta N_c} \right)^2 \epsilon_{k'} \, , \tag{3.59}$$

or

$$\mathcal{E}_{k'} \equiv \left(\frac{\hat{n}_0}{N_c - \Delta N_c} - 1 \right) \epsilon_{k'} \, , \tag{3.60}$$

and so on.[5] The coupling in Hamiltonian (3.56) has to obey the constraint (3.47) since otherwise, the gaplessness of the memory modes would be offset just like in the number conserving case.

For the number conserving system (3.16), in section 3.3, we have offered some analytic understanding of why in the numerical solution one does not observe efficient occupation transfer among the memory sectors. In essence, the reason is that the level-splitting $\Delta\mathcal{E} = \mathcal{E}_{k'} - \mathcal{E}_k$ in relation to the mixing coefficient $C_{k,k'}$ stays large.

If these conditions are likewise fulfilled in the system (3.56), the number non-conserving nature of the interactions does not change the picture. To see this explicitly, note that (3.56) is diagonalized by the Bogoliubov transformation

$$\hat{a}_k = u\hat{\alpha}_k - v\hat{\beta}^\dagger_{k'}\,, \qquad \hat{a}'_{k'} = u\hat{\beta}_{k'} - v\hat{\alpha}^\dagger_k\,, \tag{3.61}$$

where

$$u^2 = 1 + v^2\,,\ v^2 = \frac{1}{2}\left(\frac{1}{\sqrt{1 - \frac{4C^2_{k,k'}}{(\mathcal{E}_k + \mathcal{E}_{k'})^2}}} - 1\right)\,. \tag{3.62}$$

Near $n_0 = N_c$, from Eqs. (3.47) and (3.57) it follows that

$$v^2 \sim \frac{C^2_{k,k'}}{(\mathcal{E}_{k'})^2} \ll \frac{\epsilon_0}{\sqrt{N}\mathcal{E}_{k'}}\,, \qquad u^2 \simeq 1\,, \tag{3.63}$$

resulting in a highly suppressed rate of occupation transfer among the memory sectors. Thus it can not free the control mode $\hat{a}_0$ from the memory burden on a relevant time scale.

As for higher order operators such as, e.g., $\hat{a}_k\hat{a}'_{k'_1}\cdots\hat{a}'_{k'_l}$, their coefficients are suppressed by extra powers of $1/N_c$. Those operators, whether number conserving or not, are therefore not able to significantly enhance the decay rate.

[5] Even a gap function such as, e.g., $\mathcal{E}_{k'} \equiv \left(1 - \frac{N_c - \Delta N_c}{\hat{n}_0}\right)\epsilon_{k'}$ would be admissible since here we are not restricted by renormalizability and only interested in the regime of $n_0 \gg 1$.

Chapter 4

Manifestation of Memory Burden in Black Holes and De Sitter

4.1 Black Holes

4.1.1 Parameter Mapping

We now proceed to apply our findings to black holes. Of course, we will assume that the investigated quantum system with enhanced memory capacity reflects some fundamental aspects of how information is stored in black holes. Ideally, we want to avoid being limited to any particular microscopic theory of a BH and instead utilize universal properties that all such theories should incorporate. For instance, it is expected that the existence of modes that become gapless near a macrostate associated with a black hole is such a universal property. Without such gapless excitations, it would be impossible to account for the microstate entropy of a black hole. Another fact of importance is that the Bekenstein-Hawking entropy [10] scales with the black hole mass M as

$$S = 4\pi G_N M^2 \,, \tag{4.1}$$

where G_N is Newton's constant. Thus, the number of gapless modes that a black hole can accommodate is directly linked to its mass. Therefore, any reduction in M must impact the energy gaps of its memory modes. Specifically, as a black hole evaporates, some previously gapless modes must acquire gaps. This process, because of the information stored in those modes, then leads to a memory burden effect that opposes the decrease of the black hole's mass. This is the primary insight we gain about black holes from our analysis. To gain a more quantitative understanding, we aim to set the parameters of our toy model as close as possible to the corresponding characteristics of a black hole.

For this purpose, we can use the microscopic theory of the black hole quantum N-portrait [19] as a rough guideline. While we aim to keep our analysis as general as possible, the microscopic theory is helpful for establishing an exact parameter correspondence between a black hole and the simple Hamiltonian presented here. Furthermore, it demonstrates how effectively the toy model captures the essential features of the phenomenon.

The quantum N-portrait proposes that a black hole with a Schwarzschild radius of $r_g = 2G_N M$ is a bound state of soft gravitons. These constituent gravitons contribute to the gravitational self-energy with a characteristic wavelength given by r_g. Their occupation number is critical in the sense that it renders a set of other modes near-gapless. Those other modes thus correspond to the memory modes of the toy model, while the constituent gravitons play the role of the control mode.

If the occupation number of the control mode were not critical, the memory modes would correspond to free gravitons with very high frequencies and correspondingly large energy cost for information stored in them. These gapless modes are assumed to account for the Bekenstein-Hawking entropy (4.1).

Within the toy model presently investigated, the system's decay is modeled through the coupling of $\hat{a}_0$ to $\hat{b}_0$, whose occupations are denoted n_0 and m_0. The quantum depletion of the n_0 into the initially vanishing m_0 is what plays the role of Hawking radiation [11]. As the m_0 increases at the expense of n_0, the memory burden effect is setting in sooner or later. The mode $\hat{b}_0$ is in fact only pseudo-external because the model (3.16) can oscillate back. Hence the mapping on a truly decaying black hole holds only up to a limited time. However, this is sufficient to draw our conclusions.[1].

The validity of our model is limited for another reason. Black holes can exist for any mass value M, requiring a tower of momentum mode sets where one of them becomes gapless for each M. However, our model only includes two sets of momentum modes. Therefore, as soon as a third set would begin to get occupied, our model can no longer be applied to a black hole. Furthermore, the prototype model (3.16) is number conserving, whereas in quantum field theory particle number is not conserved. However, as we have explained in section 3.3.2, this difference does not affect our conclusions.

The parameters of Hamiltonian (3.16) can be chosen to replicate the typical information-theoretic properties of a black hole. To achieve this, we first set the elementary gap to $\epsilon_0 = r_g^{-1}$, ensuring that the energy of Hawking quanta is correctly represented by r_g^{-1}. Next, we require that $K = S$ to achieve the desired entropy. As a result, a typical pattern will have $N_m = S/2$ since, for large black holes where $S \gg 1$, the number of patterns with different N_m is negligible. An estimate of the memory mode gap can be obtained as follows. Because a Schwarzschild black hole is spherically symmetric, states can be labeled by their quantum numbers (l, m) of angular harmonics. The degeneracy of each level scales with l. Assuming that the energy of the modes is mainly in their angular rather than radial motion, all the states until $l \sim \sqrt{K}$ need to be occupied in order to amount to a number of K modes. The highest mode then has an energy of $\epsilon_k = \sqrt{K}\epsilon_0$, which we use to estimate the free gap of the memory modes. The relative energy split among levels is not significant for our discussion. It should be noted that this means the modes are Planckian, $\epsilon_k \sim 1/\sqrt{G_N}$. Lastly, the critical occupation number N_c can be chosen freely, but for specificity, we set

[1]The bilinear coupling between modes is motivated as the simplest possible coupling that is able to effectively describe energy transfer between degrees of freedom. In order to model a decay more precisely, one could instead consider a coupling to many species, $\frac{C_0}{\sqrt{F}} \sum_{f=1}^{F} \hat{a}_0 \hat{b}_f^\dagger + h.c.$ (all with the same gap $\epsilon_f = \epsilon_0$), which could e.g., represent momentum modes of a field-theoretic system. In the limit of large F, one can achieve strict decay with the same rate as in (3.16).

$N_c = S$, motivated by the quantum N-Portrait. With that choice, the total energy of the system also equals the mass of a Schwarzschild black hole of entropy S: $M = N_c\epsilon_0$.

To summarize, the above fixes some of the parameters of (3.16) in terms of a black hole's entropy and Schwarzschild radius as follows:

$$\begin{aligned} &\epsilon_0 = r_g^{-1}\,, \qquad N_c = S\,, \qquad K = S\,, \qquad N_m = S/2\,, \\ &\epsilon_k = \sqrt{S} r_g^{-1}\,. \end{aligned} \tag{4.2}$$

As for the couplings $C_{k,k'}$ and all $\tilde{C}_{k,l}$, they all must be of the same order since the gravitational coupling is universal. Therefore, Eq. (3.24) results in the strongest bound on the couplings,

$$C_{k,k'} \sim \tilde{C}_{k,l} \lesssim \frac{\epsilon_0}{S}\,. \tag{4.3}$$

This constraint as mentioned earlier is the mildest possible one and application to black holes might actually require stronger bounds. Another issue arising in the black hole application is the following. Just like there are the external Hawking modes, whose role is played by the $\hat{b}_0$-mode, there are of course also free modes of higher momenta. In particular, there exist external modes of the same momenta as the memory modes $\hat{a}_k$. Let us denote those by $\hat{b}_k$. Being external, these modes are of course not subjected to the assisted gaplessness and instead satisfy the dispersion relations of free quanta. Thus they have much higher frequencies, on the order of their momenta, $\epsilon_k = \sqrt{S}\epsilon_0$. The situation is effectively described by the following addition to the Hamiltonian:

$$\begin{aligned} \hat{H}_{\text{higher}} = &\sum_{k=1}^{K} \epsilon_k \hat{b}_k^\dagger \hat{b}_k + \sum_{k=1}^{K} C_k \left(\hat{a}_k^\dagger \hat{b}_k + \hat{b}_k^\dagger \hat{a}_k\right) \\ &+ \sum_{k'=1}^{K'} C_{k'} \left(\hat{a}_{k'}'^\dagger \hat{b}_{k'} + \hat{b}_{k'}^\dagger \hat{a}_{k'}'\right)\,. \end{aligned} \tag{4.4}$$

The highest possible values of the couplings C_k are determined by the consistency requirement that they do not offset the gaplessness of the effective $\hat{a}_k$-modes. For $n_0 = N_c$, the corresponding coupling matrix reads

$$\begin{pmatrix} 0 & C_k \\ C_k & \epsilon_0\sqrt{S} \end{pmatrix}\,. \tag{4.5}$$

Requiring that the vanishing gap be disturbed by at most $\epsilon_0/\sqrt{S}$, leads to $C_k^2/(\epsilon_0\sqrt{S}) \lesssim \epsilon_0/\sqrt{S}$, i.e., $C_k \lesssim \epsilon_0$. Therefore, due to the strong level splitting, a transfer of occupation from $\hat{a}_k$ to $\hat{b}_k$ is highly suppressed and the $\hat{b}_k$ effectively do not get populated during the evolution. This protects the information carried by the memory modes from getting carried away by external modes. As has been argued in ref. [28], the above observation constitutes a microscopic explanation of why a black hole initially releases energy but almost no information.

While this behaviour is often considered mysterious and specific o black holes, the above shows that rather it is a universal property of systems that are in a state of enhanced

memory capacity due to assisted gaplessness. The microscopic explanation lies in the large level splitting between the memory modes subjected to the assisted gaplessness and their free counterparts.

We do not include the $\hat{b}_k$-modes in the numerical simulations since they barely get occupied. As for the constraint on the coupling C_0, since the gravitational interaction scales with energy, the above consideration implies

$$C_0 \lesssim \frac{\epsilon_0}{\sqrt{S}} \,. \tag{4.6}$$

4.1.2 Implications of Numerical Findings

When we employ the parameter scalings (4.2), which we have argued in the previous section to be appropriate for a black hole, only the couplings C_0 and $C_{\rm m}$ as well as ΔN_c are independent of S. The constraint (4.6) on C_0, however, does depend on S. There is also a bound on ΔN_c, which is implied by Eq. (3.21):

$$\Delta N_c \gg 1 \,. \tag{4.7}$$

Thus, putting together the observed scalings of C_m and Γ (Eqs. (3.31)-(3.33)), we obtain

$$C_{\rm m} \sim S^{-0.5+\beta_C} (\Delta N_c/S)^{0.2} \gtrsim S^{-0.7+\beta_C} \,, \tag{4.8}$$

and[2]

$$\Gamma \sim S^{-1.7+\beta_\Gamma} \,. \tag{4.9}$$

From Eq. (4.8) it follows that in order to obey the constraint (4.3) on the S-dependence of C_m, the scaling of C_m with K must be bounded as

$$\beta_C \lesssim -0.3 \,. \tag{4.10}$$

Likewise, one sees from Eq. (4.9) that the rewriting-facilitated decay rate is as high as the Hawking rate, $\Gamma \sim 1$, only if

$$\beta_\Gamma \gtrsim 1.7 \,. \tag{4.11}$$

Let us investigate whether our numerical results for the K-scaling of C_m and Γ can accommodate the requirements of Eqs. (4.10) and (4.11). As a first method, let us confront the actual results for $K = 6, 8$ with the values for $K = 6, 8$ allowed by the combination of the result for $K = 4$ and the constraints Eqs. (4.10) and (4.11). For that purpose, in Fig. 3.4, we plot a curve through the rewriting value at $K = 4$ that saturates the bounds (4.10) and (4.11). Even though many rewriting values exist at $K = 6, 8$, it can be seen that none of them obeys both the bounds (4.10) and (4.11).[3]

[2] Since $\Delta N_c/S \to 0$, the rate Γ becomes independent of ΔN_c.

[3] In fact, none of them fulfills either condition, except for one data point at $K = 6$. It has a sufficiently high rate, but its coupling strength $C_m = 0.74$ is far too big to satisfy the bound (4.10).

As a second way to assess the compatibility, let us compare the constraints (4.10) and (4.11) with the estimates (3.36) and (3.37). Although β_C might be small enough, it can be seen that β_Γ is vastly different.

The above clearly indicates that for large black holes, Γ never achieves the speed corresponding to the rate of Hawking-radiation, $\Gamma \sim 1$. Therefore, within the parameter space we have been able to access, we can conclude that the semiclassical description breaks down when the memory burden sets in even if it is alleviated via rewriting.

A newly created black hole that has radiated away only a small fraction of its mass is expected to be described well by the semiclassical approximation and to thus decay with $\Gamma \sim 1$. As we have now seen, the investigated model (3.28) with black hole scalings fails this requirement, since rewriting does not sufficiently alleviate the memory burden effect and the onset of the latter is effectively immediate. Thus, in black holes, this onset must be delayed. Within the prototype model, an effective parametrization of such delay has been introduced in terms of the parameter p in (3.12). As discussed in 3.1.2, the onset of the memory burden effect can be delayed at most until n_0 has lost order one of its initial occupation, corresponding to the black hole losing order one of its initial mass.

When the memory burden effect does set in, we have seen that the decay rate slows down. Let us attempt to quantify this slowdown. For this, we are going to assume that Γ in the system (3.12) (with a parameter value $p \gg 1$ and including the coupling to another set of memory modes) behaves analogously to the system investigated here. From (3.9), we see that in order to realize $\Gamma \sim 1$ before the onset of backreaction, a coupling $C_0 \sim 1/S$ is needed. This modifies Eq. (4.9) as follows:

$$\Gamma \sim S^{-2.4+\beta_\Gamma} \,. \tag{4.12}$$

As discussed above, β_Γ cannot be reliably determined. However, we have found no indications that the rates Γ might grow with K (see Eq. (3.37)). It thus appears conservative to estimate $\beta_\Gamma \lesssim 0$. We are thus left with

$$\Gamma \lesssim \frac{1}{S^2} \,. \tag{4.13}$$

Therefore, in the absence of competing effects, a black hole's evaporation has to slow down dramatically at the latest after it has lost on the order of half of its initial mass.

4.1.3 Black Hole Metamorphosis

In light of our result, a pressing question is what the possible evolution of a black hole is beyond half-decay. The possibilities for such evolution are in stark contrast to what is rather commonly assumed, namely, that a black hole evaporates in self-similar fashion. More explicitly, based on extrapolation from the semiclassical result of thermal evaporation, a black hole is commonly described beyond half-decay in terms of a time-dependent mass $M(t)$, with corresponding time-dependent Schwarzschild-radius and temperature, $r_g =$

$2G_N M(t)$ and $T = (8\pi G_N M(t))^{-1}$. However, what is overlooked in such a description is the fact that the Hawking result is derived only in the limit

$$G_N \to 0,\ M \to \infty,\ r_g = \text{finite}\,. \tag{4.14}$$

In this limit, also $S \to \infty$. For finite-valued parameters, therefore, the semiclassical description necessarily breaks down before the black hole has evaporated completely. Quantitative arguments independent of the specific microscopic theory of a black hole have been provided in ref. [24]. The deviations from thermal emission are quantified by the order parameter $\dot{T}/T^2$, which from $\dot{M} \sim r_g^{-2}$ follows to be

$$\dot{T}/T^2 \sim 1/S\,. \tag{4.15}$$

One thus sees that only in the strict limit (4.14) thermality is recovered and a self-similar evolution is exact [82, 83]. Without committing to any microscopic model one can therefore not exclude that corrections to thermal emission of order $\sim 1/S$ do not accumulate to give an order-one effect over the course of $\sim S$ emissions. In other words, the built-in control parameter of the Hawking treatment (4.15) indicates a breakdown of the description after roughly half-decay.

Turning to the particular microscopic black hole model of the N-Portrait, we also find a mechanism of how the breakdown happens [19, 27, 25, 31]: After losing on the order of half of its constituent gravitons, the black hole state is maximally entangled. This results in a back-reaction strong enough for the semiclassical treatment to break down.

Yet another microscopic mechanism of departure from self-similar evolution due to quantum effects is discovered in the present study. The memory burden, to which black holes are expected to be subjected by virtue of being states of maximal entropy, induces a new source of quantum back-reaction. In that way, the information stored in the memory modes results in a quantum hair that has a significant influence at later stages via the memory burden effect. The classical no-hair theorems [84, 85, 86, 87, 88, 89, 90] do not constrain such quantum hair.

As we have found in our prototype model with parameter scalings appropriate to black holes, the decay rate has to slow down dramatically after half-decay. In principle, we can only speculate on what this implies for black hole evolution beyond half-decay. The two logical possibilities seem to be: 1) An effective stabilization due to a slow-down of the decay; 2) A classical transition into non-linear gravitational waves. The latter possibility arises since after the description in terms of a classical black hole stops being valid, one can no longer exclude a new classical instability occurring in the system. From now on, we are going to concentrate on the former possibility, which of course would have interesting implications in the context of dark matter studies.

Correspondingly, as a result of the slowed-down decay, from here on we are going to assume an extended black hole lifetime

$$\tilde{\tau} \gtrsim r_g S^{1+k}\,, \tag{4.16}$$

where k quantifies the slowdown of the evaporation as compared to the semiclassical rate, $\Gamma \sim r_g^{-1}$. The emission spectrum after half-decay is of course no longer a thermal one. Nevertheless, we are going to suppose a typical wavelength of emitted particles on the order of the initial Schwarzschild-radius $\sim r_g$ for as long as the mass of the black hole is on the order of the initial mass.

We would like to emphasize that we cannot exclude increased emission of much shorter wavelength particles once the memory burden has come into effect. The reason is that with increasing gap of the memory modes, their conversion into quanta with free dispersion becomes less suppressed. Such conversion may well be part of how a black hole's information gets released after it has lost a sizeable portion of its mass. This constitutes a specific mechanism for the release of information from the black hole after Page's time [91].

4.2 Small Primordial Black Holes as Dark Matter

There is a longstanding idea that dark matter could in part or fully consist of primordial black holes (PBHs) [92, 93, 94, 95]. In this context, an effective stabilization of black holes through the memory burden effect is expected to open up the parameter space. For a complete analysis of the constraints on the initial PBH abundances, one would of course need a more definite knowledge of the black hole evolution past half-decay. In the following, we are first going to present some qualitative considerations on how the constraint landscape is affected by quasi-stabilization. For a quantitative example, we then give estimates for one specific PBH mass.

4.2.1 Effects on Bounds

There is a large variety of bounds on PBH abundances, depending on their assumed mass spectrum (see ref.s [96, 13] for a review). Both the strength and the extent in the mass of many of the bounds are rooted in the naive extrapolation of the semiclassical approximation. If the assumption of Hawking evaporation until the end of a black hole's life is dropped the parameter space is correspondingly reshaped significantly.

Assuming Hawking evaporation past half-decay, one obtains that PBHs with masses $M \lesssim M_* \equiv 5 \cdot 10^{14} g$ would have vanished until today[13]. On the other hand, an effective stabilization setting in around half-decay allows also smaller PBHs to persist until the present epoch. Therefore, many of the bounds on masses $M \lesssim M_*$ are changed. Specifically, a new mass range below M_* of PBHs as dark matter is now allowed. Let us now qualitatively discuss examples of how existing constraints are altered. We start with bounds coming from the observation of the galactic gamma-ray background, using as guidance ref. [97]. Due to the relative proximity, photons from PBHs in the Milky Way halo would mostly be due to instantaneous emission rather than past emission. Therefore the range of existing bounds here naively includes only masses $M \gtrsim M_*$. Since the extrapolation of Hawking evaporation throughout the black hole evolution results in a final speed-up of radiation, the strongest bound is on M around M_*. By contrast, a slowdown of evaporation

around half-decay would strongly relax the bound close to M_*, since PBHs of such initial masses would already be in the stabilized phase. Similarly, the newly opened-up range of masses $M \lesssim M_*$ would be mildly bounded by observations of the galactic gamma-ray background. On the flip side, the continued emission of such small PBHs would in principle also allow for their detection. We are going to return to this in our quantitative example.

For another illustration, we can look at the effects on bounds coming from BBN, following ref. [98]. With Hawking evaporation valid throughout a black hole's life, PBHs with masses $M \lesssim M_N \equiv 10^{10}$g would have vanished by the onset of BBN. Thus their abundance is commonly regarded as unbounded by BBN. If, however, such small PBHs still exist at that time due to a slowdown after half-decay, there are again bounds implied by BBN. Similarly to the situation of the diffuse galactic photons, the bounds in this mass range can be expected to be rather mild, because the PBHs by the time would already have been slowed down in their decay. Also similarly to the galactic gamma-ray background, the strongest BBN bound on the masses $M \sim M_N$ would be relaxed. BBN bounds on masses $M \gg M_N$ are unaffected by memory burden, since for the early stage of evaporation the semiclassical approximation is still good.

4.2.2 Specific Example

We now look at a specific example where estimates indicate that small PBHs with $M \ll M_*$ can account for all of the dark matter. We would like to emphasize that we are merely providing rough estimates and neither try to revisit all the various bounds nor look at the entire mass range. For this purpose, let us take the case of PBHs with a monochromatic spectrum at $M \sim 10^8$g. Taking into account our numerical result (4.13), for definiteness, we are going to suppose a slowed down rate $\tilde{\Gamma}$ of black hole evaporation due to the set-in of memory burden by two powers of the initial black hole entropy: $\tilde{\Gamma} \sim r_g^{-1}/S^2$. For the black hole lifetime, this corresponds to $k = 2$ in (4.16), meaning that the extended lifetime $\tilde{\tau}$ is given by $\tilde{\tau} \gtrsim S^2\tau$. Here, τ is the common lifetime obtained from the extrapolated semiclassical evolution (see e.g., ref. [13]). For our mass example, that leads to $\tilde{\tau} \gtrsim 10^{49}$ s, which of course by far exceeds the age of the present universe.

We are going to look at two types of bounds on the possible PBH abundance. The first kind of constraints are unrelated to black hole evaporation and thus are the same as for MACHOs with the same mass. To the best of our knowledge, the abundance of MACHOs of $M \sim 10^8$g is unbounded (see e.g., ref.s [13, 99]). As a side remark, such bounds would be similar to those for N-MACHOs [100]. In the remainder of this section, we are going to consider the second category of constraints, which is related to the fact that the PBHs radiate, albeit with a slowed-down rate.

Let us estimate whether the detection of photons can bound the exemplary PBH scenario. As reasoned earlier, the expected energy of particles radiated by the slowed-down black hole is still on the order of the initial black hole temperature, $T_{\rm BH} = M_p^2/(8\pi M) \sim 10^5$ GeV. Let us first consider the galactic gamma-ray background. If the Milky Way halo

is largely constituted by PBHs, we can estimate that they cause a diffuse photonic flux of

$$\Phi \sim n_{\mathrm{BH}}\, R\, \tilde{\Gamma} \sim 10^{-34}/(\mathrm{cm}^2\mathrm{s})\,, \tag{4.17}$$

where $R \sim 2 \cdot 10^{24}\,\mathrm{cm}$ is the typical radius of our galaxy's halo and n_{BH} is the number density of PBHs in there. The density is roughly given in terms of the Milky Way mass $M_{\mathrm{MW}} \sim 2 \cdot 10^{42}\,\mathrm{kg}$ as $n_{\mathrm{BH}} \sim M_{\mathrm{MW}}/(MR^3)$.

The above estimate corresponds to about one photon hitting our planet in 10^8 years and thus appears far below reliable detection thresholds. Indeed, to the best of our knowledge, no observational lower bounds exist for the diffuse flux of photons with energy $E_\gamma \sim 10^5\,\mathrm{GeV}$. For comparison, in the case of $E_\gamma \sim 10^3\,\mathrm{GeV}$, the flux is observed to be on the order of $10^{-10}/(\mathrm{cm}^2\mathrm{s})$ [101].

The above consideration pertains to the direct emission of photons. There is also secondary photon emission, resulting from other emitted particles that subsequently decay into photons. This kind of photon emission is dominated by pion decay. However, the effective rate for secondary emission is only higher than the primary rate by an order of magnitude, $\tilde{\Gamma}_S \sim 10\tilde{\Gamma}$ (see ref. [97]). In conclusion, therefore, the galactic gamma-ray background does not appear to constrain our mass example.

Now let us consider the extra-galactic gamma-ray background as a possible source of bounds. If cold dark matter is mostly due to PBHs of our exemplary mass, they will cause a flux due to secondary photon emission which is roughly given by (see ref. [98])

$$\Phi \sim \frac{\rho_{\mathrm{DM}}}{M}\tilde{\Gamma}\, t_0 \sim 10^{-31}/(\mathrm{cm}^2\mathrm{s})\,. \tag{4.18}$$

Here, $\rho_{\mathrm{DM}} \sim 2 \cdot 10^{-30}\,\mathrm{g/cm}^3$ is the present energy density of dark matter in the Universe and $t_0 \sim 4 \cdot 10^{17}\,\mathrm{s}$ is the age of the Universe. Like in the galactic case, the minuteness of this flux does not allow for observational exclusion. The above flux is only due to secondary photon emission because there exists a cosmic gamma-ray horizon effectively absorbing the primarily emitted photons (see e.g., ref. [102]).

As for the detection of particles other than photons, no constraints appear to arise for our PBH mass example either, unless their emission were to drastically exceed photon emission.

In summary, none of the observations we have considered puts a bound on our numerical example of PBHs of mass $M \sim 10^8\mathrm{g}$ and thus it appears that such PBHs can constitute all dark matter. As we have remarked, this does not constitute a full investigation.

In closing, we remark that apart from the constraints considered above, there is a third category of constraints. In the case of a direct encounter of a black hole with our planet, the related gravitational and seismic disturbances provide another detection mechanism. Seismic perturbations have been considered in ref. [103] for the case of PBHs of $M \gg M_*$. In the case of smaller PBHs as enabled by stabilization after half-decay, their number would be higher and thus encounters would occur more often. Therefore, it is possible that for some range of small masses, PBHs are much more easily detected via direct encounter as compared to via particle emission.

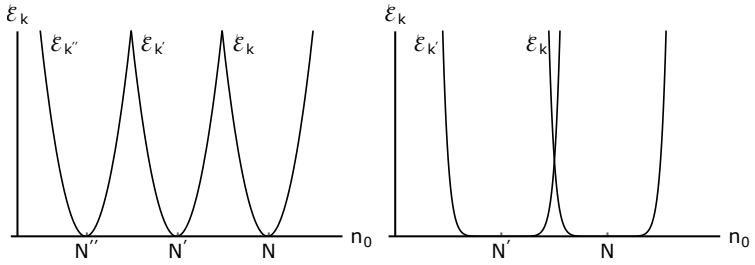

(a) Small p. (b) Large p.

Figure 4.1: Highly schematic plots (for even values of p) of the energy thresholds of the memory modes for the case of black holes. Different degenerate minima exist, corresponding to different possible black hole masses.

4.3 De Sitter

The application to de Sitter spacetime and to the inflationary stage of the universe can proceed with a high degree of analogy to the above application to black holes. An important difference is related to the fact that, for the case of pure de Sitter spacetime, the positive vacuum energy density Λ represents a fixed *theory* parameter. By contrast, the black hole mass constitutes a state parameter, with different possible values allowed within the same theory. The energy landscape for the memory modes corresponding to the black hole case is qualitatively shown in fig. 4.1.

For pure de Sitter on the other hand, minima that potentially exist for values $n_0 = N_c', N_c'', \ldots$ must not be degenerate with the minimum at N_c, which is set by Λ, but instead must lie higher. This is required by the matching to the semiclassical description of de Sitter. Correspondingly, the offset among the minima in the semiclassical limit, $S \to \infty$, must scale in such a way that only the minimum $n_0 = N_c$ survives.

This may be parametrized in terms of the following modification of the part of the Hamiltonian describing the memory sectors and their interaction with the control mode:

$$\Delta\hat{H} = \left(1 - \frac{\hat{n}_0}{N_c}\right)^p \sum_{k\neq 0} \epsilon_k \hat{n}_k + \left(\left(1 - \frac{\hat{n}_0}{N_c'}\right)^p + \left(1 - \frac{\hat{n}_0}{N_c}\right)^q\right) \sum_{k'\neq 0} \epsilon_{k'}' \hat{n}_{k'}' + \ldots . \tag{4.19}$$

Here, $q > 0$ and otherwise unknown. The resulting qualitative energy landscape is shown in Fig. 4.2.

For inflation, H is determined by the interaction with the inflaton degree of freedom. For as long as de Sitter represents a good approximation to the slow-rolling inflationary spacetime, the situation is the same as for pure de Sitter.

If the offsets quantified by q are significant, rewriting is suppressed and thus the memory burden effect is inevitable. If they are negligible, there is in principle the chance of rewriting. Motivated by the latter possibility, let us investigate the possible speed of rewriting-facilitated decay of de Sitter.

The scaling of the parameters in the model (3.16) that is appropriate to de Sitter is completely analogous to the case of black holes and given in terms of the Hubble scale H

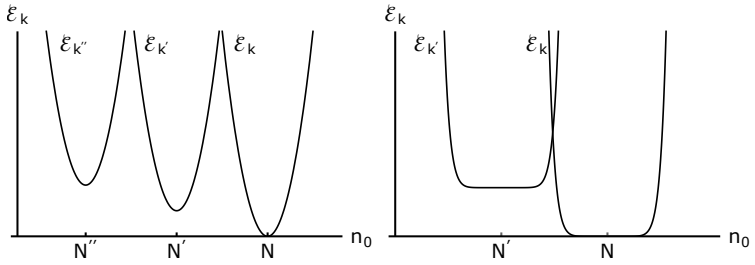

(a) For small p, the minima are narrow.

(b) For large p, the minima are wide.

Figure 4.2: Highly schematic plots (for even values of p) of the energy thresholds of the memory modes in a theory with cosmological constant. Only around a single value of n_0 gapless modes emerge.

and the de Sitter entropy $S = M_P^2/H^2$. The Gibbons-Hawking radiation is characterized by the temperature $T \sim H$ and thus we have $\epsilon_0 = H$. Since the number of memory modes K scale as the entropy, we also have $K \sim S$. The total energy contained in a de Sitter patch is given by $E_{dS} \sim SH$, which motivates the choice $N_c \sim S$. As for the free gaps of the memory modes, ϵ_k, they can again be determined without committing to an explicit microscopic description. The quantum numbers of the memory modes are constrained by the de Sitter symmetry that must be present in the classical limit. In particular, the presence of spherical symmetry allows for the same argument as in the case of black holes, implying $\epsilon_m \sim \sqrt{S}\epsilon_0$. Likewise, regarding the parameters C_0, C_m, and ΔN_c, the arguments of the case of black holes apply and therefore they are bounded in the same way in terms of ϵ_0 and S.

Therefore, the conclusions for the possibility of rewriting in de Sitter coincide with those for black holes: The parameter p must be high enough to allow for an initial phase of near-semiclassical evolution by delaying the onset of the memory burden. After a number of $\sim S$ emissions, the memory burden sets in, and rewriting is too slow to effectively circumvent it: The rate is slowed down by at least a factor of $1/S^2$. Alternatively, the offsets in (4.19) parametrized by q are strong enough to eliminate rewriting altogether.

As with BHs, we can of course not exclude the onset of other effects of quantum backreaction. However, what can be excluded is the particular case of an appearance of a classical instability leading to a disintegration into gravitational lumps. In contrast to BHs, this is not possible for de Sitter since the latter is tied to a source and furthermore is not localized.

In any case, after $t_Q \sim SH^{-1}$, Gibbons-Hawking radiation effectively stops. The growth of the effective gaps of the memory modes at the same time enhances the rate of information release via the coupling (4.4), manifesting in non-thermal particle creation. Both effects combine to a deviation from the semiclassical evolution given by the thermal Gibbons-Hawking radiation.

4.4 Summary

The present study constitutes a quantitative analysis following ideas of ref. [28]. As has been argued there (for more references, see the introduction II), systems with a high memory capacity, which include systems with high entropy, at the microscopic level are in a state around which it possesses near-gapless degrees of freedom. The corresponding near-vanishing energy cost of storing quantum information in those modes gives rise to the effective degeneracy of a high number of states. When such a system moves away from that state, which in particular must happen in the course of a decay of the system, the increasing energy cost of the memory results in a backreaction resisting such evolution. This is the so-called memory burden effect [28], which is universal to such systems. In particular, this effect has to be present in de Sitter and black holes as systems of maximal entropy.

It has been argued [28] that in the absence of an efficient way of releasing the stored quantum information to the environment, there is only one possible way of avoiding or alleviating the memory burden effect after its onset. Namely, if the system can synchronize the decay with rewriting the information onto another set of degrees of freedom, which become gapless at a later stage of the decay. The aim of the present work has been to quantify the possible speed of such rewriting-facilitated decay. To this end, we have investigated a prototype system, which has been proposed in ref. [28] as the simplest possible model that exhibits memory burden as well as the possibility of rewriting. Such a model of course does not constitute a full microscopic description of the more complicated systems like black holes or de Sitter. Correspondingly, we cannot capture or exclude the onset of potential further effects of quantum backreaction in those systems. Instead, the model promises to capture the universal aspects of the memory burden effect.

For the application to black holes and de Sitter, we have argued that for either case, most of the model parameters are constrained by their appropriate scaling with the entropy S. With those scalings, the results of our numerical time-evolution of the model reveal that rewriting-powered decay is by far not fast enough to account for the initial stage of near-semiclassical particle emission of black holes or de Sitter and thus the memory burden effect in those systems has to set in with a delay. We have argued that the onset must take place the latest after $\sim S$ emissions. For the time of the onset, t_Q, our results imply a drastic slowdown of the decay rate, as shown for example in (4.13). We have argued that the increased gaps of the information-carrying modes also lead to a reduced suppression of the release of the stored quantum information to the environment. Both the slowdown and the information release constitute a deviation from the semiclassical thermal particle creation.

Regarding an inflationary phase of the universe, we can be sure that the graceful exit has taken place before t_Q because the semiclassical description of de Sitter can accommodate observations with good accuracy. However, if the duration of inflation has come close enough to t_Q, the beginning deviations from the semiclassical evolution will manifest in detectable imprints in the primordial density fluctuations. A quantitative analysis requires a separate investigation. Remarkably, the quantum information accessible in this way is

one that cannot be erased by an inflationary evolution and thus constitutes a primordial cosmic memory.

For black holes, our findings imply in particular that a black hole that has lost half of its mass is not equivalent to a young black hole of the same mass. Instead, the information stored constitutes a quantum hair, whose effect becomes strong at later stages of the decay. We have pointed out that due to the breakdown of the classical description after t_Q, a plausible candidate for a competing strong effect of quantum backreaction is given by the appearance of a classical instability, giving rise to the disintegration of the black hole into nonlinear gravitational waves. As pointed out in sec. 2.6, such instability may give rise to an additional instability in the form of non-gradual quantum decay. Both the scenario of extreme slowdown of decay and that of destabilization constitute a dramatic deviation from a self-similar evolution of a black hole. An effective stabilization due to a slowdown has interesting consequences for the dark matter candidacy of primordial black holes (PBHs). Small PBHs, that are commonly assumed to have evaporated by now or earlier, would instead still be present. Thus, a commonly excluded parameter space would be reopened. To demonstrate this, we have considered a specific numerical example for which stabilized small PBHs appear to be able to constitute all of the dark matter.

Appendix A

Appendix Part I

In this appendix, we are going to provide the details to the perturbative quantum calculations of part I.

A.1 General Relations

Combinatorics and factorization of amplitude

For definiteness, the following discussion is going to refer to the first example, i.e., the example of section 2.2. We comment on the extension to the other cases where needed.

The rate is given in terms of the amplitude A as

$$\Gamma_{n\phi\to 2\chi} = \frac{1}{T}\int d\Pi_{2\chi}\left|A\,\delta^4\left(\ldots\right)(2\pi)^4\right|^2 , \tag{A.1}$$

where the integration is over the phase space of the two final particles. In the case where several particles in either the initial or final state belong to the same *species*, the same Wick contraction generally gives rise to several different diagrams. A simple example of this would be the $t-$ and $u-$channel of $e^+e^-\to\gamma\gamma$. The number of different diagrams corresponds to the number of different distributions of the identical particles on the external legs. These arise upon projecting a given Wick contraction on the initial and final state. The number of diagrams may grow as strongly as factorially with the number of identical particles n in an external state, as can be seen as follows. It is convenient to assume the normalization

$$\left[\hat{a}_{\vec{k}},\hat{a}^\dagger_{\vec{q}}\right] = \frac{(2\pi)^3}{V}\delta^3\left(k-q\right) , \tag{A.2}$$

for which number eigenstates have unit norm. Via canonical commutation of the field operator this implies

$$\hat{\phi}^+(x) = \int\frac{d^3k}{(2\pi)^3}\sqrt{\frac{V}{2\omega_k}}e^{-ikx}\hat{a}_{\vec{k}}\,,\quad \hat{\phi}=\hat{\phi}^+ + h.c.\,. \tag{A.3}$$

Projecting a given Wick contraction on an external state of n identical particles which all are in a different 1-particle state involves the structure

$$\prod_{j=1}^{n} \hat{\phi}^{+}(x_j) \prod_{m=1}^{n} \hat{a}^{\dagger}_{\vec{q}_m} \; |0\rangle = n! \prod_{j=1}^{n} \frac{e^{-iq_j x_j}}{\sqrt{2\omega_{q_j} V}} |0\rangle \,, \tag{A.4}$$

where all the $\vec{q}_m$ are supposed to be different. The factor of $n!$ at the level of the unsquared amplitude can be seen to emerge. In the case of the n particles being in the final state, the phase space integration over n identical particles comes of course with an extra factor of $1/n!$ at the level of the amplitude squared.

In the case of n identical particles in the initial state, it is possible that some of them are in the same one-particle state or *mode*. In the extreme case of all n identical bosons occupying the same mode, one has a reduction of the effective multiplicity by a factor of $n!^{-1/2}$, as can be seen from

$$\prod_{j=1}^{n} \hat{\phi}^{+}(x_j) \frac{\left(\hat{a}^{\dagger}_{\vec{p}}\right)^n}{\sqrt{n!}} \; |0\rangle = \frac{n!}{\sqrt{n!}} \frac{e^{-ip\sum_{j=1}^{n} x_j}}{(2\omega_p V)^{n/2}} |0\rangle \,. \tag{A.5}$$

This is the relevant case for the process $n \to 2$ with condensate kinematics. In that case, all the diagrams are actually the same and there is literally just an effective multiplicity of $n!^{1/2}$ at the amplitude level. In the same way, the leading order diagram relevant to the process of the second example $(n/2, n/2 \to 2)$ comes with an effective multiplicity of $(n/2)!^{2/2}$.

Due to the above, a convenient way of bookkeeping in the case we approximate A in terms of only one specific shape of Wick contraction is the following:

$$A = \frac{W}{v!} \cdot S_i \cdot S_f \cdot d \,. \tag{A.6}$$

Here, v is the number of vertices and the factor $1/v!$ is the expansion coefficient in the Dyson series for the S-matrix operator at order v, W is the number of Wick contractions giving rise to the same shape, S_i and S_f are the effective multiplicities of the diagram resulting from the mechanism of (A.5). d is the value of the diagram itself and can be factorized as

$$d = N \cdot D \cdot E \,, \tag{A.7}$$

where N is the product of numerators of propagators, vertices, and polarizations of external particles; D is the factor due to the denominators of propagators; E a factor due to the external particles except for their polarizations. For the kinematics under consideration,

$$nm = \left(m_\chi^2 + k^2\right)^{1/2} \,, \tag{A.8}$$

the latter is always (also for the processes in examples 2 and 3) given by

$$E = (2mV)^{-\frac{n}{2}} (nmV)^{-1} \,. \tag{A.9}$$

Initial-state Bose enhancement

For the generic case, in which part of the initial N condensate bosons go unscattered,

$$N \to (N-n) + 2\,, \tag{A.10}$$

there is an effective combinatoric enhancement. To see how it depends on N and n, we observe

$$\begin{aligned}\langle n'_{\vec{p}}| \prod_{j=1}^{n} \hat{\phi}^+(x_j) |(n+n')_{\vec{p}}\rangle &= \langle n'_{\vec{p}}| \sqrt{\frac{(n+n')!}{n'!}\frac{n!}{n!}} \frac{e^{-ip\sum_{j=1}^{n} x_j}}{(2\omega_p V)^{n/2}} |n'_{\vec{p}}\rangle \\ &= \binom{n+n'}{n}^{1/2} \langle 0| \prod_{j=1}^{n} \hat{\phi}^+(x_j) |n_{\vec{p}}\rangle\,, \end{aligned} \tag{A.11}$$

where in the last equality, (A.5) has been used.

The same result is obtained at order g^{2n} and with the kinematics (A.8) when including into the PSI the final $n' = N - n$ ϕ-particles. In that case the additional $n'!^{-1}$ from the PSI is balanced by the additional factor of $\sqrt{n'!}$ appearing at the amplitude level:

$$\frac{1}{n'!}\left(\prod_{j=1}^{n'} \frac{V}{(2\pi)^3}\int d^3q_j\right) \left|\langle \vec{q}_1, \vec{q}_2, \ldots, \vec{q}_{n'}|n'\rangle\right|^2 = 1\,, \tag{A.12}$$

as can be seen using (A.2) and (A.5).

Therefore, the rate for the process (2.8) in examples 1 and 3 is given by

$$\Gamma \equiv C_{Nn}\Gamma_{n\to 2}\,, \quad C_{Nn} = \binom{N}{n}\,. \tag{A.13}$$

Similarly, for the process of example 2,

$$\frac{N}{2} + \frac{N}{2} \to \frac{N-n}{2} + \frac{N-n}{2} + 2\,, \tag{A.14}$$

the rate is given by

$$\Gamma \equiv C_{Nn}\Gamma_{\frac{n}{2},\frac{n}{2}\to 2}\,, \quad C_{Nn} = \binom{N/2}{n/2}^2\,. \tag{A.15}$$

Final-state Bose enhancement

In this appendix, we are going to derive (2.19), the effective Bose enhancement for the process (2.8) that arises due to preexisting nonzero occupation of the created χ-modes. This represents simply a generalization of derivation for the case of $n = 2$, which can be found in ref. [104]. An analogous consideration goes through for the processes examples 2 and 3.

Because of unbroken rotation invariance, one has for the expected number of created χs $n_{\vec{k}} = n_{-\vec{k}} = n_k$, where $n_{\vec{k}} \equiv \langle t_0|\hat{a}^\dagger_{\vec{k}}\hat{a}_{\vec{k}}|t_0\rangle$ and $k \equiv |\vec{k}|$. When taking into account processes of χs going to ϕs, it is important to note that processes with ϕ-quanta in modes $\vec{k} \neq 0$ have a lesser number of factors of N compared to g^2. Therefore the rate of those processes vanishes in the limit (2.1). For finite N, these processes are of course sources of quantum breaking. For sufficiently large N, it is enough to consider only the processes of condensate re-population. A given momentum k kinematically fixes the number n of ϕ-quanta either annihilated or created. The time-evolved state $|t\rangle$ will in general feature entanglement as well as a mean number of ϕs smaller than N. As an approximation for large N, we may still take $|t\rangle$ as a number state $|N, n_k\rangle$, i.e., a state with χ-occupation of n_k for all $|\vec{k}| = k$, as well as a number N of condensate ϕ-quanta. The possible further conversions in either direction are then

$$N\phi + 2n_k\chi \to (N-n)\,\phi + 2\,(n_k+1)\,\chi \tag{A.16}$$

and

$$(N+n)\,\phi + 2\,(n_k-1)\,\chi \leftarrow N\phi + 2n_k\chi\,. \tag{A.17}$$

The effective rate of χ-creation is then given by the difference

$$\Gamma_{\mathit{eff}} \equiv \dot{n}_k = \Gamma_\to - \Gamma_\leftarrow = \Gamma_{n\phi\to 2\chi}(f_\to - f_\leftarrow)\,, \tag{A.18}$$

where the factors $f_\to, f_\leftarrow$ are due to both initial-state and final-state combinatoric enhancement. Their dependence on N, n, n_k is derived below. Importantly, $\Gamma_\leftarrow$ results from integrating over the two χ-momenta just as $\Gamma_\to$ and hence they have the *same* kinematic factor $\sqrt{s-4m_\chi^2}$:

$$\Gamma_{n\phi\to 2\chi} = \frac{1}{T}\int d\Pi_{2\chi}\left|A\,\delta^4\,(\ldots)\,(2\pi)^4\right|^2\,, \tag{A.19}$$

where m_χ^2 may include the condensate contribution in the time-dependent or time-averaged form. The combinatorics related to the matrix elements are

$$\begin{aligned} n!\cdot 1!^2\cdot f_\to &\equiv \left|\langle (N-n)(n_k+1)^2|\hat{b}^n\hat{a}^\dagger_{-\vec{k}}\hat{a}^\dagger_{+\vec{k}}|Nn_k^2\rangle\right|^2 = N(N-1)\cdots(N-n+1)(n_k+1)^2 \\ &= n!\cdot\binom{N}{n}\cdot 1!^2\cdot\binom{n_k+1}{1}^2 \end{aligned} \tag{A.20}$$

and

$$\begin{aligned} n!\cdot 1!^2\cdot f_\leftarrow &\equiv \left|\langle (N+n)(n_k-1)^2|(\hat{b}^\dagger)^n\hat{a}_{-\vec{k}}\hat{a}_{+\vec{k}}|Nn_k^2\rangle\right|^2 = (N+1)(N+2)\cdots(N+n)n_k^2 \\ &= n!\cdot\binom{N+n}{n}\cdot 1!^2\cdot\binom{n_k}{1}^2\,. \end{aligned} \tag{A.21}$$

The factors $n!\cdot 1!\cdot 1!$ are left explicit, because they are already included in $\Gamma_{n\phi\to 2\chi}$ and therefore not to be included in the fs. We therefore have

$$f_\to - f_\leftarrow = (n_k+1)^2\binom{N}{n} - n_k^2\binom{N+n}{n} = \binom{N}{n}\left(n_k^2 - n_k^2 + 2n_k + 1 + \mathcal{O}\left(\frac{n^2n_k^2}{N}\right)\right)\,. \tag{A.22}$$

Thus, absorbing the initial state Bose enhancement into the definition $\Gamma \equiv \binom{N}{n} \Gamma_{n\phi\to 2\chi}$, one has due to the final state Bose enhancement

$$\dot{n}_k \sim (1 + 2n_k)\,\Gamma\,, \tag{A.23}$$

and for $n_k \gtrsim 1$, one has a time-evolution approximately given by $n_k \sim \exp(2\Gamma t)$.

Phase space integration

For a scalar condensate initial state from examples 1 and 2, there is no angular momentum and the phase space integration is trivial. Including the final state factor of E, it gives

$$\frac{1}{2!}\left(\frac{V}{(2\pi)^3}\int d^3p\right)^2 (2E_pV)^{-2}(2\pi)^4\delta^4(\ldots)\,VT = \frac{1}{16\pi}VT\sqrt{1-\frac{n_0^2}{n^2}}\,, \tag{A.24}$$

where $1/2!$ is present only for the two final particles of the same species.

Uniform representation of result

For convenience, the result can be organized by strength of scaling with n in the following way:

$$\Gamma_{n\to 2} = Kn^A\sqrt{1-\frac{n_0^2}{n^2}}B^n n^{Cn}\,. \tag{A.25}$$

A.2 Leading Order Diagram for Case 1

For calculation in the $\phi^2\chi^2$-case, the following relations apply. The first factor in (A.6) contributes

$$\frac{W}{v!} = \frac{2^v v!}{v!}, \quad v = n/2\,. \tag{A.26}$$

The effective multiplicities in (A.6) are

$$S_i \cdot S_f = \frac{n!}{n!^{1/2}}\cdot 2!\,. \tag{A.27}$$

The propagators contribute to d the factor

$$D = \prod_{l=1}^{n/2-1}\left(q_l^2 - m_\chi^2\right)^{-1} = (-1)^{n/2-1}m^{2-n}\,n^2\,2^{-n}\,(n/2)!^{-2}\,, \tag{A.28}$$

where q_l^μ denote the the virtual momenta in the diagram. The vertices merely contribute

$$N = \left(\frac{g^2}{\mathcal{N}_c}\right)^v\,. \tag{A.29}$$

Due to the absence of angular momentum of the initial state, the phase space integration is trivial and is given by (A.24). The resulting tree-level rate for $n\phi \to 2\chi$ for $\mathcal{N}_c = 1$ is thus

$$\Gamma_{n\phi\to 2\chi} = \frac{1}{4\pi} V m^4 \sqrt{1-\frac{n_0^2}{n^2}}\, n^4 \left(\frac{g^2}{4Vm^3}\right)^n \frac{n!}{(n/2)!^4}\,. \tag{A.30}$$

A.3 Leading Order Diagram for Case 2

For calculation in the first scalar QED example, the following relations apply. The first factor in (A.6) contributes again

$$\frac{W}{v!} = \frac{2^v v!}{v!}, \quad v = n/2\,. \tag{A.31}$$

Due to the distinguishability of s^+ and s^-, the effective multiplicities in (A.6) are now

$$S_i \cdot S_f = \frac{(n/2)!^2}{(n/2)!} \cdot 2!\,. \tag{A.32}$$

The denominators of propagators are the same as in the previous case and thus again

$$D = \prod_{l=1}^{n/2-1} \left(q_l^2 - m_\chi^2\right)^{-1} = (-1)^{n/2-1} m^{2-n}\, n^2\, 2^{-n}\, (n/2)!^{-2}\,, \tag{A.33}$$

where q_l^μ denote the the virtual momenta in the diagram. The product of vertices and numerators of the propagators is different from the previous case only by the scalar product of the external polarizations, $\epsilon_\mu^*(k,r)\epsilon^{*\mu}(k',r') \equiv \epsilon^{*2}$ such that

$$N = g^{2v}\epsilon^{*2}\,. \tag{A.34}$$

The phase space integration is again given by (A.24) and thus the resulting tree-level rate for $\frac{n}{2}s^- + \frac{n}{2}s^+ \to 2\gamma$ is

$$\Gamma_{\frac{n}{2},\frac{n}{2}\to 2\gamma} = \frac{1}{4\pi} V m^4 \sqrt{1-\frac{n_0^2}{n^2}}\, n^4 \left(\frac{g^2}{4Vm^3}\right)^n \frac{\sum_{r,r'} |\epsilon^{*2}|^2}{(n/2)!^2}\,. \tag{A.35}$$

The effective rate $\Gamma = C_{Nn}\Gamma_{\frac{n}{2},\frac{n}{2}\to 2\gamma}$ is the same as in the scalar case despite the absence of the factor $\frac{n!}{(n/2)!^2} \sim 2^n$ in the above result. This factor is compensated by the different relation of N and ϕ_0 (due to the different normalization of the mass term).

A.4 Leading Order Diagrams for Case 3

The process is $n\gamma \to s^+s^-$, where we consider all photons in the same linear polarization. For such polarization, both the 3- and the 4-vertex are non-zero. Thus the leading order amplitude can be split as

$$A_n = \sum_{j=0}^{n/2} \delta A_{j,n-j}\,, \tag{A.36}$$

where $\delta A_{j,n-j}$ is based on the sum of diagrams with a number j of 4−vertices and $2n-2j$ of 3−vertices. In the following we are going to find $\delta A_{n,0}$ and $\delta A_{0,n}$, based on the diagrams with all-4-vertices and all-3-vertices, respectively. The approximation of the rate based on only $\delta A_{n,0}$ is denoted as $\delta\Gamma_4$ and that based on $\delta A_{0,n}$ as $\delta\Gamma_3$.

Calculation of $\delta A_{0,n}$

The number n could be odd but has to be even for comparison with $\delta A_{n,0}$. In the factorization (A.6), one has

$$\delta A_{0,n} = \frac{W}{v!}\cdot\frac{n!}{\sqrt{n!}}\cdot 1\cdot d_{0,n}\,, \tag{A.37}$$

where $W = v! = n!$. For the product of propagator denominators contributing to $d_{0,n}$, one has

$$D = \prod_{l=0}^{n-1}\frac{i}{q_l^2 - m_e^2} = i^{n-1}\frac{(-1)^{n-1}n^2m^2}{m^{2n}n!^2}\,, \tag{A.38}$$

where $q_l^\mu = lm\delta_0^\mu - k^\mu$ is the virtual momentum in the propagator after the lth insertion of a single external photon leg. Therefore, using the Stirling approximation for the factorial,

$$|D|^2 \sim \frac{m^4}{4\pi^2}n^2\frac{e^{4n}}{m^{4n}}\frac{1}{n^{4n}}\,. \tag{A.39}$$

For the product of vertices N, one has

$$N = \prod_{l=1}^{n}(-ig)\,\epsilon_\mu(p)\left(q_{l-1}^\mu + q_l^\mu\right) = (-ig)^n\left(-2(-k_z)\right)^n = \tag{A.40}$$

$$= (-ig)^n\left(2\cos\theta\frac{\sqrt{s}}{2}\sqrt{1-\frac{n_0^2}{n^2}}\right)^n \tag{A.41}$$

and therefore

$$|N|^2 = \left(1-\frac{n_0^2}{n^2}\right)^n g^{2n}m^{2n}n^{2n}\left(\cos\theta\right)^{2n}\,. \tag{A.42}$$

The trivial part of the phase space integration (PSI) over E^2 and $|(2\pi)^4\delta^4(\ldots)|^2$ gives $(\delta^4(0) = VT/(2\pi)^4)$

$$(2mV)^{-n}\left(\frac{V}{(2\pi)^3}\int\frac{d^3k}{2E_kV}\right)^2(2\pi)^4\delta^4\left(\ldots\right)VT\left(\cos\theta\right)^{2n} = \tag{A.43}$$

$$= (2mV)^{-n}\frac{1}{8\pi}VT\sqrt{1-\frac{n_0^2}{n^2}}\frac{1}{4\pi}\int d\Omega\left(\cos\theta\right)^{2n}\,. \tag{A.44}$$

The remaining $\cos\theta$-dependent part of the PSI is

$$\frac{1}{4\pi}\int d\Omega\left(\cos\theta\right)^{2n} = \frac{1}{4\pi}2\pi\frac{2}{2n+1} = \frac{1}{2n}\left(1+\mathcal{O}\left(1/n\right)\right)\,. \tag{A.45}$$

There is no symmetry factor, because the final particles are not identical. For bookkeeping purposes, below, the contributions to the quantities K, A, B, C from the representation (A.25) below are ordered by origin as contribution from combinatorics and factor $1/T$, trivial $\cos\theta$-independent PSI, $\cos\theta$-dependent PSI, $\cos\theta$-independent part of $|N|^2$, $\cos\theta$-independent part of $1/|D|^2$:

$$B = 1 \cdot \frac{1}{2mV} \cdot 1 \cdot g^2 m^2 n^2 \sqrt{1 - \frac{n_0^2}{n^2}}^2 \cdot \frac{e^4}{m^4 n^4} \tag{A.46}$$

$$B^n = \left(\frac{e^4}{2}\frac{g^2}{Vm^3n^2}\right)^n \left(1 - \frac{n_0^2}{n^2}\right)^n \tag{A.47}$$

$$A = 0 + 0 - 1 + 0 + 2 = 1 \tag{A.48}$$

$$K = \frac{1}{T} \cdot \frac{1}{8\pi} VT \cdot \frac{1}{2} \cdot 1 \cdot \frac{m^4}{4\pi^2} = \frac{1}{64\pi^3} V m^4 \tag{A.49}$$

Calculation of $\delta A_{n,0}$

n is even. The contribution $\delta A_{n,0}$ factorizes as:

$$\delta A_4 = \frac{W}{v!} \cdot \frac{n!}{\sqrt{n!}} \cdot 1 \cdot d_{n,0}\,, \tag{A.50}$$

where $W = v! = (n/2)!$ The product of propagator denominators contributes to $d_{n,0}$ the factor

$$D = \prod_{l=0}^{n/2-1} \frac{i}{q_l^2 - m_e^2} = i^{n/2-1} \frac{(-1)^{n/2-1} n^2 m^2}{m^n 2^n \left(\frac{n}{2}\right)!^2}\,. \tag{A.51}$$

Therefore, using the Stirling approximation for the factorial,

$$|D|^2 \sim \frac{m^4}{\pi^2} n^2 \frac{e^{2n}}{m^{2n}} \frac{1}{n^{2n}}\,. \tag{A.52}$$

For N, one has

$$N = \prod_{l=1}^{n/2} \left(-ig^2\right) \epsilon^2(p) = i^{n/2} g^n\,, \quad |N|^2 = g^{2n}\,. \tag{A.53}$$

For $d_{n,0}$, there are no $\cos\theta$-dependent factors arising and the PSI is given by (A.24) with only the symmetry factor absent. For comparability with $\delta\Gamma_3$ in the bookkeeping below, the $\cos\theta$-dependent part of the PSI will be separated as a trivial factor of 1. The below ordering of the contributions to the quantities K, A, B, C from (A.25) is the same as in the case of $\delta\Gamma_3$:

$$B = 1 \cdot \frac{1}{2mV} \cdot 1 \cdot g^2 \cdot \frac{e^2}{m^2 n^2}\,, \quad B^n = \left(\frac{e^2}{2}\frac{g^2}{Vm^3n^2}\right)^n \tag{A.54}$$

$$A = 0 + 0 + 0 + 0 + 2 = 2 \tag{A.55}$$

$$K = \frac{1}{T} \cdot \frac{1}{8\pi} VT \cdot 1 \cdot 1 \cdot \frac{m^4}{\pi^2} = \frac{1}{8\pi^3} V m^4 \tag{A.56}$$

Conclusion

The result based on only $\delta A_{n,0}$ is given in terms of the leading order rate for the 2-scalar model as $\delta\Gamma_4 = 2^{-n-1}\Gamma_{n\phi\to 2\chi}$. The origin of these factors becomes clear when comparing the derivations: The internal selectron does not give a factor 2 at each vertex, accounting for a factor of 2^{-n}. The distinguishability of the final particles accounts for the remaining factor of $2!/2!^2 = 1/2$.

Let us now compare $\delta\Gamma_3$ and $\delta\Gamma_4$. Based on the above results, we have

$$\frac{\delta\Gamma_3}{\delta\Gamma_4} = \frac{1}{8}\cdot\frac{1}{n}\cdot e^{2n}\left(1-\frac{n_0^2}{n^2}\right)^n \sim \frac{1}{8}\frac{1}{n}e^{2n}\begin{cases} \left(1+\mathcal{O}\left(\frac{n_0^2}{n}\right)\right) & , \quad n \gg n_0 \\ \left(\frac{2\delta}{n_0}+\mathcal{O}\left(\frac{\delta^2}{n_0^2}\right)\right)^n & , \quad n = n_0+\delta\,, \quad \delta \ll n_0 \end{cases} . \tag{A.57}$$

One can see that $\delta A_{0,n}$ dominates far away from threshold, but $\delta A_{n,0}$ dominates close to the threshold. This corresponds to the fact that each 3-vertex results in a factor of the final selectrons' 3-momentum, which is much smaller than their mass m_e near threshold but larger sufficiently far from threshold.

A.5 SBT-Diagram

Two scalars

There are a single cross coupling vertex $g^2\chi^2\phi^2/\mathcal{N}_c$ and $v-1$ quartic self coupling vertices $\gamma\phi^4/\mathcal{N}_s$, where $v = n/2$.

The factorization (A.6) gives

$$\delta A_{SBT} = \frac{W}{v!}\cdot\frac{n!}{\sqrt{n!}}\cdot 2!\cdot d_{SBT}\,, \tag{A.58}$$

with

$$\frac{W}{v!} = \frac{v!}{v!}\frac{4!^{v-1}}{3!^{n/3}}2!, \quad v = n/2\,. \tag{A.59}$$

The calculation of D in (A.7) follows ref. [58]. If $l = 0, 1, \ldots$ labels the virtual momenta in the propagators after the lth branching, then

$$q_l^2 = \frac{(\frac{n}{2}m)^2}{3^{2l}}\,. \tag{A.60}$$

To make the calculation feasible, one can replace $q_l^2 - m^2$ by fq_l^2, where from

$$\frac{8}{9}q_l^2 \le (q_l^2 - m^2) < q_l^2, \quad \forall\, l\,, \tag{A.61}$$

it follows for the value of f that

$$\frac{8}{9} < f < 1\,. \tag{A.62}$$

Then, with $2 \cdot 3^L = n$, one has

$$D = \prod_{l=0}^{L-1} (q_l^2 - m^2)^{-2\cdot 3^l} = \frac{1}{(fm^2)^{\frac{n}{2}-1}} \frac{3^3}{2^2} n^2 \frac{1}{3^{\frac{3}{2}n}} \,. \tag{A.63}$$

For N, one simply has

$$N = \frac{g^2}{\mathcal{N}_c} \prod_{l=0}^{L-1} \left(\frac{\gamma}{\mathcal{N}_s}\right)^{2\cdot 3^l} = \frac{g^2}{\mathcal{N}_c} \left(\frac{\gamma}{\mathcal{N}_s}\right)^{\frac{n}{2}-1} \,. \tag{A.64}$$

The factors resulting from the phase space integration are given by (A.24). Overall, in the representation of (A.25), one thus has

$$B^n = \left(\frac{B_0 \gamma}{V m^3}\right)^n, \quad B_0 = \frac{4!/\mathcal{N}_s}{f \cdot 2 \cdot 3!^{\frac{2}{3}} \cdot 3^3} \sim \frac{1}{10 \mathcal{N}_s} \tag{A.65}$$

$$A = 4 \tag{A.66}$$

$$K = \frac{1}{T} \frac{1}{16\pi} VT \frac{g^4/\mathcal{N}_c^2}{(4!\gamma/\mathcal{N}_s)^2} (fm^2)^2 \frac{3^6}{2^4} 2!^4 \tag{A.67}$$

$$\equiv V m^4 \frac{K_0 g^4}{\gamma^2}, \quad K_0 \sim 10^1, \quad \mathcal{N}_c = 1, \mathcal{N}_s = 4! \,. \tag{A.68}$$

Scalar QED

For the case of photon creation from the scalar electron-positron condensate (sec. 2.3), the internal legs branching out in the diagram belong to the complex scalar and therefore the calculation is highly analogous to the one presented in the two-scalar case.

For the Proca-case (sec. 2.4), the loop induced 4-vertex of the two-scalar case (2.70) has an analog arising from the loop-induced terms

$$g^4 \left(A_\mu A^\mu\right)^2 \,, \quad \frac{g^4}{m_e^2} A_\mu A^\mu F_{\alpha\beta} F^{\alpha\beta} \,, \ldots \,. \tag{A.69}$$

Further 4-vertices are all $\mathcal{O}\left(m_e^{-2}\right)$ or $\mathcal{O}\left(m_e^{-4}\right)$. For the kinematics in question, all virtual momenta in the SBT-diagram satisfy $q_l^2 \ll m_e^2$ and thus the non-derivative term $\left(A_\mu A^\mu\right)^2$ dominates over the remaining terms.

The only remaining difference with the two-scalar case is then the numerator structure of the photon propagator. However, this plays no role in the diagram at hand: The initial photon polarizations are $\epsilon^\mu \propto \delta_z^\mu$ and project out all the orthogonal ones in the photon propagator, in particular the ones $\epsilon^\mu \propto q_l^\mu \propto \delta_0^\mu$. Thus the numerator can be replaced by $\eta^{\alpha\beta}$ and the calculation reduces to the one of the $\chi^2\phi^2$-model.

Appendix B

Appendix Part II

In this appendix, we document how we determined the parameter scalings cited in (3.31) - (3.34).

To find the dependence of both the rewriting values of C_m and the associated rates Γ on a given parameter $X \in \{N_c, \epsilon_m, C_0, \Delta N_c, K\}$, we have time evolved the system for different choices of X, while keeping fixed the remaining parameters at the values stated in (3.30). For each individual choice of X, the simulations have been repeated for many values of the coupling, $C_m \in [0, 1]$ (or a larger interval), with a sampling step $\delta C_m = 10^{-3}$ or smaller.

Among the values of C_m thus sampled we have defined those as rewriting values for which the amplitude n_0 exceeded by a factor of 1.2 or more the free amplitude of n_0, i.e., that of the case of $C_m = 0$. In the case of neighboring rewriting values (i.e., values differing only by the increment δC_m), we only selected that with the highest value of Γ. Around that value, since we have found the rate to depend on C_m rather sensitively, we have then repeated simulations with the smaller sampling step of $\delta C_m = 5 \cdot 10^{-5}$. The eventually selected pair of (C_m, Γ) within such finer sampling was then determined as that with the highest rate.

Below, we further explain our procedure and present the obtained data and fits.

N_c-Scaling

Fig. B.1 shows the data used to find the dependence of (C_m, Γ) on N_c. While varying N_c, ΔN_c has also been varied with $N_c/\Delta N_c$ is fixed. To fit the rewriting values, the function $f_C(N_c) = a \left(\frac{N_c}{22}\right)^{-b}$ has been used. The fit result is $a \approx 0.275$ and $b \approx 0.911$. To fit the rates, the function $f_\Gamma(N_c) = A \left(\frac{N_c}{22}\right)^{-B}$ has been used. The fit result is $A \approx 4.46 \cdot 10^{-5}$ and $B \approx 1.14$.

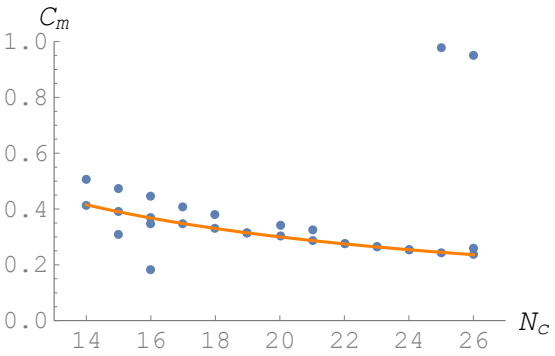

(a) Rewriting values of C_{m}.

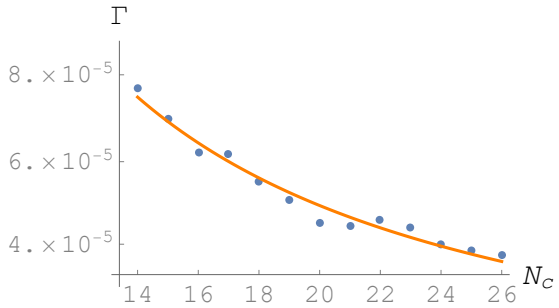

(b) Rates Γ at those rewriting values.

Figure B.1: Data and fits for the rewriting values of C_m and the rates Γ as function of N_c. ΔN_c has been varied to keep $N_c/\Delta N_c$ fixed.

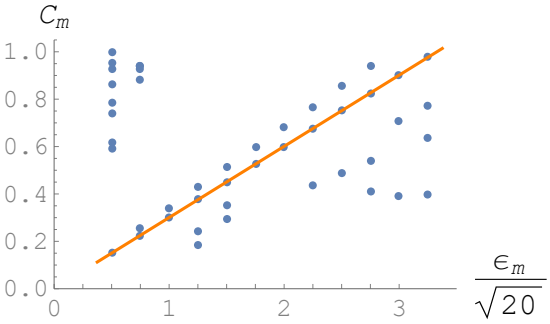

(a) Rewriting values of C_{m}.

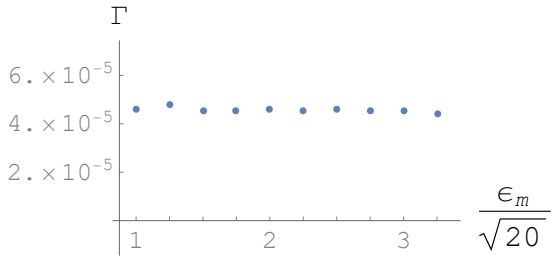

(b) Rates Γ at those rewriting values.

Figure B.2: Data and fit for the rewriting values of C_m and the rates Γ as function of ϵ_m.

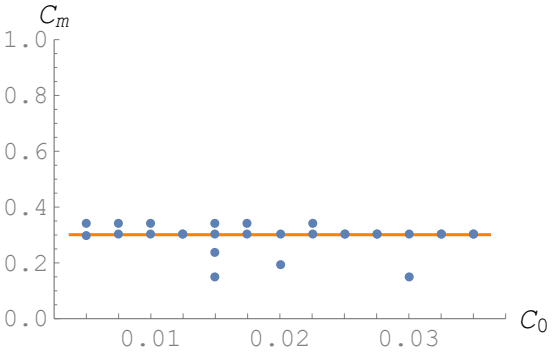

(a) Rewriting values of C_m.

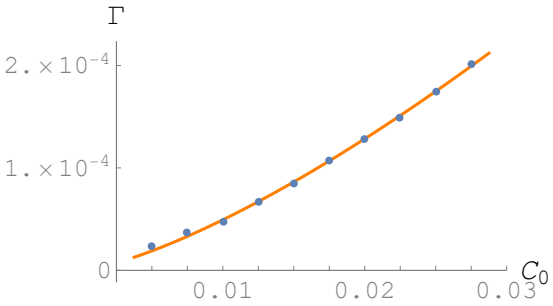

(b) Rates Γ at those rewriting values.

Figure B.3: Data and fits for the rewriting values of C_m and the rates Γ as function of C_0.

ϵ_m-Scaling

Fig. B.2 shows the data used to find the dependence of (C_m, Γ) on ϵ_m. To fit the rewriting values, the function $f_C(\epsilon_m) = a\epsilon_m$ has been used. The fit result is $a \approx 0.300$. The dependence of the rate Γ on ϵ_m can be seen to be negligible compared to its dependence on other parameters.

C_0-Scaling

Fig. B.3 shows the data used to find the dependence of (C_m, Γ) on C_0. The dependence of the rewriting values on C_0 can be observed to be negligible compared to its dependence on other parameters. To fit the rates, the function $f_\Gamma(C_0) = AC_0^B$ has been used. The fit result is $A \approx 2.85 \cdot 10^{-2}$ and $B \approx 1.38$.

ΔN_c-Scaling

Fig. B.4 shows the data used to find the dependence of (C_m, Γ) on ΔN_c. To fit the rewriting values, the function $f_C(\Delta N_c) = a\left(\frac{\Delta N_c}{12}\right)^b$ has been used. The fit result is $a \approx 0.300$ and $b \approx 0.207$. [1] To fit the rates, the function $f_\Gamma(\Delta N_c) = A\left(1 - B\frac{\Delta N_c}{20}\right)$ has been used. The fit result is $A \approx 1.38 \cdot 10^{-4}$ and $B \approx 1.07$.

[1] A second scaling behavior with $b \approx -0.130$ can also be observed. Since $\Delta N_c/N_c \to 0$ in the limit of a large system, this scaling would be even less favorable for rewriting and we consequently do not consider it.

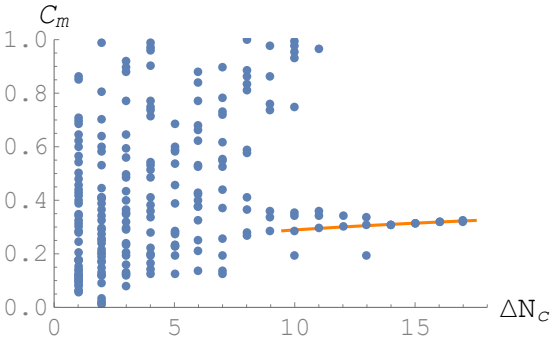

(a) Rewriting values of C_m.

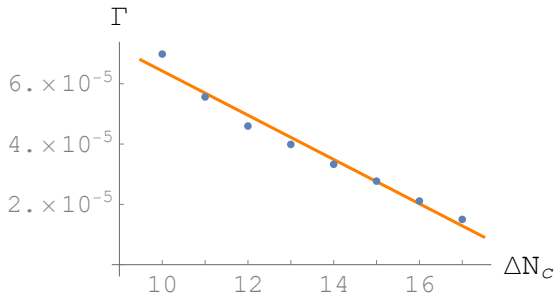

(b) Rates Γ at those rewriting values.

Figure B.4: Data and fits for the rewriting values of C_m and the rates Γ as function of ΔN_c.

K-Scaling

The exponential growth of the size of the Hilbert space with the number of modes is a limiting factor for the numerical investigation of the K-dependence. For this reason, we have been restricted to choices of up to $K = 8$. While varying K, we have also varied $N_m = K/2$ in order to exclude effects due to a relative change of occupation of the memory modes. For $K = 2$, the system appears to behave in a non-generic way, motivating us to exclude that K-choice. This leaves as available choices $K = 4, 6, 8$.

A further challenge is due to the fact that the duration of simulations for $K = 8$ is already rather long. Performing refined scans around rewriting values in order to precisely determine the rate is thus not feasible, especially since a large number of rewriting values exists for $K = 8$. As a solution, we have restricted the selection of rewriting values to those with at least one neighboring rewriting value (i.e., separated by only the increment $\delta C_m = 10^{-3}$). For those, the rates have been determined through a refined scan. The same procedure has been applied to the cases $K = 4$ and $K = 6$ as well. Fig. 3.4 shows the rewriting values thus selected and the associated rates.

List of Figures

Bibliography

[1] G. Dvali and L. Eisemann, "Perturbative understanding of nonperturbative processes and quantumization versus classicalization", *Phys. Rev. D* **106** (2022) 125019 [2211.02618].

[2] G. Dvali, L. Eisemann, M. Michel and S. Zell, "Universe's Primordial Quantum Memories", *JCAP* **1903** (2019) 010 [1812.08749].

[3] G. Dvali, L. Eisemann, M. Michel and S. Zell, "Black hole metamorphosis and stabilization by memory burden", *Phys. Rev. D* **102** (2020) 103523 [2006.00011].

[4] S. Zell, *The quantum substructure of gravity*, Ph.D. thesis, Munich U., 7, 2019. 10.5282/edoc.24429.

[5] M. Michel, *Quantum Gravity and Quantum Information: On Systems of Enhanced Microstate Entropy*, Ph.D. thesis, Munich U., 2021. 10.5282/edoc.28578.

[6] J.F. Donoghue, "General relativity as an effective field theory: The leading quantum corrections", *Physical Review D* **50** (1994) 3874.

[7] C.W. Misner, K.S. Thorne and J.A. Wheeler, *Gravitation*, W. H. Freeman, San Francisco (1973).

[8] R. Narayan, "Black holes in astrophysics", *New Journal of Physics* **7** (2005) 199.

[9] J.D. Bekenstein, "A Universal Upper Bound on the Entropy to Energy Ratio for Bounded Systems", *Phys. Rev. D* **23** (1981) 287.

[10] J.D. Bekenstein, "Black holes and entropy", *Phys. Rev.* **D7** (1973) 2333.

[11] S. Hawking, "Particle Creation by Black Holes", *Commun. Math. Phys.* **43** (1975) 199.

[12] V. Mukhanov, *Physical Foundations of Cosmology*, Cambridge University Press, Oxford (2005), 10.1017/CBO9780511790553.

[13] B. Carr, K. Kohri, Y. Sendouda and J. Yokoyama, "Constraints on primordial black holes", *Reports on Progress in Physics* **84** (2021) 116902.

[14] H.J. Treder, "The Planckions as largest elementary particles and as smallest test bodies", *Found. Phys.* **15** (1985) 161.

[15] G. 't Hooft, "Graviton Dominance in Ultrahigh-Energy Scattering", *Phys. Lett. B* **198** (1987) 61.

[16] G. Dvali and C. Gomez, "Self-Completeness of Einstein Gravity", 1005.3497.

[17] G. Dvali, G.F. Giudice, C. Gomez and A. Kehagias, "UV-Completion by Classicalization", *JHEP* **08** (2011) 108 [1010.1415].

[18] G. Dvali, "Strong Coupling and Classicalization", *Subnucl. Ser.* **53** (2017) 189 [1607.07422].

[19] G. Dvali and C. Gomez, "Black Hole's Quantum N-Portrait", *Fortsch. Phys.* **61** (2013) 742 [1112.3359].

[20] G. Dvali, "Entropy Bound and Unitarity of Scattering Amplitudes", *JHEP* **03** (2021) 126 [2003.05546].

[21] G. Dvali, *Area Law Saturation of Entropy Bound from Perturbative Unitarity in Renormalizable Theories*, 2019.

[22] A.H. Guth, "The Inflationary Universe: A Possible Solution to the Horizon and Flatness Problems", *Phys. Rev. D* **23** (1981) 347.

[23] G.W. Gibbons and S.W. Hawking, "Cosmological Event Horizons, Thermodynamics, and Particle Creation", *Phys. Rev.* **D15** (1977) 2738.

[24] G. Dvali, "Non-Thermal Corrections to Hawking Radiation Versus the Information Paradox", *Fortsch. Phys.* **64** (2016) 106 [1509.04645].

[25] G. Dvali and C. Gomez, "Black Hole's 1/N Hair", *Phys. Lett.* **B719** (2013) 419 [1203.6575].

[26] G. Dvali, D. Flassig, C. Gomez, A. Pritzel and N. Wintergerst, "Scrambling in the Black Hole Portrait", *Phys. Rev.* **D88** (2013) 124041 [1307.3458].

[27] G. Dvali and C. Gomez, "Quantum Compositeness of Gravity: Black Holes, AdS and Inflation", *JCAP* **1401** (2014) 023 [1312.4795].

[28] G. Dvali, "A Microscopic Model of Holography: Survival by the Burden of Memory", 1810.02336.

[29] W.R. Inc., "Mathematica, Version 13.3",

[30] G. Dvali and C. Gomez, "Black Holes as Critical Point of Quantum Phase Transition", *Eur. Phys. J.* **C74** (2014) 2752 [1207.4059].

[31] G. Dvali and C. Gomez, "Black Hole Macro-Quantumness", 1212.0765.

[32] G. Dvali and C. Gomez, "Quantum Exclusion of Positive Cosmological Constant?", *Annalen Phys.* **528** (2016) 68 [1412.8077].

[33] G. Dvali, C. Gomez and S. Zell, "Quantum Break-Time of de Sitter", *JCAP* **1706** (2017) 028 [1701.08776].

[34] G. Dvali, "S-Matrix and Anomaly of de Sitter", *Symmetry* **13** (2020) 3 [2012.02133].

[35] G. Dvali, "Quantum gravity in species regime", 2103.15668.

[36] L. Berezhiani, G. Dvali and O. Sakhelashvili, "de Sitter space as a BRST invariant coherent state of gravitons", *Phys. Rev. D* **105** (2022) 025022 [2111.12022].

[37] G. Dvali and S. Zell, "Classicality and Quantum Break-Time for Cosmic Axions", *JCAP* **07** (2018) 064 [1710.00835].

[38] L. Berezhiani and M. Zantedeschi, "Evolution of coherent states as quantum counterpart of classical dynamics", *Phys. Rev. D* **104** (2021) 085007 [2011.11229].

[39] L. Berezhiani, G. Cintia and M. Zantedeschi, "Background-field method and initial-time singularity for coherent states", *Phys. Rev. D* **105** (2022) 045003 [2108.13235].

[40] F. Kühnel, "Thoughts on the Vacuum Energy in the Quantum N-Portrait", *Mod. Phys. Lett. A* **30** (2015) 1550197 [1408.5897].

[41] F. Kuhnel and M. Sandstad, "Corpuscular Consideration of Eternal Inflation", *Eur. Phys. J. C* **75** (2015) 505 [1504.02377].

[42] L. Berezhiani, "On Corpuscular Theory of Inflation", *Eur. Phys. J. C* **77** (2017) 106 [1610.08433].

[43] L. Kofman, A.D. Linde and A.A. Starobinsky, "Towards the theory of reheating after inflation", *Phys. Rev. D* **56** (1997) 3258 [hep-ph/9704452].

[44] G. Dvali, C. Gomez and A. Kehagias, "Classicalization of Gravitons and Goldstones", *JHEP* **11** (2011) 070 [1103.5963].

[45] G. Dvali, C. Gomez, R.S. Isermann, D. Lüst and S. Stieberger, "Black hole formation and classicalization in ultra-Planckian 2→N scattering", *Nucl. Phys. B* **893** (2015) 187 [1409.7405].

[46] G. Dvali, "Classicalization Clearly: Quantum Transition into States of Maximal Memory Storage Capacity", 1804.06154.

[47] T.W.B. Kibble, "Frequency Shift in High-Intensity Compton Scattering", *Phys. Rev.* **138** (1965) B740.

[48] J. Ellis, "TikZ-Feynman: Feynman diagrams with TikZ", *Comput. Phys. Commun.* **210** (2017) 103 [1601.05437].

[49] N.D. Birrell and P.C.W. Davies, *Quantum Fields in Curved Space*, Cambridge Monographs on Mathematical Physics, Cambridge Univ. Press, Cambridge, UK (2, 1984), 10.1017/CBO9780511622632.

[50] V. Mukhanov and S. Winitzki, *Introduction to quantum effects in gravity*, Cambridge University Press (6, 2007).

[51] L. Landau and S. Lifshitz, E., *Mechanics, Vol.1, pp. 80-84*, Butterworth-Heinemann (1976).

[52] L. Eisemann, "Schwinger Pair-Creation from Multi-Photon Annihilation Processes", Master's thesis, Munich U., 2016.

[53] M.S. Marinov and V.S. Popov, "Electron-Positron Pair Creation from Vacuum Induced by Variable Electric Field", *Fortsch. Phys.* **25** (1977) 373.

[54] E. Brezin and C. Itzykson, "Pair production in vacuum by an alternating field", *Phys. Rev. D* **2** (1970) 1191.

[55] A. Ringwald, "Pair production from vacuum at the focus of an X-ray free electron laser", *Phys. Lett. B* **510** (2001) 107 [hep-ph/0103185].

[56] J.S. Schwinger, "On gauge invariance and vacuum polarization", *Phys. Rev.* **82** (1951) 664.

[57] S.R. Coleman and E.J. Weinberg, "Radiative Corrections as the Origin of Spontaneous Symmetry Breaking", *Phys. Rev. D* **7** (1973) 1888.

[58] H. Goldberg, "Breakdown of perturbation theory at tree level in theories with scalars", *Phys. Lett. B* **246** (1990) 445.

[59] J.M. Cornwall, "On the High-energy Behavior of Weakly Coupled Gauge Theories", *Phys. Lett. B* **243** (1990) 271.

[60] D. Flassig, A. Pritzel and N. Wintergerst, "Black holes and quantumness on macroscopic scales", *Phys. Rev. D* **87** (2013) 084007 [1212.3344].

[61] A. Kovtun and M. Zantedeschi, "Breaking BEC", *JHEP* **07** (2020) 212 [2003.10283].

[62] G. Dvali and R. Venugopalan, "Classicalization and unitarization of wee partons in QCD and gravity: The CGC-black hole correspondence", *Phys. Rev. D* **105** (2022) 056026 [2106.11989].

[63] F. Gelis, E. Iancu, J. Jalilian-Marian and R. Venugopalan, "The Color Glass Condensate", *Ann. Rev. Nucl. Part. Sci.* **60** (2010) 463 [1002.0333].

[64] G. Dvali and O. Sakhelashvili, "Black-hole-like saturons in Gross-Neveu", *Phys. Rev. D* **105** (2022) 065014 [2111.03620].

[65] D.J. Gross and A. Neveu, "Dynamical Symmetry Breaking in Asymptotically Free Field Theories", *Phys. Rev. D* **10** (1974) 3235.

[66] D. Amati, M. Ciafaloni and G. Veneziano, "Superstring Collisions at Planckian Energies", *Phys. Lett. B* **197** (1987) 81.

[67] D. Amati, M. Ciafaloni and G. Veneziano, "Classical and Quantum Gravity Effects from Planckian Energy Superstring Collisions", *Int. J. Mod. Phys. A* **3** (1988) 1615.

[68] D.J. Gross and P.F. Mende, "String Theory Beyond the Planck Scale", *Nucl. Phys. B* **303** (1988) 407.

[69] D.J. Gross and P.F. Mende, "The High-Energy Behavior of String Scattering Amplitudes", *Phys. Lett. B* **197** (1987) 129.

[70] A. Addazi, M. Bianchi and G. Veneziano, "Glimpses of black hole formation/evaporation in highly inelastic, ultra-planckian string collisions", *JHEP* **02** (2017) 111 [1611.03643].

[71] G. Dvali, A. Franca, C. Gomez and N. Wintergerst, "Nambu-Goldstone Effective Theory of Information at Quantum Criticality", *Phys. Rev.* **D92** (2015) 125002 [1507.02948].

[72] G. Dvali and M. Panchenko, *Black Hole Type Quantum Computing in Critical Bose-Einstein Systems*, 2015.

[73] G. Dvali and M. Panchenko, "Black Hole Based Quantum Computing in Labs and in the Sky", *Fortsch. Phys.* **64** (2016) 569 [1601.01329].

[74] G. Dvali, *Critically excited states with enhanced memory and pattern recognition capacities in quantum brain networks: Lesson from black holes*, 2017.

[75] G. Dvali, "Black Holes as Brains: Neural Networks with Area Law Entropy", *Fortsch. Phys.* **66** (2018) 1800007 [1801.03918].

[76] G. Dvali, "Area law microstate entropy from criticality and spherical symmetry", *Phys. Rev.* **D97** (2018) 105005 [1712.02233].

[77] G. Dvali, M. Michel and S. Zell, "Finding Critical States of Enhanced Memory Capacity in Attractive Cold Bosons", *EPJ Quant. Technol.* **6** (2019) 1 [1805.10292].

[78] G. Dvali, *Unitarity Entropy Bound: Solitons and Instantons*, 2019.

[79] G. Dvali, O. Kaikov and J.S.V. Bermúdez, "How special are black holes? correspondence with objects saturating unitarity bounds in generic theories", *Physical Review D* **105** (2022) .

[80] T. Tao, *Topics in Random Matrix Theory*, vol. 132 of *Graduate studies in mathematics*, AMS (2012).

[81] M. Michel and S. Zell, "TimeEvolver: A program for time evolution with improved error bound", *Computer Physics Communications* **277** (2022) 108374.

[82] G. Dvali and C. Gomez, "Landau–Ginzburg limit of black hole's quantum portrait: Self-similarity and critical exponent", *Phys. Lett.* **B716** (2012) 240 [1203.3372].

[83] V.F. Foit and N. Wintergerst, "Self-similar Evaporation and Collapse in the Quantum Portrait of Black Holes", *Phys. Rev.* **D92** (2015) 064043 [1504.04384].

[84] R. Ruffini and J.A. Wheeler, "Introducing the black hole", *Phys. Today* **24** (1971) 30.

[85] J.B. Hartle, "Long-range neutrino forces exerted by kerr black holes", *Phys. Rev.* **D3** (1971) 2938.

[86] J.D. Bekenstein, "Transcendence of the law of baryon-number conservation in black hole physics", *Phys. Rev. Lett.* **28** (1972) 452.

[87] J.D. Bekenstein, "Nonexistence of baryon number for static black holes", *Phys. Rev.* **D5** (1972) 1239.

[88] J.D. Bekenstein, "Nonexistence of baryon number for black holes. ii", *Phys. Rev.* **D5** (1972) 2403.

[89] C. Teitelboim, "Nonmeasurability of the baryon number of a black-hole", *Lett. Nuovo Cim.* **3S2** (1972) 326.

[90] C. Teitelboim, "Nonmeasurability of the lepton number of a black hole", *Lett. Nuovo Cim.* **3S2** (1972) 397.

[91] D.N. Page, "Information in black hole radiation", *Phys. Rev. Lett.* **71** (1993) 3743 [hep-th/9306083].

[92] Y.B. Zel'dovich and I.D. Novikov, "The Hypothesis of Cores Retarded during Expansion and the Hot Cosmological Model", *Sov. Astron.* **10** (1967) 602.

[93] S. Hawking, "Gravitationally collapsed objects of very low mass", *Mon. Not. Roy. Astron. Soc.* **152** (1971) 75.

[94] B.J. Carr and S. Hawking, "Black holes in the early Universe", *Mon. Not. Roy. Astron. Soc.* **168** (1974) 399.

[95] G.F. Chapline, "Cosmological effects of primordial black holes", *Nature* **253** (1975) 251.

[96] B. Carr, F. Kuhnel and M. Sandstad, "Primordial Black Holes as Dark Matter", *Phys. Rev.* **D94** (2016) 083504 [1607.06077].

[97] B.J. Carr, K. Kohri, Y. Sendouda and J. Yokoyama, "Constraints on primordial black holes from the Galactic gamma-ray background", *Phys. Rev.* **D94** (2016) 044029 [1604.05349].

[98] B.J. Carr, K. Kohri, Y. Sendouda and J. Yokoyama, "New cosmological constraints on primordial black holes", *Phys. Rev.* **D81** (2010) 104019 [0912.5297].

[99] MACHO, EROS collaboration, "EROS and MACHO combined limits on planetary mass dark matter in the galactic halo", *Astrophys. J. Lett.* **499** (1998) L9 [astro-ph/9803082].

[100] G. Dvali, E. Koutsangelas and F. Kuhnel, "Compact Dark Matter Objects via N Dark Sectors", *Phys. Rev.* **D101** (2020) 083533 [1911.13281].

[101] Fermi-LAT collaboration, "The spectrum of isotropic diffuse gamma-ray emission between 100 MeV and 820 GeV", *Astrophys. J.* **799** (2015) 86 [1410.3696].

[102] T. Kneiske, K. Mannheim and D. Hartmann, "The Gamma-ray horizon", *AIP Conf. Proc.* **587** (2001) 358.

[103] Y. Luo, S. Hanasoge, J. Tromp and F. Pretorius, "Detectable seismic consequences of the interaction of a primordial black hole with Earth", *Astrophys. J.* **751** (2012) 16 [1203.3806].

[104] V. Mukhanov, *Physical Foundations of Cosmology*, Cambridge University Press, Oxford (2005), 10.1017/CBO9780511790553.

Acknowledgements

My deep thanks and appreciation go to my supervisor, Gia Dvali, who provided me with an extraordinary opportunity to do research in his group. To work with him and under his insightful guidance on the intriguing projects he suggested has been an enthralling experience. I am particularly grateful for his willingness to share his profound insights into physics, which he conveyed with inspiring clarity during various settings, including lectures, seminars, group discussions, and personal conversations.

I also wish to thank Gia Dvali, Andreas Weiler, Harald Weinfurter, and Til Birnstiel as well as Thomas Kuhr and Monika Aidelsburger for making up my PhD committee.

Throughout my doctoral studies, I have been fortunate to engage in enlightening dialogues and thought-provoking discussions that span beyond the realm of physics. I would like to extend my gratitude to the individuals who have generously shared their knowledge and broadened my horizons. I am particularly appreciative of my research collaborators, Marco Michel and Sebastian Zell. The constructive and disciplined approach and the willingness to help each other within the projects and beyond have made collaborating a pleasure. Furthermore, I am grateful to Max Warkentin and Karanbir Tiwana for the enriching conversations and camaraderie we enjoyed both as fellow physics enthusiasts and trusted friends. I feel fortunate to have shared an office space with them and Otari Sakhelashvili. The friendly atmosphere and mutual support have turned this period into a cherished memory. My appreciation extends to all other group members for their shared passion for the subject and the readiness to help each other. I would also like to express my special thanks to Herta Wiesbeck-Yonis for her warm and friendly disposition and indispensable assistance in navigating academic bureaucracy.

Moreover, I wish to express my gratitude to my academic institution, LMU, for fostering my growth from the master's studies until the PhD. In particular, I would like to mention the inspiring and rich lectures of Prof. Slava Mukhanov, which at the beginning of my master's program reaffirmed to me the possibility of a profound understanding of physics and certainly contributed to my decision to pursue a PhD.

I am indebted to my friends for their continued support, with a special mention to Hüseyin Vural for his wise counsel on all kinds of matters. The immeasurable and humbling support I have received from Maria, Andreas, and Jakob has provided the very foundation for this endeavour. Their presence and memory have served as a guiding light, illuminating every stage of this journey. Lastly, I am grateful to Garam for her unwavering and generous support, valuable advice, and love, which have been constant sources of inspiration and

encouragement.